

INFORMATION TO USERS

This manuscript has been reproduced from the microfilm master. UMI films the text directly from the original or copy submitted. Thus, some thesis and dissertation copies are in typewriter face, while others may be from any type of computer printer.

The quality of this reproduction is dependent upon the quality of the copy submitted. Broken or indistinct print, colored or poor quality illustrations and photographs, print bleedthrough, substandard margins, and improper alignment can adversely affect reproduction.

In the unlikely event that the author did not send UMI a complete manuscript and there are missing pages, these will be noted. Also, if unauthorized copyright material had to be removed, a note will indicate the deletion.

Oversize materials (e.g., maps, drawings, charts) are reproduced by sectioning the original, beginning at the upper left-hand corner and continuing from left to right in equal sections with small overlaps.

Photographs included in the original manuscript have been reproduced xerographically in this copy. Higher quality 6" x 9" black and white photographic prints are available for any photographs or illustrations appearing in this copy for an additional charge. Contact UMI directly to order.

ProQuest Information and Learning
300 North Zeeb Road, Ann Arbor, MI 48106-1346 USA
800-521-0600

UMI[®]

**MULTIUSER WIRELESS COMMUNICATION OVER
TIME AND FREQUENCY SELECTIVE CHANNELS**

By

Tamer Adel Kadous

A DISSERTATION SUBMITTED IN PARTIAL FULFILLMENT OF THE
REQUIREMENTS FOR THE DEGREE OF

DOCTOR OF PHILOSOPHY
(ELECTRICAL ENGINEERING)

at the

UNIVERSITY OF WISCONSIN – MADISON

2001

UMI Number: 3012417

Copyright 2001 by
Kadous, Tamer Adel

All rights reserved.

UMI[®]

UMI Microform 3012417

Copyright 2001 by Bell & Howell Information and Learning Company.

All rights reserved. This microform edition is protected against
unauthorized copying under Title 17, United States Code.

Bell & Howell Information and Learning Company
300 North Zeeb Road
P.O. Box 1346
Ann Arbor, MI 48106-1346

Copyright 2001 by Tamer Adel Kadous

All Rights Reserved

A dissertation entitled

Multiuser Wireless Communication Over Time and Frequency
Selective Channels

submitted to the Graduate School of the
University of Wisconsin-Madison
in partial fulfillment of the requirements for the
degree of Doctor of Philosophy


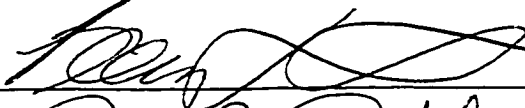
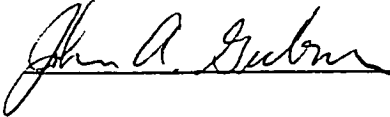
by

Tamer Adel Kadous

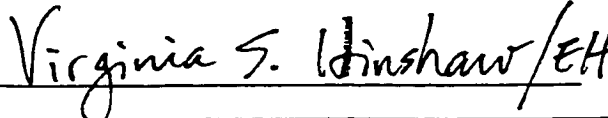
Date of Final Oral Examination: April 12, 2001

Month & Year Degree to be awarded: **December** **May** 2001 **August**

Approval Signatures of Dissertation Committee

	
_____ Professor	_____ Professor
	_____

Signature, Dean of Graduate School



Dedicated to my dear friend Sameh Zeitoun,
may Allah bestow His mercy on him.

ACKNOWLEDGEMENTS

Many thanks and appreciation goes first and foremost to Almighty Allah (God) who gave me the determination and patience to finish this dissertation. All my supplications and prayers for Him, Almighty, to accept my humble effort and devotion over the years to achieve this goal.

Many people have contributed in different ways to the conception and development of this dissertation. This is my special opportunity to say thank you to:

- My advisor, Professor Akbar Sayeed for his direction, criticism, insight and financial support.
- Many Professors in Electrical and Computer Engineering and Math departments who were my valuable resources. Among those: Professor John Gubner, Professor James Bucklew, Professor Barry Van Veen and Professor Hans Schneider.
- Professor Louis Scharf at University of Colorado Boulder for his valuable suggestions on Chapter 3.
- Professor Parameswaran Ramanathan and professor Richard Brualdi for their contributions as members of my dissertation committee.
- My friends and colleagues in the wireless communication group, including: Eko Onggosanusi, Jianzhong Zhang, Kraiyut Tantinarawat, Ashwin Ganesan, Kerry Wong and Ke Liu for the valuable discussions, and the lot of fun.
- My friends at the Engineering Hall, including: Seyfullah Halit Oguz, Ahmet Aydilek, Cabir Vural and Hussien Kettani who have made my experience in the University of Wisconsin-Madison more fun and enjoyable.

On the nonacademic side, Heartfelt thanks to:

- My wife Nermeen. Her patience, understanding and love throughout the course of my doctoral degree made things much easier.
- My daughter Mariam who contributed all the time she should get from her father.
- My parents and in-laws for their endless support throughout this course.
- My brothers, sisters-in-law, and my friends who have been a continuous source of encouragement and support.
- The Muslim brothers in the Islamic Center of Madison. Their enquiries, prayers and support over the years made this city like a home for me.

Contents

Acknowledgements		ii
List of Tables		viii
List of Figures		ix
1 Introduction		1
1.1 Challenges in Multiuser Communication Systems		1
1.2 CDMA Systems for Dispersive Channels		3
1.3 Thesis Overview		5
2 Preliminaries		8
2.1 Notation		8
2.2 Channel Model		9
3 Decentralized Multiuser Detection for Time-Varying Multipath Channels		11
3.1 Introduction		11
3.2 Canonical Multipath-Doppler Coordinates		14
3.3 Receiver Design in the Canonical Coordinates		17
3.3.1 Primary Coordinates: Minimal Complexity Reception		18
3.3.2 Primary and Secondary Coordinates: Enhanced Reception		19
3.4 Performance Analysis		22
3.4.1 Limiting Solution at High SNR		25
3.4.2 Probability of Error		26

3.4.3	Near-Far Resistance	28
3.4.4	Choice of Secondary Coordinates	30
3.5	Illustrative Examples	31
3.6	Implementation Issues	34
3.6.1	Adaptive Implementations	34
3.6.2	Channel Estimation	36
3.7	Conclusion	37
3.8	Figures	38
4	A Novel Framework for MC-CDMA Reception in the Presence of Imperfections	48
4.1	Introduction	48
4.2	System Model	50
4.2.1	MC-CDMA Transmitter	51
4.2.2	Conventional MC-CDMA Receiver	52
4.3	The Proposed Framework	53
4.3.1	General Receiver Structure	54
4.3.2	Receiver Performance	57
4.4	Reception in the Presence of Fast Fading	60
4.5	Reception in the Presence of Frequency Offset	61
4.5.1	Frequency Offset Correction in Slow Fading Channels	62
4.5.2	Frequency Offset Correction in Fast Fading Channels	63
4.6	Reception in the Presence of Phase Noise	63
4.7	Numerical Results	66
4.8	Alternative Representation	69

4.9	Conclusion	71
4.10	Figures	71
5	A New Signaling Scheme for Time and Frequency Dispersive Channels	80
5.1	Introduction	80
5.2	Time-Frequency Signaling	82
5.3	Near-Optimal Choice of T_o and B_o	85
5.4	Signal Reception and Performance	87
5.5	Intuitive Mapping Between MC-CDMA and TF-CDMA Systems	90
5.6	Conclusion	91
5.7	Figures	91
6	Multuser Detection in Time and Frequency Dispersive Channels	96
6.1	Introduction	96
6.2	CDMA Systems	98
6.2.1	DS-CDMA System	98
6.2.2	MC-CDMA System	101
6.2.3	MC-DS-CDMA system	103
6.2.4	Special Cases	107
6.3	Time Domain- Frequency Domain Mappings	108
6.4	Equivalences	111
6.4.1	Equivalences in FS Channel	113
6.4.2	Equivalences in TS Channel	119
6.4.3	Equivalences in TFS Channel	121

6.5 Numerical Results	127
6.6 Conclusion	128
7 Conclusions and Future Research	139
A The Necessary Condition for (3.47) to Hold	143
B The Proof of Proposition 1, Chapter 5	145
C The Proof of (6.43)	146
D The Proof of (6.63)	147
E The Proof of Lemma 1	148

List of Tables

6.1	Equivalence results for FS channel	119
6.2	Equivalence results for TS channel	121
6.3	Equivalence results for TFS channel–Part 1	126
6.4	Equivalence results for TFS channel–Part 2	126

List of Figures

- 3.1 (a) Generic linear receiver structure based on canonical multipath-Doppler coordinates. (b) Interpretation of the MMSE receiver in (3.20) and (3.21). The matrix filter \mathbf{C} suppresses MAI in the primary coordinates \mathbf{z}_p by using the secondary coordinates \mathbf{z}_s . The filter \mathbf{w}_p further suppresses MAI in the residual \mathbf{e} and performs diversity combining. 39
- 3.2 A schematic illustrating active and inactive coordinates. Active coordinates correspond to multipath-Doppler basis signals that lie within the channel spread. Inactive coordinates correspond to basis functions outside the channel spread. 39
- 3.3 Receiver SINR versus relative power of each interfering user for different number of secondary coordinates (D_s). Long times scales with respect to interference coherence time ($T_{obs} \gg T_{coh,i}$). (a) 1 interfering user ($N_i = 9$). (b) 3 interfering users ($N_i = 27$). Notice the saturation of SINR as $N_{tot} = D_p + D_s = 9 + D_s$ increases beyond $N_i + 1$ 40
- 3.4 Receiver SINR as a function of SNR of desired user for different values of D_s . Three interfering users with the same power as the desired user. (a) $T_{obs} < T_{coh,i}$ ($N_i = 3$). (b) $T_{obs} \gg T_{coh,i}$ ($N_i = 27$). Note that the receiver moves from an MAI-limited regime to a noise-limited regime as D_s increases beyond $N_i + 1 - D_p$ (-5 for (a) and 19 for (b)). SINR saturates in the MAI-limited regime but increases linearly with SNR in the noise-limited regime. 41
- 3.5 Analytically computed P_e (using (3.38)) as a function of the relative power of 3 interfering users ($N_i = 27$) for different values of D_s 42

3.6	Comparison of analytically computed P_e (via (3.38)) versus Monte-Carlo averaging of (3.37) over all \mathbf{h}_k 's for different values of D_s . 3 interfering users. (a) and (b): all users with equal power. (c) and (d): interfering users are 3 times stronger than desired user. (e) and (f): interfering users are 10 times stronger. We note for large D_s the receiver performance is close to that of a single-user (MRC) receiver with 3-level diversity [1] operating in the absence of MAI.	43
3.7	Near-far resistance, computed using (3.41) for 3 different realizations of \mathbf{h}_k 's, as a function of D_s . There are 3 interfering users that are 5 times stronger than the desired user.	44
3.8	Analytically computed P_e for different choices of secondary coordinates as a function of the relative power of 3 interfering users. (a) $D_s = 12$ (b) $D_s = 30$. Notice that the relatively small difference in performance between different choices, especially for larger D_s	45
3.9	Structures for adaptive implementation. (a) Parallel structure, and (b) Serial structure. The serial structure is particularly suited to blind channel estimation from the eigenstructure of \mathbf{e}	46
3.10	A representative plot of the channel estimation error as a function of SNR of desired user for different value of D_s . 3 interfering users that are 10 times stronger than desired user. Notice the monotonic decrease in error for $D_s \geq N_i = 3$	47
4.1	The MC-CDMA transmitter.	72
4.2	(a) The spectrum of SC-CDMA signal. (b) The spectrum of a MC-CDMA signal.	72

4.3	Coefficients associated with the the active and inactive subcarriers at the receiver for $M_l = M_u = 2$	73
4.4	The normalized energy captured by the m^{th} coefficient. (a) Fast fading channels with $B_dT = 2$. (b) Slowly fading channel in the presence of frequency offset with $f_{off}T = 0.8$. (c) $B_dT = 2$, $f_{off}T = 0.8$	74
4.5	(a) Normalized energy captured by the m^{th} coefficient in the presence of phase noise. (b) The number of coefficients M whose normalized power exceeds a threshold $\epsilon = 0.1, 0.01$ as a function of B_oT	75
4.6	(a) System performance as a function of fast fading parameter B_dT at $SNR = 10dB$. (b) System performance as a function of frequency offset parameter $f_{off}T$ at $SNR = 10dB$	76
4.7	(a) System performance as a function of B_dT at $SNR = 10dB$ and $f_{off}T = 0.3$. (b) System performance as a function of $f_{off}T$ at $SNR = 10dB$ and $B_dT = 0.3$	77
4.8	Receiver performance in the presence of phase noise at $SNR = 10dB$. (a) P_e as a function of B_oT for $M=10$. (b) P_e as a function of M for $B_oT = 0.8$. (c) Same as (a) when all subcarriers are used for transmission.	79
5.1	The TF-CDMA transmitter.	92
5.2	Time-frequency support of basis signals. (a) Fourier basis used in multicarrier systems in slow fading channels. (b) The proposed short-time Fourier basis in fast fading channels.	93
5.3	A digital implementation for the TF-CDMA transceiver.	94

- 5.4 (a) Comparison between the P_e of a conventional MC-CDMA system, the proposed TF-CDMA system and the MC-CDMA system introduced in Chapter 4 as a function of $T B_d$. There are two resolvable multipaths ($L = 2$) and SNR=10dB. The simulation results are based on Monte-Carlo simulation of 50,000 symbols via Jakes Model. The performance of the proposed TF-CDMA and MC-CDMA proposed systems are almost the same and improve with faster fading, in contrast to the degradation in performance of the conventional system. (b) The P_e of the proposed TF-CDMA system as a function of SNR for different values of $T B_d$ ($L = 2$). The increase in the slope of the P_e curve with increasing $T B_d$ (higher Doppler diversity) is evident. 95
- 6.1 The transmitter structure for different CDMA systems. (a) DS-CDMA system where $q_k[p]$ is the p^{th} entry of the k^{th} user signature code. (b) MC-CDMA system where $\tilde{q}_k[n]$ is the n^{th} entry of the k^{th} user signature code. (c) MC-DS-CDMA system where $\hat{q}_k[p, n]$ is the $(p, n)^{th}$ entry of the k^{th} user signature code. 130
- 6.2 The code distribution in time and frequency domains. (a) DS-CDMA system. (b) MC-CDMA system. (c) MC-DS-CDMA system. 132
- 6.3 DS-CDMA and MC-CDMA systems in FS channel. The DS-CDMA system exhibits multipath in time domain due to frequency selectivity. The MC-CDMA system is diagonal since each subcarrier encounters non selective fading in the frequency domain. 133

- 6.4 DS-CDMA and MC-CDMA systems in a TS channel. The MC-CDMA system exhibits multiple Doppler components in the frequency domain due to time selectivity. The DS-CDMA system is diagonal since each basis waveform (chip) encounters non selective fading in the time domain. 134
- 6.5 Diagonalizing a TFS channel via a TF-CDMA system starting from a MC-CDMA system. The bandwidth is divided into N_f sub-bands each contains N_t subcarriers that are faded similarly. To diagonalize TFS channel, each basis waveform duration is reduced by N_t , its bandwidth is increased by N_t so as the new basis waveforms encounter non selective fading in time and frequency. (a) MC-CDMA system. (b) TF-CDMA. 135
- 6.6 Diagonalizing TFS channel via TF-CDMA system starting from a DS-CDMA system. The symbol duration is divided into N_f time slots each contains N_f time samples that fade similarly. To diagonalize the TFS channel, each basis waveform bandwidth is reduced by N_f , its duration is increased by N_f so as the new basis waveforms encounter flat fading in time and frequency. (a) DS-CDMA system. (b) TF-CDMA. 136
- 6.7 Various systems performance over FS channel for $K = 20$ as a function of SNR . (a) $SINR$. (b) P_e 137
- 6.8 The performance of MC-CDMA, DS-CDMA and TF-CDMA systems over TFS channel for $K = 20$ as a function of SNR and at $B_d T = 0.2$. (a) $SINR$. (b) P_e 138

CHAPTER 1

INTRODUCTION

Wireless communication systems play an indispensable role in the rapidly evolving global information infrastructure. The increasing demand for personal communication services, wireless internet services, and the trend toward mobile computing is pushing the technology towards higher data rate applications. However, the hostile wireless propagation medium at the heart of modern communication poses formidable challenges to achieve this goal. Code Division Multiple Access (CDMA) has emerged as a key wireless communication technology as for meeting these challenges. CDMA systems are wide-band communication systems where signature code is assigned to each user to distinguish his/her signal from the users. There are three main types of CDMA systems that use the signature code in time, frequency, or time and frequency domains, respectively. This thesis contributes new solutions to a variety of problems in CDMA wireless communication systems.

1.1. Challenges in Multiuser Communication Systems

The major challenges posed by the wireless medium are:

Channel Propagation Dynamics: The highly dynamic and varied communication environments encountered in most wireless scenarios entail complex propagation dynamics that have a severe impact on system performance [2]. In particular, frequency selective fading due to multipath propagation and time selective fading due to Doppler effects (caused by the relative motion between end-users) make reliable wireless communication a challenging task. Coherent communication requires accurate

channel estimation and tracking commensurate with the rate of channel variations. Moreover, after determining the channel response, it is necessary to design receivers that compensate for the channel distortion. Interestingly, the same propagation effects that produce harsh channel characteristics also provide two inherent sources of diversity – multipath and Doppler diversity [1, 3].¹ With appropriate system design, channel diversity can be exploited to enhance system performance. Two key channel parameters in this context are the channel coherence bandwidth Δf_c and the channel coherence time Δt_c .²

Multiaccess Interference (MAI): This source of interference is due to multiple users accessing the channel simultaneously. This is one of the most significant factors limiting the performance of CDMA communication systems. The problem of MAI is particularly acute in near-far scenarios [4] in which a strong nearby interferer can disrupt reception of a highly attenuated desired signal. Strict power control among all users or interference suppression techniques are necessary for reliable communications. The problem becomes more challenging in the presence of multipath-Doppler propagation effects.

Complexity: In addition to the above challenges, an overriding constraint in practical applications is the complexity of the system. Digital Signal Processing (DSP) techniques are playing a key role in this context. For practical implementation, DSP algorithms face two main constraints. First, the need for low-power solutions, especially for the battery-powered mobile handset. This factor dictates low computational complexity. Second, the need for communication in rapidly changing mobile environ-

¹Antenna arrays exploits the spatial dimension for diversity. However, this thesis considers single antenna systems.

² Δf_c (Δt_c) is the frequency (time) span over which the channel is strongly correlated.

ments requires low structural complexity to enable fast adaptation. The next section briefly describes the three CDMA systems considered in this thesis.

1.2. CDMA Systems for Dispersive Channels

A key consideration in the design of CDMA systems in dispersive channels is the interaction between the underlying signal space and the channel. Denote the overall symbol duration by T and its essential two-sided bandwidth by B . The time-bandwidth product is denoted by $N \approx TB$ which is the dimension of the signal space. A CDMA system with such time-bandwidth product can support up to approximately N users by employing signature codes of length N . In general, the signature code is transmitted over a set of basis waveforms, each of which has a time duration T_o and essential two-sided bandwidth B_o . In Direct Sequence (DS)-CDMA [1], the basis waveforms are *narrow* time slots denoted by chips. In this case, $T_o = \frac{T}{N}$ and $B_o = B$. In Multi-Carrier (MC)-CDMA [5, 6, 7], the basis waveforms are narrowband subcarriers. In this case, $T_o = T$ and $B_o = \frac{B}{N}$. The MC-DS-CDMA [8, 5, 9] is the hybrid case which uses a grid of $N_t \times N_f$ basis waveforms ($N = N_t N_f$). In this case, $T_o = \frac{T}{N_t}$ and $B_o = \frac{B}{N_f}$.

The effects of channel on the three CDMA signaling schemes are determined by two factors: channel selectivity and channel dispersion. The channel is frequency (time) selective if the transmitted signal is subjected to different fading coefficients across its bandwidth (duration). Particularly, for any signaling scheme, the channel is frequency (time) selective if the overall bandwidth (duration) $B > \Delta f_c$ ($T > \Delta t_c$). The channel is dispersive in time if it exhibits multipath components and is dispersive in frequency if it exhibits multiple Doppler components. Whether or not the channel is dispersive depends on the relation between the duration, T_o , and bandwidth, B_o , of

basis waveforms and the channel coherence time Δt_c and coherence bandwidth Δf_c . In particular, the channel is dispersive in time if it is frequency selective per basis waveform (i.e. $B_o > \Delta f_c$), dispersive in frequency if it is time selective per basis waveform (i.e. $T_o > \Delta t_c$), and dispersive in time and frequency if it is time and frequency selective per basis waveform (i.e. $B_o > \Delta f_c$ and $T_o > \Delta t_c$). If the channel is non-dispersive for a particular signaling scheme, we say that this scheme diagonalizes the channel.³ For example, in a purely frequency selective channel ($B > \Delta f_c$, $T \ll \Delta t_c$), the DS-CDMA system is time dispersive and a well-known detector for this system that restores performance loss due to dispersion and exploits multipath diversity is the Rake receiver. The MC-CDMA system on the other hand is diagonal, and depending on the choice of T_o and B_o the MC-DS-CDMA could be time dispersive or diagonal. In purely time selective channel ($B \ll \Delta f_c$, $T > \Delta t_c$), the MC-CDMA system is frequency dispersive, the DS-CDMA system is diagonal, and again the MC-DS-CDMA could be frequency dispersive or diagonal. In time and frequency selective channels ($B > \Delta f_c$, $T > \Delta t_c$), the DS-CDMA is time dispersive, the MC-CDMA is frequency dispersive, and depending on the choice of T_o and B_o , the MC-DS-CDMA could be purely time dispersive, purely frequency dispersive, time and frequency dispersive, or diagonal.

³The notion of diagonalization comes from the fact that for non dispersive channels, the received signal vector (projection of the received signal onto the set of basis waveforms) is the transmitted one point-wise multiplied by a set of fading coefficients. That is, the basis functions serve as eigenfunctions of the channel – they pass through the channel without interference.

1.3. Thesis Overview

The new contributions in this thesis address a variety of issues in the design of CDMA systems operating over dispersive channels. A key underlying theme is an integrated approach to addressing the challenges due to channel propagation effects, MAI and system complexity.

Chapter 2 provides some background materials on notation and the channel model used throughout the thesis.

In **Chapter 3** we introduce a decentralized multiuser receiver for DS-CDMA system [10, 11]. The receiver design is based on a set of basis waveforms – *canonical multipath-Doppler modes*– that were recently explored in [12, 3, 13]. The canonical modes are derived from a fundamental characterization of channel propagation dynamics in terms of *uniformly spaced* discrete multipath delays and Doppler shifts of the signaling waveform. The receiver exploits the notion of *primary* and *secondary* coordinates. The primary coordinates contain the desired signal energy, facilitate exploiting channel diversity and also provide minimal complexity suppression of MAI that corrupts the primary coordinates. Additional degrees of freedom for MAI suppression are incorporated via *secondary* coordinates, that do not contain the desired signal, but only MAI. The complexity of the receiver can be tailored to achieve a desired level of performance by adjusting the number of secondary coordinates. The receiver easily lends itself for adaptive implementation that only requires the knowledge of the desired user’s signature code.

In **Chapter 4** we study some of the imperfections encountered in MC-CDMA systems over time-varying channels. Due to the longer symbol duration in comparison with single carrier systems, MC systems are more sensitive to various imperfections, includ-

ing phase noise and frequency offsets (due to local oscillators) and Doppler spreading due to temporal channel variations. The performance of current systems is significantly limited by these imperfections because they disperse the transmitted power in a particular subcarrier into adjacent subcarriers, thereby causing interference between the subcarriers at the receiver. We propose a receiver structure that combats these impairments in an integrated fashion. The receiver is based on a canonical model for the received signal that efficiently captures the effects of all impairments. The information transmitted on a particular subcarrier is decoded by processing a small subset of subcarriers surrounding the desired subcarrier. The proposed receiver fully compensates for frequency offsets as well as phase noise, thereby eliminating the performance loss due to these factors. Furthermore, in contrast to existing designs, it delivers improved performance under fast fading by exploiting Doppler diversity.

In **Chapter 5**, we introduce a set of basis waveforms that serve as approximately eigenfunctions for under-spread time-and frequency-selective channel. Such a signaling scheme significantly facilitate transceivers design since the basis waveforms minimally interfere with each other as they pass through the channel. The resulting system is a properly designed MC-DS-CDMA system that is a hybrid between DS-CDMA and MC-CDMA systems.

Chapter 6 builds on the insights developed in the previous chapters to develop a unified framework for describing and analyzing DS-CDMA, MC-CDMA, and MC-DS-CDMA systems operating over arbitrary time and frequency selective channels. The framework clearly reveals the effect of the channel on the three systems and also provides a choice of comparing the performance of linear Minimum Mean Square Error (MMSE) multiuser receiver in the three systems. We derive conditions under which

the different systems exhibit near-identical performance under a variety of channel assumptions. The notion of time-frequency duality plays a key role in the development of the framework. It is used to develop mappings that relate the various systems and expose their equivalence under appropriate channel conditions.

Chapter 7 briefly discusses some avenues for future research suggested by the work in this thesis.

CHAPTER 2

PRELIMINARIES

This chapter paves the way for the analysis in this thesis by introducing notation adopted throughout as well as the channel model under consideration.

2.1. Notation

The following conventions are used throughout the paper:

$\lfloor x \rfloor$: Denotes the largest integer smaller than x .

$\lceil x \rceil$: Denotes the smallest integer larger than x .

\mathbf{x}^T : The transpose of vector \mathbf{x} .

\mathbf{x}^H : The conjugate transpose of vector \mathbf{x} .

$\mathbf{x}(l)$: An l -places shifted version (to the right) of the vector \mathbf{x} , that is

$$\mathbf{x}(l) = \left[\underbrace{0 \ \dots \ 0}_l \ x[0] \ x[1] \ \dots \ x[N-l-1] \right]^T \text{ and } x[n] \text{ is the } n^{\text{th}} \text{ entry of vector } \mathbf{x}. \text{ If } l < 0, \text{ the shift is to the left.}$$

$\mathbf{A} \odot \mathbf{B}$: The Hadamard product between \mathbf{A} and \mathbf{B} , i.e. point-wise multiplication between the different elements of \mathbf{A} and \mathbf{B} .

$\text{diag}\{\mathbf{x}\}$: Diagonal matrix whose entries are those of vector \mathbf{x} .

$\mathbf{A}(n_1 : n_2)$: The sub-matrix built by the $(n_1)^{\text{th}}$, $(n_1 + 1)^{\text{th}}$, \dots , n_2^{th} columns of \mathbf{A} .

\mathbf{I}_N : The identity matrix of dimension N .

$\mathbf{1}_N$: $N \times 1$ vector with unity entries.

$\mathbf{0}_N$: $N \times 1$ vector with zero entries.

$E[\cdot]$: The expected value.

$$\mathbf{R}_{\mathbf{x},\mathbf{y}} : \mathbb{E} [\mathbf{x}\mathbf{y}^H].$$

Finally, we note that throughout the thesis, lower case boldface letters denote vectors and upper case boldface letters denote matrices.

2.2. Channel Model

We assume that all users have identical channel *statistics*, however, different users encounter independent channel realizations. We adopt the Wide Sense Stationary Uncorrelated Scattering (WSSUS) model [1, 14] which is characterized by a randomly time-varying impulse response $c_k(t, \tau)$ for user k . For fixed τ , $c_k(t, \tau)$ is modeled as a complex WSS Gaussian process in t . The channel response for different values of τ is uncorrelated. The time varying transfer function of the channel is

$$\tilde{c}_k(t, f) = \int_{-\infty}^{\infty} c_k(t, \tau) e^{-j2\pi f\tau} d\tau \quad (2.1)$$

Under the WSSUS assumption, $\tilde{c}_k(t, f)$ is a WSS process in both t and f . The statistics of $\tilde{c}_k(t, f)$ are characterized by the *spaced-time, spaced-frequency* correlation function $\phi(\Delta t, \Delta f) = \mathbb{E} [\tilde{c}_k(t, f) \tilde{c}_k^*(t - \Delta t, f - \Delta f)]$ which is fixed for all users. Under the assumption that all multipaths have the same *spaced-time* correlation function, $\phi_{\Delta t}(\Delta t) = \mathbb{E} [\tilde{c}_k(t, \cdot) \tilde{c}_k^*(t - \Delta t, \cdot)]$, $\phi(\Delta t, \Delta f)$ becomes separable [15],

$$\phi(\Delta t, \Delta f) = \phi_{\Delta t}(\Delta t) \psi_{\Delta f}(\Delta f) \quad (2.2)$$

where $\psi_{\Delta f}(\Delta f) = \mathbb{E} [\tilde{c}_k(\cdot, f) \tilde{c}_k^*(\cdot, f - \Delta f)]$ is the *spaced-frequency* correlation function. The duration over which the channel is strongly correlated is called the *coherence time*, Δt_c . Define the *Doppler power spectrum* function to be

$\Phi_{\theta}(\theta) = \int_{-\infty}^{\infty} \phi_{\Delta t}(\Delta t) e^{-j2\pi\Delta t\theta} d\Delta t$. The support of $\Phi_{\theta}(\theta)$ is called the *Doppler spread*,

$2B_d$, of the channel; $\Phi_\theta(\theta) = 0$, $|\theta| > B_d$. The coherence time and Doppler spread are inversely related: $\Delta t_c \approx \frac{1}{2B_d}$.

The channel power at different values of τ is called the *multipath intensity profile*: $\Psi_\tau(\tau) = \text{E} [|c_k(\cdot, \tau)|^2]$. The support of $\Psi_\tau(\tau)$ is called the *multipath spread* of the channel and is denoted T_m ; $\Psi_\tau(\tau) = 0$ for $\tau < 0$ or $\tau > T_m$. The Fourier transform of $\Psi_\tau(\tau)$ is the *spaced-frequency* correlation function $\psi_{\Delta f}(\Delta f) = \int_{-\infty}^{\infty} \Psi_\tau(\tau) e^{-j2\pi\Delta f\tau} d\tau$. The frequency span over which the channel is strongly correlated is called the *coherence bandwidth*, Δf_c . Coherence bandwidth and multipath spread are inversely related: $\Delta f_c \approx \frac{1}{T_m}$.

Throughout the thesis, we denote the duration of the overall signaling waveform with T and its essential bandwidth with B . At the different parts of the thesis, we may consider purely frequency selective channels ($B > \Delta f_c$, $T \ll \Delta t_c$), purely time selective channels ($B \ll \Delta f_c$, $T > \Delta t_c$) and/or the general time and frequency selective channels ($B > \Delta f_c$, $T > \Delta t_c$). As mentioned before in Chapter 1, the channel is frequency (time) selective if the transmitted signal is subjected to different fading coefficients across its bandwidth (duration). We denote the diversity order due to frequency selectivity (multipath diversity) by $L + 1$ where $L = \lceil BT_m \rceil$ while the diversity order due to time selectivity (Doppler diversity) by $2M + 1$ where $M = \lceil B_d T \rceil$.

CHAPTER 3

DECENTRALIZED MULTIUSER DETECTION FOR TIME-VARYING MULTIPATH CHANNELS

3.1. Introduction

Code Division Multiple Access (CDMA) has emerged as a promising core wireless technology for meeting the physical layer challenges of modern communication networks. Innovative signal processing is playing a key role in the design of high-performance CDMA receivers. Major signal processing challenges stem from three key factors that have a significant impact on CDMA system performance: *channel propagation effects* manifested as multipath dispersion, multipath fading, and temporal variations or Doppler effects; *multiaccess interference (MAI)*; and, *complexity* of the signal processing algorithms. Furthermore, these factors affect system performance in an inter-related fashion and have to be addressed jointly.

For signaling waveforms of duration T and bandwidth B , the dimension of the overall signal space is approximately¹ $N_o \approx TB$ (see, e.g., [16]). In direct-sequence CDMA systems, N_o is proportional to the spreading gain $N = \frac{T}{T_c}$, where T_c is the chip duration. Centralized receivers, which have the knowledge of spreading codes of all users, represent the signal space in terms of symbol-rate sampled outputs of the matched filters for different users [17]. Decentralized receivers, which have knowledge of only the spreading code of desired user, represent the space in terms of N -dimensional

¹More precisely, $N_o = (B + 2B_d)(T + T_m)$, where T_m is the multipath spread and B_d is the Doppler spread of the channel [1]. However, the terms other than TB are relatively small since $T_m \ll T$ and $B_d \ll B$, typically.

chip-rate sampled² outputs of the matched filter for the desired user. If the number of (strong) users, K , is smaller than N_o , it is most advantageous to operate in the lower-dimensional subspace containing the multiuser signal. While centralized receivers directly accomplish this, decentralized receivers rely on the data itself to adaptively estimate the multiuser subspace (see, e.g., [18, 17, 19, 20]). For desired performance of adaptive decentralized receivers in realistic time-varying scenarios, it is extremely important to map the received signal to a lower-dimensional subspace to enable reliable estimation of requisite statistics and rapid tracking. However, most existing decentralized receiver designs operate in the full (N) dimensional chip-rate sampled space which can result in unacceptably poor performance in realistic time-varying scenarios (see, e.g., [21]). Multipath propagation effects distort the signal and make the problem even more challenging. While there has been considerable recent research on decentralized reception over multipath channels (see, e.g., [18, 22, 23, 24, 25]), it falls short of jointly addressing the key issues of propagation effects, MAI suppression and receiver complexity, primarily due to the lack of an appropriate framework relating these aspects of receiver design. In particular, there is no systematic approach for effecting a judicious complexity versus performance tradeoff.

In this chapter, we introduce receiver design in *canonical multipath-Doppler coordinates* as an integrated framework for combating time-varying multipath distortion, suppressing MAI, and managing receiver complexity. The canonical coordinates are derived from a fundamental characterization of channel propagation dynamics in terms of *uniformly spaced* discrete multipath delays and Doppler shifts of the signaling waveform. These waveforms capture the essential degrees of freedom in the received signal

²Or oversampled outputs to cover all $N_o \geq N$ dimensions.

and constitute a canonical *fixed* basis for representing it. Consequently, processing in canonical coordinates eliminates the need for estimating arbitrary delays and Doppler shifts. While dispersion effects are often considered a nuisance to MAI suppression, canonical multipath-Doppler coordinates provide a natural partitioning of the signal space that enables exploitation of propagation effects for MAI suppression and diversity processing. A key notion in our framework is that of *primary* and *secondary* coordinates [12]. The primary coordinates of a desired user depend on its multipath and Doppler spreads and define a canonical low-dimensional subspace for capturing its signal energy. The primary coordinates facilitate maximal exploitation of channel diversity [3] and minimum-complexity MAI suppression. However, additional degrees of freedom are needed in general to adequately suppress the MAI that corrupts the desired signal in the primary coordinates. These additional degrees of freedom are furnished by the *secondary coordinates*. The secondary coordinates may include the active coordinates of *other users* (centralized reception) [13, 12], or *inactive* coordinates of the *desired user* (decentralized reception) [12] that do not contain the desired signal but only the MAI. The generic receiver structure is depicted in Figure 3.1(a). The signal space partitioning in terms of primary/secondary coordinates provides a systematic approach for tailoring receiver complexity to achieve a desired level of performance.

The next section develops the notion of canonical multipath-Doppler coordinates. Section 3.3 derives a decentralized minimum-mean-squared-error (MMSE) receiver structure in terms of primary and secondary coordinates. Performance analysis in Section 3.4 guides the choice of design parameters. Examples illustrating various facets of the framework are presented in Section 3.5. Practical issues related to channel esti-

mation and adaptive/blind implementations are discussed in Section 3.6. Concluding remarks are provided in Section 3.7.

3.2. Canonical Multipath-Doppler Coordinates

This section provides a brief discussion of the concept of canonical multipath-Doppler coordinates that underlies our framework [3, 12]. The complex baseband received waveform $r(t)$ for a *single* symbol of a *single* user is given by

$$r(t) = s(t - \tau_s) + n(t), \quad (3.1)$$

$$s(t) = \int_0^{T_m} \int_{-B_d}^{B_d} C(\theta, \tau) q(t - \tau) e^{j2\pi\theta t} d\theta d\tau, \quad (3.2)$$

where $s(t)$ is the information bearing signal, τ_s is the user delay, $n(t)$ is complex AWGN, and $q(t)$ denotes the spread-spectrum signaling waveform of duration T . Channel propagation is characterized by the multipath-Doppler *spreading function* $C(\theta, \tau) = \int c(t, \tau) e^{-j2\pi\theta t} dt$ and $c(t, \tau)$ is defined in Section 2.2 (with the subscript k removed for simplicity). $C(\theta, \tau)$ accounts for the temporal and spectral dispersion produced by the channel [14]. T_m and B_d denote the *multipath* and *Doppler spreads* of the channel, respectively and defined in Section 2.2.³

The key idea behind canonical multipath-Doppler coordinates is that the receiver “sees” only *finitely many* degrees of freedom in the signal due to the inherently finite duration T and essentially finite bandwidth B of the transmitted waveform $q(t)$ [3, 12, 14]. These essential degrees of freedom are captured by the following fundamental

³We assume negligible intersymbol interference, $T_m \ll T$, that is often the case in CDMA channels. However, the channel is frequency selective ($T_m > T_c$) in most cases, thereby affording multipath diversity.

characterization [3, 12, 14, 26]

$$\begin{aligned} s(t - \tau_s) &\approx \frac{1}{TB} \sum_{l=L_s}^{L_s+L_a} \sum_{m=-M_a}^{M_a} \bar{C} \left(\frac{m}{T}, \frac{l}{B} \right) q \left(t - \frac{l}{B} \right) e^{j \frac{2\pi m t}{T}} \\ &= \sum_{l=L_s}^{L_s+L_a} \sum_{m=-M_a}^{M_a} H(m, l) q_{ml}(t), \end{aligned} \quad (3.3)$$

which corresponds to a uniform sampling of the multipath-Doppler plane. $\bar{C}(\theta, \tau)$ is a time-frequency smoothed version of $C(\theta, \tau)$ that arises due to the time- and band-limited nature of $q(t)$. $L_s = \lfloor \tau_s B \rfloor$ denotes the representation of the delay τ_s . The number of degrees of freedom, $(L_a + 1)(2M_a + 1)$, is determined by the normalized multipath and Doppler spreads, $L_a = \lceil T_m B \rceil$ and $M_a = \lceil T B_d \rceil$ and is proportional to the products $T_m B_d$ and TB . We note that the Doppler components (index m) in (3.3) capture the temporal channel variations encountered *within* a symbol duration. Temporal variations over symbols are captured by the variations in the channel coefficients, $\{H(m, l)\}$, over symbols.

The channel characterization (3.3) defines the canonical multipath-Doppler coordinates. It asserts that the received signal $s(t - \tau_s)$ belongs to an $(L_a + 1)(2M_a + 1)$ -dimensional subspace spanned by the *fixed* basis

$$q_{ml}(t) = q \left(t - \frac{l}{B} \right) e^{j \frac{2\pi m t}{T}}, \quad (3.4)$$

$l = L_s, L_s + 1, \dots, L_s + L_a$, $m = -M_a, \dots, 0, \dots, M_a$, generated by discretely delayed and Doppler-shifted versions of the spread-spectrum signaling waveform $q(t)$ [3, 12]. These basis waveforms define the *active* coordinates, $\Xi_a = \{(l, m) : L_s \leq l \leq L_s + L_a, -M_a \leq m \leq M_a\}$, carrying the signal energy. Each user corresponds to unique active coordinates defined by its spreading waveform $q(t)$ and the channel spread parameters. The front-end processing for representing a received symbol in the

canonical coordinates consists of projection (despreading) onto the basis waveforms of the form (3.4)

$$z_{ml} = \int r(t)q_{ml}^*(t)dt, \\ l = L_1, \dots, L_2, \quad m = -M_1, \dots, 0, \dots, M_2. \quad (3.5)$$

In (3.5), L_1, L_2, M_1 , and M_2 are chosen to always include the *active* coordinates. However, *inactive* coordinates, $\Xi_{ia} = \{(l, m) \notin \Xi_a\}$, corresponding to canonical delays and Doppler shifts *outside* the channel spread, may also be used to aid in MAI suppression. Figure 3.2 illustrates the notion of active/inactive coordinates. Canonical coordinates, taken together for all users and symbols of interest, along with corresponding channel coefficients, constitute sufficient statistics for demodulation—*all signal processing can be performed in the canonical coordinates.*

An important implication of the canonical representation (3.3) is that regardless of the actual physical distribution of multipath delays and Doppler shifts, virtually all information is contained in the uniformly spaced canonical coordinates [3, 12]. The main error in (3.3) is due to the bandlimited approximation and can be made arbitrarily small by sufficient oversampling in multipath, and by including sufficiently many terms in the summation 3.3. In particular, for direct-sequence CDMA, B is inversely related to the chip duration $T_c = T/N$, where N is the spreading gain, and oversampling by a factor \mathcal{O} corresponds to $B = \mathcal{O}/T_c$ in (3.3) and (3.4).

3.3. Receiver Design in the Canonical Coordinates

For simplicity, we illustrate multiuser reception for the case of synchronized user transmissions and BPSK signaling.⁴ The received signal for a single symbol admits the canonical representation

$$r(t) = \sum_{k=1}^K b_k s_k(t) + n(t), \quad (3.6)$$

$$s_k(t) \approx \frac{1}{TB} \sum_{l=0}^{L_{k,a}} \sum_{m=-M_{k,a}}^{M_{k,a}} H_k(m, l) q_{k,ml}(t), \quad (3.7)$$

where b_k denotes the symbol, $\{q_{k,ml}(t)\}$ the canonical multipath-Doppler basis waveforms, and $\{H_k(m, l)\}$ the corresponding canonical channel coefficients of the k^{th} user. The above signal representation provides a natural (dictated by channel dispersion effects) *a priori* partitioning of the signal subspace that can be leveraged for MAI suppression. Centralized receivers represent the subspace in terms of *active* coordinates of all users [13]. Decentralized reception is based on an alternative representation in terms of active (primary) and inactive (secondary) coordinates of the desired user. The focus of this paper is on decentralized reception.

We illustrate the key ideas behind the framework with decentralized MMSE receiver design and begin by assuming the knowledge of the channel coefficients of the desired user. In Section 3.6, we discuss blind channel estimation issues and blind implementations of the proposed receivers. The overall generic receiver structure is shown in Figure 3.1(a). The objective is to choose the primary and secondary filters \mathbf{w}_p and \mathbf{w}_s to yield an MMSE estimate of the bit b_1 of the desired user:

$$\hat{b}_1 = \text{sign} \left\{ \text{Re} \left(\mathbf{w}^H \mathbf{z} \right) \right\} = \text{sign} \left\{ \text{Re} \left(\mathbf{w}_p^H \mathbf{z}_p + \mathbf{w}_s^H \mathbf{z}_s \right) \right\}. \quad (3.8)$$

⁴Asynchronous scenarios can be treated analogously by considering twice as many interfering users and by processing a block of symbols [17]. The essential ideas presented here remain unchanged.

3.3.1. Primary Coordinates: Minimal Complexity Reception

The primary coordinates for user 1 of dimension $D_p = (L_{1,a} + 1)(2M_{1,a} + 1)$ take the form⁵

$$\mathbf{z}_p = b_1 \mathbf{Q}_{11} \mathbf{h}_1 + \sum_{k=2}^K b_k \mathbf{Q}_{1k} \mathbf{h}_k + \mathbf{v}_p = b_1 \mathbf{g}_1 + \mathbf{i}_p + \mathbf{v}_p, \quad (3.9)$$

where \mathbf{Q}_{jk} is the $D_p \times D_p$ matrix of cross-correlations between the *active* basis waveforms $\{q_{j,ml}(t) : (m, l) \in \Xi_{j,a}\}$ and $\{q_{k,ml}(t) : (m, l) \in \Xi_{k,a}\}$ of users j and k , respectively, \mathbf{h}_k denotes the $D_p \times 1$ vector of channel coefficients, $H_k(m, l)$, of the k^{th} user, and \mathbf{v}_p denotes $D_p \times 1$ Gaussian noise vector with correlation matrix $\sigma^2 \mathbf{Q}_{11}$. The powers of different users are absorbed in \mathbf{h}_k 's, a notation that is adopted throughout the thesis. The first term $\mathbf{g}_1 = \mathbf{Q}_{11} \mathbf{h}_1$ in (3.9) constitutes the signal part in \mathbf{z}_p , while the second term \mathbf{i}_p constitutes the MAI component. Note that all the signal energy of the desired user is contained in \mathbf{g}_1 . In the absence of MAI ($\mathbf{i}_p = \mathbf{0}$), only the primary coordinates are needed and the optimal receiver is the generalized RAKE receiver that exploits joint multipath-Doppler diversity via maximal-ratio-combining (MRC): $\mathbf{w}_p^{\text{MRC}} = \mathbf{h}_1$ [3]. In the presence of MAI, the fact that the desired signal belongs to the one-dimensional subspace spanned by \mathbf{g}_1 can be exploited for suppressing \mathbf{i}_p in (3.9). Given \mathbf{g}_1 , the MMSE receiver based only on the primary coordinates is given by

$$\mathbf{w}_p^{\text{MMSE}} = \mathbf{R}_{\mathbf{z}_p, \mathbf{z}_p}^{-1} \mathbf{g}_1 \quad (3.10)$$

$$\mathbf{R}_{\mathbf{z}_p, \mathbf{z}_p} = \mathbf{g}_1 \mathbf{g}_1^H + \sum_{k=2}^K \mathbf{Q}_{1k} \mathbf{E}[\mathbf{h}_k \mathbf{h}_k^H] \mathbf{Q}_{1k}^H + \sigma^2 \mathbf{Q}_{11}. \quad (3.11)$$

Here, $\mathbf{R}_{\mathbf{z}_p, \mathbf{z}_p}$ is the correlation matrix of the primary coordinates. This MMSE receiver works in the low-dimensional primary coordinates to provide *minimal-complexity* MAI suppression while *maximally* exploiting the available (multipath-Doppler) diversity to

⁵For simplicity, we assume the same number of primary coordinates for all users.

combat fading.

3.3.2. Primary and Secondary Coordinates: Enhanced Reception

Secondary (inactive) coordinates \mathbf{z}_s can be progressively incorporated into the receiver, via the lower branch in Figure 3.1(a), to improve its MAI suppression capability. The secondary coordinates take the form

$$\mathbf{z}_s = \sum_{k=2}^K b_k \widetilde{\mathbf{Q}}_{1k} \mathbf{h}_k + \mathbf{v}_s = \mathbf{i}_s + \mathbf{v}_s, \quad (3.12)$$

where $\widetilde{\mathbf{Q}}_{1k}$ is the $D_s \times D_p$ matrix of cross-correlation between D_s *inactive* basis waveforms of user 1 and the D_p *active* basis waveforms of user k . The $D_s \times 1$ Gaussian noise vector \mathbf{v}_s has correlation matrix $\sigma^2 \widetilde{\mathbf{Q}}_s$, where $\widetilde{\mathbf{Q}}_s$ is the matrix of correlations between the secondary basis waveforms of user 1. Note that a particularly attractive feature of the secondary (*inactive*) coordinates \mathbf{z}_s is that they are signal free — they are only correlated with the noise and MAI component of \mathbf{z}_p .⁶

The MMSE receiver operating on both the primary and secondary coordinates solves the following problem

$$\mathbf{w}_o = \arg \min_{\mathbf{w}} \mathbb{E} \left[|b_1 - \mathbf{w}^H \mathbf{z}|^2 \right] \quad (3.13)$$

where $\mathbf{z} = \begin{bmatrix} \mathbf{z}_p \\ \mathbf{z}_s \end{bmatrix}$ and $\mathbf{w} = \begin{bmatrix} \mathbf{w}_p \\ \mathbf{w}_s \end{bmatrix}$. The solution to (3.13) is the Wiener filter and

⁶Note that in (3.12) we are assuming that $\widetilde{\mathbf{Q}}_{11} \approx 0$; that is, the active and inactive basis waveforms are roughly orthogonal. This assumption is based on the autocorrelation properties of spreading codes. However, our approach can be readily extended to account for nonzero correlations as well. In particular, we may use a linearly transformed version of the inactive coordinates that lie in the orthogonal component of the active subspace.

takes the form

$$\begin{aligned} \mathbf{w}_o &= \begin{bmatrix} \mathbf{w}_{o,p} \\ \mathbf{w}_{o,s} \end{bmatrix} = \mathbf{R}_{z,z}^{-1} \bar{\mathbf{g}}_1, \quad \text{where} \\ \mathbf{R}_{z,z} &= \begin{bmatrix} \mathbf{R}_{z_p,z_p} & \mathbf{R}_{z_p,z_s} \\ \mathbf{R}_{z_s,z_p} & \mathbf{R}_{z_s,z_s} \end{bmatrix} \end{aligned} \quad (3.14)$$

where $\bar{\mathbf{g}}_1 = \begin{bmatrix} \mathbf{g}_1 \\ \mathbf{0} \end{bmatrix}$ (since the secondary coordinates are signal-free). The submatrices are given by (3.11) and

$$\mathbf{R}_{z_p,z_s} = \sum_{k=2}^K \mathbf{Q}_{1k} \mathbf{E}[\mathbf{h}_k \mathbf{h}_k^H] \tilde{\mathbf{Q}}_{1k}^H \quad (3.15)$$

$$\mathbf{R}_{z_s,z_s} = \sum_{k=2}^K \tilde{\mathbf{Q}}_{1k} \mathbf{E}[\mathbf{h}_k \mathbf{h}_k^H] \tilde{\mathbf{Q}}_{1k}^H + \sigma^2 \tilde{\mathbf{Q}}_s. \quad (3.16)$$

By using the block matrix inversion formula [27] we can expand $\mathbf{R}_{z,z}^{-1}$ as

$$\mathbf{R}_{z,z}^{-1} = \begin{bmatrix} \mathbf{R}_{e,e}^{-1} & -\mathbf{R}_{e,e}^{-1} \mathbf{C}^H \\ -\mathbf{C} \mathbf{R}_{e,e}^{-1} & (\mathbf{R}_{z_s,z_s} - \mathbf{R}_{z_s,z_p} \mathbf{R}_{z_p,z_p}^{-1} \mathbf{R}_{z_p,z_s})^{-1} \end{bmatrix}, \quad (3.17)$$

where

$$\mathbf{C} = \mathbf{R}_{z_s,z_s}^{-1} \mathbf{R}_{z_s,z_p}, \quad \mathbf{e} = \mathbf{z}_p - \mathbf{C}^H \mathbf{z}_s, \quad (3.18)$$

$$\mathbf{R}_{e,e} = \mathbf{R}_{z_p,z_p} - \mathbf{R}_{z_p,z_s} \mathbf{R}_{z_s,z_s}^{-1} \mathbf{R}_{z_s,z_p}. \quad (3.19)$$

Using (3.16) and (3.17) we can explicitly characterize $\mathbf{w}_{o,p}$ and $\mathbf{w}_{o,s}$ as

$$\mathbf{w}_{o,p} = \mathbf{R}_{e,e}^{-1} \mathbf{g}_1, \quad (3.20)$$

$$\mathbf{w}_{o,s} = -\mathbf{C} \mathbf{w}_{o,p} = -\mathbf{C} \mathbf{R}_{e,e}^{-1} \mathbf{g}_1. \quad (3.21)$$

The solution for the primary and secondary filters in (3.20) and (3.21) has an intuitively appealing interpretation as illustrated in Figure 3.1(b). Conditioned on a fixed

value of the $\mathbf{g}_1 = \mathbf{Q}_{11}\mathbf{h}_1$, the matrix \mathbf{C} is the linear MMSE estimator of \mathbf{z}_p from \mathbf{z}_s ($\hat{\mathbf{z}}_p = \mathbf{C}^H\mathbf{z}_s$) and $\mathbf{R}_{\mathbf{e},\mathbf{e}}$ is the covariance matrix of the corresponding estimation error \mathbf{e} . Thus, the filter \mathbf{C} optimally exploits the secondary coordinates \mathbf{z}_s to suppress MAI in \mathbf{z}_p (since \mathbf{z}_s is uncorrelated with the signal component \mathbf{g}_1 in \mathbf{z}_p). The filter $\mathbf{w}_{o,p}$ then optimally suppresses the MAI remaining in the residual error \mathbf{e} by forming an MMSE estimate of \hat{b}_1 from \mathbf{e} (compare with the solution in (3.11) based on the primary coordinates only). The number of secondary coordinates D_s can vary between zero (only primary coordinates) and $N_o - D_p$ (covering the entire signal space). As we will see, depending on the number of dominant interfering users, near-optimal performance can be achieved with significantly low-dimensional ($D_p + D_s \ll N$) processing.

We note that most of the decentralized receivers proposed in the literature are based on chip-rate sampled processing. The received signal is sampled every chip duration and the resultant N -dimensional vector is processed by an N -tap filter which may be chosen based on the MMSE criterion. In practice, the N -tap MMSE receiver has to be implemented adaptively. For large N , there are too many degrees of freedom to allow reliable estimation and tracking of the MMSE filter taps. Thus, it is necessary to develop MMSE detectors with fewer number of taps (degrees of freedom). *Ad hoc* lower dimensional representations for the filter are often considered (see, for example, [28]). Other approaches based on subspace tracking was presented in [29, 23]. In our framework, the natural signal space partitioning in terms of active/inactive coordinates provides a systematic approach to controlling receiver complexity. The detector operates in an $N_{tot} = D_s + D_p \leq N$ dimensional subspace. The complexity of the receiver can be progressively increased, by increasing D_s , to achieve a desired level of performance.

We also note that the proposed receiver only requires knowledge of $\mathbf{g}_1 = \mathbf{Q}_{11}\mathbf{h}_1$ and $\mathbf{R}_{z,z}$. \mathbf{Q}_{11} only depends on the spreading code of the desired user and $\mathbf{R}_{z,z}$ can be readily estimated from data. This solution assumes the knowledge of \mathbf{h}_1 of the desired user. In Section 3.6.2, we will see that the structure of \mathbf{e} can be exploited for blindly estimating \mathbf{h}_1 .

3.4. Performance Analysis

In this section, we assess the performance of the proposed MMSE receiver structure under varying conditions. Let T_{obs} be the time scale over which the performance of the receiver is assessed. Our analysis is based on two distinct time scales depending on how T_{obs} compares $T_{coh,d}$, the coherence time of the channel seen by the *desired* user. Essentially, $T_{coh,d}$ is the time duration over which the channel coefficients \mathbf{h}_1 (and hence \mathbf{g}_1) remain approximately constant. The coherence time is roughly equal to the reciprocal of the channel Doppler spread ($1/B_d$) [1]. For $T_{obs} < T_{coh,d}$, the desired user's signal exhibits a fixed direction determined by \mathbf{g}_1 and the channel is effectively equivalent to an AWGN channel. Thus, the probability of error (P_e) is governed by the instantaneous signal-to-interference-to-noise ratio $\text{SINR}(\mathbf{g}_1)$ [30].⁷ Over time scales significantly longer than $T_{coh,d}$, i.e. $T_{obs} \gg T_{coh,d}$, the desired user's signal can exhibit up to $D_p = (L_{1,a} + 1)(2M_{1,a} + 1)$ degrees of freedom and the average P_e is computed by averaging $\text{SINR}(\mathbf{g}_1)$ over the statistics of \mathbf{g}_1 . We analyze the receiver over both time scales and also investigate measures of near-far resistance [17] that are appropriate in the two scenarios.

⁷Note that SINR is really a function of all \mathbf{h}_k 's. However, for sufficiently effective MAI suppression, the residual MAI can be lumped to Gaussian noise [30].

Another factor that affects system performance is the degrees of freedom exhibited by the interference. This depends on how T_{obs} compares to the coherence time of the interference, $T_{coh,i}$.⁸ If $T_{obs} < T_{coh,i}$, the MAI exhibits up to $N_i = (K - 1)$ degrees of freedom in the full dimensional space since each interfering user exhibits a fixed direction within its active subspace ($E[\mathbf{h}_k \mathbf{h}_k^H] \approx \mathbf{h}_k \mathbf{h}_k^H$ in (3.11), (3.15) and (3.16)). On the other hand, if $T_{obs} \gg T_{coh,i}$, the MAI can exhibit up to $N_i = (K - 1)D_p$ degrees of freedom, since each interfering user can exhibit up to D_p directions in its active subspace due to the time-variations in the channel coefficients.⁹ Clearly, in the detector subspace, spanned by the active and inactive basis vectors, the MAI cannot exhibit more than $N_{tot} = D_p + D_s$ degrees of freedom. However, unless $N_{tot} \geq N_i + 1$, the receiver will not be near-far resistant. As long as $N_i + 1 < N$, we can choose D_s to ensure $N_{tot} \geq N_i + 1$. Our analysis will clearly show the dependence of performance on N_i and N_{tot} .

To facilitate analysis, we first derive alternate expressions for the optimum solution. Let $\mathbf{y} = \mathbf{z} - \bar{\mathbf{g}}_1 = \mathbf{i} + \mathbf{v}$ denote the signal-free component of the canonical coordinates

$$\mathbf{y} = \begin{bmatrix} \mathbf{y}_p \\ \mathbf{y}_s \end{bmatrix} = \begin{bmatrix} \mathbf{z}_p \\ \mathbf{z}_s \end{bmatrix} - \begin{bmatrix} \mathbf{g}_1 \\ \mathbf{0} \end{bmatrix} = \begin{bmatrix} \mathbf{i}_p \\ \mathbf{i}_s \end{bmatrix} + \begin{bmatrix} \mathbf{v}_p \\ \mathbf{v}_s \end{bmatrix}. \quad (3.22)$$

The correlation matrix of \mathbf{y} is of the form

$$\begin{aligned} \mathbf{R}_{\mathbf{y},\mathbf{y}} &= \mathbf{R}_{\mathbf{z},\mathbf{z}} - \bar{\mathbf{g}}_1 \bar{\mathbf{g}}_1^H = \mathbf{R}_{\mathbf{i},\mathbf{i}} + \mathbf{R}_{\mathbf{v},\mathbf{v}} \\ &= \begin{bmatrix} \mathbf{R}_{\mathbf{i}_p,\mathbf{i}_p} & \mathbf{R}_{\mathbf{i}_p,\mathbf{i}_s} \\ \mathbf{R}_{\mathbf{i}_s,\mathbf{i}_p} & \mathbf{R}_{\mathbf{i}_s,\mathbf{i}_s} \end{bmatrix} + \sigma^2 \begin{bmatrix} \mathbf{Q}_{11} & \mathbf{0} \\ \mathbf{0} & \tilde{\mathbf{Q}}_s \end{bmatrix}. \end{aligned} \quad (3.23)$$

⁸For simplicity, we assume that all interfering users experience the same coherence time, $T_{coh,i}$ (which may be different from $T_{coh,d}$).

⁹Note that $\text{rank}(E[\mathbf{h}_k \mathbf{h}_k^H]) \leq D_p$.

Without loss of generality assume that $\mathbf{R}_{\mathbf{v},\mathbf{v}} = \sigma^2\mathbf{I}$; that is $\mathbf{Q}_{11} = \mathbf{I}$ and $\tilde{\mathbf{Q}}_s = \mathbf{I}$.¹⁰ Let

$$\begin{aligned} \mathbf{R}_{\mathbf{i},\mathbf{i}} &= \begin{bmatrix} \mathbf{V}_I & \mathbf{V}_\perp \end{bmatrix} \begin{bmatrix} \mathbf{\Lambda} & \mathbf{0} \\ \mathbf{0} & \mathbf{0} \end{bmatrix} \begin{bmatrix} \mathbf{V}_I^H \\ \mathbf{V}_\perp^H \end{bmatrix} \\ &= \begin{bmatrix} \mathbf{V}_{I,p} & \mathbf{V}_{\perp,p} \\ \mathbf{V}_{I,s} & \mathbf{V}_{\perp,s} \end{bmatrix} \begin{bmatrix} \mathbf{\Lambda} & \mathbf{0} \\ \mathbf{0} & \mathbf{0} \end{bmatrix} \begin{bmatrix} \mathbf{V}_{I,p}^H & \mathbf{V}_{I,s}^H \\ \mathbf{V}_{\perp,p}^H & \mathbf{V}_{\perp,s}^H \end{bmatrix} \end{aligned} \quad (3.24)$$

be the eigendecomposition of $\mathbf{R}_{\mathbf{i},\mathbf{i}}$, where \mathbf{V}_I contains the eigenvectors corresponding to nonzero eigenvalues ($\mathbf{\Lambda}$ is the diagonal matrix of nonzero eigenvalues) and \mathbf{V}_\perp contains the eigenvectors corresponding to the zero eigenvalues. The second equality further partitions \mathbf{V}_I and \mathbf{V}_\perp into primary and secondary coordinates. Let $\mathcal{S}_I = \text{span}(\mathbf{V}_I)$ denote the interference subspace and $\mathcal{S}_\perp = \text{span}(\mathbf{V}_\perp)$ denote the orthogonal complement of \mathcal{S}_I . Note that $\dim(\mathcal{S}_I) = \min(N_i, N_{tot})$ and $\dim(\mathcal{S}_\perp) = N_{tot} - \dim(\mathcal{S}_I)$. $\mathbf{R}_{\mathbf{y},\mathbf{y}}$ admits the eigendecomposition

$$\mathbf{R}_{\mathbf{y},\mathbf{y}} = \mathbf{V}_I \tilde{\mathbf{\Lambda}} \mathbf{V}_I^H + \sigma^2 \mathbf{V}_\perp \mathbf{V}_\perp^H \quad (3.25)$$

where $\tilde{\mathbf{\Lambda}} = \mathbf{\Lambda} + \sigma^2\mathbf{I}$. Using the block inversion formula (3.17) and (3.25) we get

$$\begin{aligned} \mathbf{R}_{\mathbf{y},\mathbf{y}}^{-1} &= \begin{bmatrix} \mathbf{R}_{\epsilon,\epsilon}^{-1} & -\mathbf{R}_{\epsilon,\epsilon}^{-1}\mathbf{C}^H \\ -\mathbf{C}\mathbf{R}_{\epsilon,\epsilon}^{-1} & (\mathbf{R}_{\mathbf{y}_s,\mathbf{y}_s} - \mathbf{R}_{\mathbf{y}_s,\mathbf{y}_p}\mathbf{R}_{\mathbf{y}_p,\mathbf{y}_p}^{-1}\mathbf{R}_{\mathbf{y}_p,\mathbf{y}_s})^{-1} \end{bmatrix} \\ &= \mathbf{V}_I \tilde{\mathbf{\Lambda}}^{-1} \mathbf{V}_I^H + \frac{1}{\sigma^2} \mathbf{V}_\perp \mathbf{V}_\perp^H \\ &= \begin{bmatrix} \mathbf{V}_{I,p} \tilde{\mathbf{\Lambda}}^{-1} \mathbf{V}_{I,p}^H & \mathbf{V}_{I,p} \tilde{\mathbf{\Lambda}}^{-1} \mathbf{V}_{I,s}^H \\ \mathbf{V}_{I,s} \tilde{\mathbf{\Lambda}}^{-1} \mathbf{V}_{I,p}^H & \mathbf{V}_{I,s} \tilde{\mathbf{\Lambda}}^{-1} \mathbf{V}_{I,s}^H \end{bmatrix} + \frac{1}{\sigma^2} \begin{bmatrix} \mathbf{V}_{\perp,p} \mathbf{V}_{\perp,p}^H & \mathbf{V}_{\perp,p} \mathbf{V}_{\perp,s}^H \\ \mathbf{V}_{\perp,s} \mathbf{V}_{\perp,p}^H & \mathbf{V}_{\perp,s} \mathbf{V}_{\perp,s}^H \end{bmatrix} \end{aligned} \quad (3.27)$$

where $\epsilon = \mathbf{e} - \mathbf{g}_1$ denotes the signal-free component of the residual estimation error \mathbf{e} ($\mathbf{R}_{\epsilon,\epsilon} = \mathbf{R}_{\mathbf{e},\mathbf{e}} - \mathbf{g}_1 \mathbf{g}_1^H$). Based on the preceding development, the optimum filter

¹⁰Otherwise, we can always prewhiten the canonical coordinates: $\mathbf{z} \rightarrow \mathbf{R}_{\mathbf{v},\mathbf{v}}^{-1/2} \mathbf{z}$, since \mathbf{Q}_{11} and $\tilde{\mathbf{Q}}_s$ are known at the receiver.

solution admits the following representations

$$\mathbf{w}_o = \mathbf{R}_{z,z}^{-1} \bar{\mathbf{g}}_1 = \frac{\mathbf{R}_{y,y}^{-1} \bar{\mathbf{g}}_1}{1 + \bar{\mathbf{g}}_1^H \mathbf{R}_{y,y}^{-1} \bar{\mathbf{g}}_1} \quad (3.28)$$

$$= \begin{bmatrix} \mathbf{w}_{o,p} \\ \mathbf{w}_{o,s} \end{bmatrix} = \frac{1}{1 + \mathbf{g}_1^H \mathbf{R}_{\epsilon,\epsilon}^{-1} \mathbf{g}_1} \begin{bmatrix} \mathbf{R}_{\epsilon,\epsilon}^{-1} \mathbf{g}_1 \\ -\mathbf{C} \mathbf{R}_{\epsilon,\epsilon}^{-1} \mathbf{g}_1 \end{bmatrix} \quad (3.29)$$

$$= \frac{1}{\sigma^2 + \mathbf{g}_1^H (\sigma^2 \mathbf{V}_{I,p} \tilde{\mathbf{\Lambda}}^{-1} \mathbf{V}_{I,p}^H + \mathbf{V}_{\perp,p} \mathbf{V}_{\perp,p}^H) \mathbf{g}_1} \begin{bmatrix} (\sigma^2 \mathbf{V}_{I,p} \tilde{\mathbf{\Lambda}}^{-1} \mathbf{V}_{I,p}^H + \mathbf{V}_{\perp,p} \mathbf{V}_{\perp,p}^H) \mathbf{g}_1 \\ (\sigma^2 \mathbf{V}_{I,s} \tilde{\mathbf{\Lambda}}^{-1} \mathbf{V}_{I,s}^H + \mathbf{V}_{\perp,s} \mathbf{V}_{\perp,s}^H) \mathbf{g}_1 \end{bmatrix} \quad (3.30)$$

where the first equality follows from (3.23) and the matrix inversion lemma [31], the second one from (3.26) and the last one from (3.27). Finally, we note that $\bar{\mathbf{g}}$ admits the following unique orthogonal decomposition

$$\begin{aligned} \bar{\mathbf{g}} &= \bar{\mathbf{g}}_I + \bar{\mathbf{g}}_{\perp}, \quad \text{where} \\ \bar{\mathbf{g}}_I &= \mathbf{V}_I \mathbf{V}_I^H \bar{\mathbf{g}} = \begin{bmatrix} \mathbf{V}_{I,p} \\ \mathbf{V}_{I,s} \end{bmatrix} \mathbf{V}_{I,p}^H \mathbf{g}_1 \quad \text{and} \\ \bar{\mathbf{g}}_{\perp} &= \mathbf{V}_{\perp} \mathbf{V}_{\perp}^H \bar{\mathbf{g}} = \begin{bmatrix} \mathbf{V}_{\perp,p} \\ \mathbf{V}_{\perp,s} \end{bmatrix} \mathbf{V}_{\perp,p}^H \mathbf{g}_1. \end{aligned} \quad (3.31)$$

In particular, \mathbf{g}_1 admits the following (nonorthogonal) decomposition

$$\mathbf{g}_1 = \mathbf{g}_{1,I} + \mathbf{g}_{1,\perp} = \mathbf{V}_{I,p} \mathbf{V}_{I,p}^H \mathbf{g}_1 + \mathbf{V}_{\perp,p} \mathbf{V}_{\perp,p}^H \mathbf{g}_1. \quad (3.32)$$

3.4.1. Limiting Solution at High SNR

From (3.30) and (3.32) it follows that

$$\lim_{\sigma^2 \rightarrow 0} \mathbf{w}_o = \lim_{\sigma^2 \rightarrow 0} \begin{bmatrix} \mathbf{w}_{o,p} \\ \mathbf{w}_{o,s} \end{bmatrix}$$

$$\begin{aligned}
&= \frac{1}{\mathbf{g}_1^H \mathbf{V}_{\perp,p} \mathbf{V}_{\perp,p}^H \mathbf{g}_1} \begin{bmatrix} \mathbf{V}_{\perp,p} \mathbf{V}_{\perp,p}^H \mathbf{g}_1 \\ \mathbf{V}_{\perp,s} \mathbf{V}_{\perp,p}^H \mathbf{g}_1 \end{bmatrix} \\
&= \frac{\bar{\mathbf{g}}_{\perp}}{\|\bar{\mathbf{g}}_{\perp}\|^2}. \tag{3.33}
\end{aligned}$$

Recall that \mathcal{S}_{\perp} is non-empty as long as $N_{tot} \geq N_i + 1$ (the total number of coordinates is greater than or equal to the dimension of the signal-plus-interference subspace). It follows from (3.33) that in the limit of high SNR ($\sigma^2 \rightarrow 0$), as long as $N_{tot} \geq N_i + 1$ the optimum filter solution converges to a unit vector in the direction of $\bar{\mathbf{g}}_{\perp} \in \mathcal{S}_{\perp}$.¹¹ That is, MAI is *completely* suppressed in the output of the MMSE receiver in the limit of high SNR if $N_{tot} \geq N_i + 1$. Thus, in the limit of high SNR, MAI with up to $N_i = D_p - 1$ degrees of freedom can be suppressed with only the primary coordinates. This means that in a sufficiently underloaded system, the primary coordinates (the upper branch in Figure 3.1(a)) are adequate for required MAI suppression. On the other hand, the augmented receiver based on both primary and secondary coordinates is capable of suppressing MAI with up to $N_i = D_p + D_s - 1$ dominant degrees of freedom. Thus, by progressively adding more secondary coordinates, we can suppress a larger number of interfering users.

3.4.2. Probability of Error

As mentioned earlier, if $T_{obs} < T_{coh,d}$, receiver performance is fairly accurately characterized by the SINR. The SINR is defined as the ratio of the desired signal power to the interference and noise power at the output of the receiver and in our formulation it takes the form $\text{SINR}(\mathbf{g}_1) = \frac{|\mathbf{w}_{o,p}^H \mathbf{g}_1|^2}{\mathbb{E}[|\mathbf{w}_o^H \mathbf{z}|^2] - |\mathbf{w}_{o,p}^H \mathbf{g}_1|^2}$. Using the various forms of the solution

¹¹This result parallels a similar result in [28] for the AWGN channel.

in (3.28)-(3.30) the SINR can be expressed as

$$\text{SINR}(\mathbf{g}_1) = \frac{\bar{\mathbf{g}}^H \mathbf{R}_{zz}^{-1} \bar{\mathbf{g}}}{1 - \bar{\mathbf{g}}^H \mathbf{R}_{zz}^{-1} \bar{\mathbf{g}}} = \frac{\mathbf{g}_1^H \mathbf{R}_{ee}^{-1} \mathbf{g}_1}{1 - \mathbf{g}_1^H \mathbf{R}_{ee}^{-1} \mathbf{g}_1} \quad (3.34)$$

$$= \bar{\mathbf{g}}^H \mathbf{R}_{yy}^{-1} \bar{\mathbf{g}} = \mathbf{g}_1^H \mathbf{R}_{ee}^{-1} \mathbf{g}_1 \quad (3.35)$$

$$= \mathbf{g}_1^H \left(\mathbf{V}_{L,p} \tilde{\Lambda}^{-1} \mathbf{V}_{L,p}^H + \frac{1}{\sigma^2} \mathbf{V}_{\perp,p} \mathbf{V}_{\perp,p}^H \right) \mathbf{g}_1. \quad (3.36)$$

Note that SINR depends on the particular value of \mathbf{g}_1 . Drawing on the discussion in [30], we argue that for sufficiently large $N_{tot} = D_p + D_s$, P_e is fairly accurately given by

$$P_e(\mathbf{g}_1) = Q\left(\sqrt{2\text{SINR}(\mathbf{g}_1)}\right), \quad (3.37)$$

over short time scales, where $Q(x) = \int_x^\infty \frac{1}{\sqrt{2\pi}} e^{-\frac{x^2}{2}} dx$. We note that the SINR is a nondecreasing function of the total number of coordinates. As we saw in Section 3.4.1, in the limit of high SNR only $N_{tot} = N_i + 1$ coordinates are necessary for suppressing N_i interferers. As we see in Section 3.5, the SINR shows relatively small improvement as N_{tot} is increased beyond $N_i + 1$ by increasing D_s (see Figure 3.3 and Figure 3.4).

To compute the P_e over time scales much longer than $T_{coh,d}$ (i.e. $T_{obs} \gg T_{coh,d}$), we need to average the conditional expression in (3.37) over the distribution of \mathbf{g}_1 .¹²

Since \mathbf{g}_1 is modeled as Gaussian, the SINR expression in (3.35) can be alternatively expressed as $\text{SINR}(\mathbf{g}_1) = \sum_{l=1}^{D_p} \mu_l \gamma_l$ where μ_l , $l = 1, 2, \dots, D_p$ are the eigenvalues of $\mathbf{R}_{ee}^{-1} \mathbf{R}_{\mathbf{g}_1, \mathbf{g}_1}$, $\mathbf{R}_{\mathbf{g}_1, \mathbf{g}_1} = \mathbf{Q}_{11} \mathbf{E}[\mathbf{h}_1 \mathbf{h}_1^H] \mathbf{Q}_{11}^H$, and γ_l , $l = 1, 2, \dots, D_p$ are independent χ^2 random variables with two degrees of freedom and $\mathbf{E}[|\gamma_l|^2] = 1$. Assuming distinct eigenvalues $\{\mu_l\}$, the P_e can be computed as [1]

$$P_e = \mathbf{E}[P_e(\mathbf{g}_1)] = \sum_{l=1}^{D_p} \frac{\pi_l}{2} \left[1 - \sqrt{\frac{\mu_l}{1 + \mu_l}} \right], \quad \text{where}$$

¹²Strictly speaking, we need to average over the distributions of all \mathbf{h}_k 's. However, along the lines of [30], we are treating the MAI collectively as Gaussian noise. Figure 3.6 supports this approximation.

$$\pi_l = \prod_{i=1, i \neq l}^{D_p} \frac{\mu_l}{\mu_l - \mu_i}. \quad (3.38)$$

3.4.3. Near-Far Resistance

Over time scales within $T_{coh,d}$, the proposed multiuser MMSE receivers are “near-far resistant” in the sense that the $\text{SINR}(\mathbf{g}_1) > 0$ even in the limit of infinite interference power as long as $\bar{\mathbf{g}}_\perp \neq \mathbf{0}$, as evident from (3.30) and (3.36)

$$\begin{aligned} \lim_{\Lambda_{jj} \rightarrow \infty} \mathbf{w}_o &= \frac{\bar{\mathbf{g}}_\perp}{\sigma^2 + \|\bar{\mathbf{g}}_\perp\|^2} \quad \text{and} \\ \lim_{\Lambda_{jj} \rightarrow \infty} \text{SINR}(\mathbf{g}_1) &= \frac{\|\bar{\mathbf{g}}_\perp\|^2}{\sigma^2} \quad (N_{tot} \geq N_i + 1), \end{aligned} \quad (3.39)$$

where Λ_{jj} denote the nonzero eigenvalues of \mathbf{R}_{ii} in (3.24). We note that in the limit of strong interference (similar to $\sigma^2 \rightarrow 0$) the optimal filter aligns itself orthogonal to the interference subspace and thus completely suppress the MAI.

We also investigate the notion of near-far resistance defined in [17, 32] based on the asymptotic relative efficiency (ARE) of the receiver. The ARE of the multiuser receiver compares its asymptotic performance (as $\sigma^2 \rightarrow 0$) in the presence of MAI relative to its performance in the absence of MAI. For time-scales within $T_{coh,d}$, the ARE is defined as

$$\nu(\mathbf{g}_1) = \sup \left\{ 0 \leq r \leq 1 : \lim_{\sigma^2 \rightarrow 0} \frac{P_e(\mathbf{g}_1, \sigma)}{Q\left(\sqrt{\frac{2r\|\mathbf{g}_1\|^2}{\sigma^2}}\right)} = 0 \right\} \quad (3.40)$$

where $P_e(\mathbf{g}_1, \sigma)$ is the error probability of the receiver in the presence of MAI as a function of σ (implicit in (3.37)), and $Q\left(\sqrt{\frac{2r\|\mathbf{g}_1\|^2}{\sigma^2}}\right)$ captures the P_e of the corresponding single-user MRC receiver. The near-far resistance is defined as [17, 32] $\eta(\mathbf{g}_1) = \inf_{\Lambda_{jj}} \nu(\mathbf{g}_1)$. From (3.36) and (3.37) we note that as $\sigma^2 \rightarrow 0$, $P_e(\mathbf{g}_1, \sigma) \approx Q\left(\sqrt{\frac{2\|\bar{\mathbf{g}}_\perp\|^2}{\sigma^2}}\right)$ from which it follows that $\nu(\mathbf{g}_1) = \frac{\|\bar{\mathbf{g}}_\perp\|^2}{\|\mathbf{g}_1\|^2}$. Since $\nu(\mathbf{g}_1)$ is independent of the interference

power, it follows that¹³

$$\eta(\mathbf{g}_1) = \nu(\mathbf{g}_1) = \frac{\|\bar{\mathbf{g}}_\perp\|^2}{\|\mathbf{g}_1\|^2} = \frac{\|\bar{\mathbf{g}}_\perp\|^2}{\|\bar{\mathbf{g}}\|^2}. \quad (3.41)$$

It is clear that $\eta(\mathbf{g}_1) = 1$ if $\bar{\mathbf{g}}$ is orthogonal to the MAI subspace \mathcal{S}_I and $\eta(\mathbf{g}_1) = 0$ if $\bar{\mathbf{g}} \in \mathcal{S}_I$. In general, as long as $N_{tot} \geq N_i + 1$ and $\bar{\mathbf{g}}_\perp \neq \mathbf{0}$, the system is near-far resistant.

As evident from (3.40), near-far resistance is also a measure of the transmitted power required in a single user receiver, relative to that in a multiuser receiver, to achieve identical performance. The value of $0 \leq \eta(\mathbf{g}_1) \leq 1$ reflects the relative loss of efficiency in a multiuser receiver in terms of the transmitted power at high SNRs. We now investigate the relative powers required in single-user and multiuser systems over time-scales much longer than $T_{coh,d}$. For this comparison, the P_e of the single-user receiver is given by averaging $Q\left(\sqrt{\frac{2\|\mathbf{g}_1\|^2}{\sigma^2}}\right)$ over the distribution of \mathbf{g}_1 . Following the discussion in Section 3.4.2, the P_e is governed by the eigenvalues of $\mathbf{R}_{\mathbf{g}_1, \mathbf{g}_1}$, say $\{\mu_{su,l} : l = 1, 2, \dots, D_p\}$, and is given by (3.38) with $\mu_l = \mu_{su,l}/\sigma^2$. Similarly, recall that the P_e of the multiuser receiver is governed by the eigenvalues of $\mathbf{R}_{\epsilon\epsilon}^{-1}\mathbf{R}_{\mathbf{g}_1, \mathbf{g}_1}$. From (3.36) we note that as $\sigma^2 \rightarrow 0$, $\sigma^2\mathbf{R}_{\epsilon\epsilon}^{-1} \approx \mathbf{P}_{\perp,p} = \mathbf{V}_{\perp,p}\mathbf{V}_{\perp,p}^H$. Thus, in the limit of high SNR the P_e of the multiuser receiver is governed by the eigenvalues of $\mathbf{P}_{\perp,p}\mathbf{R}_{\mathbf{g}_1, \mathbf{g}_1}$, say $\{\mu_{mu,l}\}$, and is given by (3.38) with $\mu_l = \mu_{mu,l}/\sigma^2$. Furthermore, for high SNR ($\mu \gg 1$) the expression for P_e in (3.38) can be simplified as [1] $P_e \approx \binom{2D_p - 1}{D_p} \prod_{l=1}^{D_p} \frac{1}{4\mu_l}$. Let r denote the transmitted power of the single user receiver relative to the multiuser

¹³Parallel to a similar result in [28] for AWGN channels.

receiver. It follows from the above approximate expression for P_e that

$$\frac{P_e(\text{multiuser})}{P_e(\text{single-user})} \approx r^{D_p} \prod_{l=1}^{D_p} \frac{\mu_{su,l}}{\mu_{mu,l}}. \quad (3.42)$$

Thus, for identical P_e in the two systems as $\sigma^2 \rightarrow 0$, the relative power of the single-user (MRC) receiver should be $r = \left[\prod_{l=1}^{D_p} \frac{\mu_{mu,l}}{\mu_{su,l}} \right]^{1/D_p}$. We note that typically $r \leq 1$ since the eigenvalues of $\mathbf{P}_{\perp,p} \mathbf{R}_{g_1, g_1}$ (multiuser) are typically smaller than the eigenvalues of \mathbf{R}_{g_1, g_1} (single-user) since $\mathbf{P}_{\perp,p}$ maps to a lower-dimensional space. Moreover, as D_p increases $r \rightarrow 1$. Thus, for a sufficiently large dimension of the primary subspace, and under sufficiently high SNR, we expect the P_e of the multiuser receiver to be very close to that of a single-user MRC receiver operating in the absence of MAI. This trend is exhibited in Figure 3.6 (discussed in Section 3.5).

3.4.4. Choice of Secondary Coordinates

There are two key issues in this context: the *number* D_s of secondary coordinates and the *choice* of the D_s coordinates from amongst all the inactive coordinates possible. The choice of D_s is primarily guided by the dimensional analysis in Section 3.4.1 on performance analysis. The main conclusion is that at high SNR, we need $D_s \approx N_i + 1 - D_p$ to adequately suppress MAI with N_i degrees of freedom. As the noise level increases, increasing D_s would in general improve performance, however, beyond a certain point we expect to see diminishing returns, as we will see in the next section. For any given D_s coordinates, the MMSE receiver is given by $\mathbf{w}_o = \mathbf{R}_{z,z}^{-1} \bar{\mathbf{g}}$ which we have seen in several forms.

Given D_s , the choice of the “best” D_s inactive coordinates is in general a difficult one: it depends on the correlation structure of primary and secondary coordinates and it

involves $\binom{N_o - D_p}{D_s}$ possibilities. One brute force approach is to choose the set of D_s coordinates that minimizes the trace of the resulting error covariance matrix $\mathbf{R}_{e,e}$ in estimating \mathbf{z}_p from \mathbf{z}_s . While a thorough discussion of this issue is beyond the scope of this paper, we note that the difference in performance between different choices may not be very significant as illustrated in Figure 3.8 discussed in the next section.

3.5. Illustrative Examples

We now illustrate various features of the framework with numerical examples. We consider a system that employs Gold codes for all users with a spreading gain of $N = 63$. The system supports $K = 4$ users in a relatively slow fading environment. A wide-sense stationary uncorrelated scattering (WSSUS) channel is simulated via the model (3.3) using 16 uniformly spaced paths per chip duration with independent, equal-power fading coefficients ($E[\mathbf{h}_k \mathbf{h}_k^H] = P_k \mathbf{I}$, where P_k is the power of the k^{th} user). All users experience a multipath spread of $T_m = 2T_c$ and negligible Doppler effects within a symbol duration ($TB_d \approx 0$; $M = 0$). An active basis corresponding to four-fold oversampling ($B = 4/T_c$ in (3.4)) is employed for the front-end processing at the receiver (see (3.5)). This corresponds to $D_p = 9$ active coordinates for each user. The background noise is such that the SNR of the desired user ($E[2\|\mathbf{g}_1\|^2/\sigma^2]$) is 20dB unless otherwise noted. All results correspond to BPSK signaling and channel coefficients of the desired user are assumed known at the receiver.

Figure 3.3 illustrates the improvement in SINR as a function of D_s . We consider the case where $T_{obs} \gg T_{coh,i}$ but $T_{obs} < T_{coh,d}$. Thus, $N_i = (K - 1)D_p$ whereas the desired user exhibits a fixed direction over T_{obs} . This artificial difference between the

coherence times of the desired and interfering users is used for illustrative purposes to simulate a system with a large number of interference degrees of freedom. The SINR is plotted as a function of the relative power, P , of each interfering user.¹⁴ Figure 3.3(a) corresponds to $K - 1 = 1$ resulting in $N_i = D_p = 9$ MAI degrees of freedom. Figure 3.3(b) corresponds to $K - 1 = 3$ resulting in $N_i = 27$.¹⁵ Note the performance of the MMSE receiver with $D_s = 0$ is significantly better than that of the MRC receiver. Furthermore, the performance of the MMSE receiver increases significantly as D_s is increased until $N_{tot} = D_p + D_s$ approaches $N_i + 1$, beyond which the performance saturates.

Figure 3.4 illustrates the variation in SINR as a function of the SNR of desired user for different D_s . There are 3 interfering users with the same power as the desired user. Figure 3.4(a) depicts the case where $T_{obs} < T_{coh,i}$ resulting in $N_i = 3$, whereas Figure 3.4(b) corresponds to the $T_{obs} \gg T_{coh,i}$ case resulting in $N_i = 27$. The figure clearly shows two regimes depending on D_s : MAI-limited regime when $D_s + D_p < N_i + 1$, and noise-limited regime when $D_s + D_p \geq N_i + 1$. While the SINR saturates in the MAI-limited regime, it increases linearly with SNR in the noise-limited regime. For fixed value of N_i , the system moves from an MAI-limited regime to a noise-limited one as D_s is increased. For example, in Figure 3.4(b), $N_i = 27$ and the system is MAI-limited for $D_s < 28 - 9 = 19$ as evident from the curves for $D_s = 0, 4$. For $D_s \geq 19$, it is noise-limited as evident from the curves for $D_s = 20, 30$.

Figure 3.5 shows the analytically computed P_e (via (3.38)) as a function of the relative power of each interfering user for different values of D_s . In this case, there are $K - 1 =$

¹⁴We assume the same relative power, P , for each interfering user: $E[\mathbf{h}_1 \mathbf{h}_1^H] = \mathbf{I}$ and $E[\mathbf{h}_k \mathbf{h}_k^H] = P\mathbf{I}$.

¹⁵The two scenarios may be interpreted as representing 9 versus 27 interfering users when $T_{obs} < T_{coh,i}$.

3 interfering users with $T_{obs} \gg T_{coh,i}$ resulting in $N_i = 27$. The improvement in performance with increasing D_s is evident. Figure 3.6 explores the validity of the P_e expression in (3.38) for a variety of scenarios. Analytical computation of P_e in (3.38) is compared with Monte-Carlo averaging of the conditional P_e expression in (3.37) over 2000 channel realizations of all 4 users. Figures 3.6(a) and 3.6(b) show the comparison for $D_s = 1$ and $D_s = 20$ in the case when all users have equal power. Figures 3.6(c)-3.6(f) show the comparison between $D_s = 1$ and $D_s = 40$ for higher interference powers. Figures 3.6(c) and 3.6(d) show the comparison for the case when the interfering users are 3 times stronger, and Figures 3.6(e) and 3.6(f) depict the case when the interfering users are 10 times stronger. Consistent with the conclusions drawn in [30], the approximation in (3.38) is fairly good and is more accurate when effective MAI in the output of the receiver is relatively small (which is true for large D_s). We note that the analytical approximation in (3.38) seems to lowerbound the actual receiver performance.

Figure 3.7 plots the near-far resistance (via (3.41)) versus D_s for three different realizations of \mathbf{h}_k 's of all users to illustrate variation in performance with channel coefficients. There are 3 interfering users with $T_{obs} < T_{coh,i}$ ($N_i = 3$) and each one is 5 times stronger than the desired user. Note that the value of η tends to converge with increasing D_s and the improvement in near-far resistance saturates as D_s is increased.

Finally, Figure 3.8 explores the effect of the choice of secondary coordinates on performance. There are 3 strong interfering users with $T_{obs} \gg T_{coh,i}$ ($N_i = 27$) and P_e is analytically computed for four different choices of secondary coordinates as a function of the relative power of each interfering user. Figure 3.8(a) corresponds to $D_s = 12$ and Figure 3.8(b) corresponds to $D_s = 30$. The best attainable performance, that of

the full-dimensional ($D_s = N - D_p$) receiver, is also plotted for comparison. Notice that the difference in performance for the four different choices is not too significant, especially for the larger value of D_s .

3.6. Implementation Issues

The proposed MMSE receiver structure requires knowledge of second-order statistics (\mathbf{R}_{zz}) of the canonical coordinates and the channel coefficients of the desired user \mathbf{h}_1 . In practice, both of these quantities have to be estimated from data. In this section we briefly discuss such implementational issues. We first discuss adaptive formulations of the receiver which assume the knowledge of \mathbf{h}_1 and infer the optimum solution directly from data by implicitly estimating \mathbf{R}_{zz} . We then discuss the estimation of \mathbf{h}_1 directly from data using one of the adaptive receiver structures.

3.6.1. Adaptive Implementations

To derive an adaptive formulation of the proposed receiver, we first cast it in the framework of Linearly Constrained Minimum Variance (LCMV) filtering [31]. In this formulation, the optimum filter $\mathbf{w}_{mv,o}$ minimizes the average output power subject to constraining the signal component to remain constant:

$$\mathbf{w}_{mv} = \arg \min_{\mathbf{w}} E [|\mathbf{w}^H \mathbf{z}|^2] \quad \text{subject to} \quad \mathbf{w}_p^H \mathbf{g}_1 = \alpha. \quad (3.43)$$

Using the method of Lagrange multipliers [31], the solution to (3.43) is given by

$$\mathbf{w}_{mv}(\mathbf{g}_1) = \frac{\alpha}{\bar{\mathbf{g}}_1^H \mathbf{R}_{z,z}^{-1} \bar{\mathbf{g}}_1} \mathbf{R}_{z,z}^{-1} \bar{\mathbf{g}}_1 = \frac{\alpha}{\mathbf{g}_1^H \mathbf{R}_{e,e}^{-1} \mathbf{g}_1} \mathbf{R}_{e,e}^{-1} \mathbf{g}_1$$

$$= \frac{\alpha}{\mathbf{g}_1^H \mathbf{R}_{\epsilon, \epsilon}^{-1} \mathbf{g}_1} \begin{bmatrix} \mathbf{R}_{\epsilon, \epsilon}^{-1} \mathbf{g}_1 \\ -\mathbf{C} \mathbf{R}_{\epsilon, \epsilon}^{-1} \mathbf{g}_1 \end{bmatrix}, \quad (3.44)$$

$$\text{mv}(\mathbf{g}_1) = \frac{\alpha^2}{\mathbf{g}_1^H \mathbf{R}_{\epsilon, \epsilon}^{-1} \mathbf{g}_1} = \frac{\alpha^2 (1 + \mathbf{g}_1^H \mathbf{R}_{\epsilon, \epsilon}^{-1} \mathbf{g}_1)}{\mathbf{g}_1^H \mathbf{R}_{\epsilon, \epsilon}^{-1} \mathbf{g}_1}. \quad (3.45)$$

Note that the solutions in (3.44) and (3.28) are identical upto a scalar.

To implement \mathbf{w}_{mv} adaptively, we formulate it as a Generalized Sidelobe Canceler (GSC) [31] to convert the constrained problem in (3.43) into an unconstrained one. Figure 3.9 shows two adaptive implementations based on the GSC approach. Figure 3.9(a) shows a parallel scheme, along the lines of Figure 3.1(a) in which \mathbf{w}_p and \mathbf{w}_s are adapted simultaneously ($D_p + D_s$ adaptive taps). Whereas the secondary filter \mathbf{w}_s is adapted unconstrained, the primary filter is decomposed as $\mathbf{w}_p = \alpha \mathbf{g}_1 + \mathbf{w}_\perp$ to satisfy the constraint in (3.43). In particular, $\mathbf{w}_\perp = \mathbf{G}^\perp \mathbf{w}_{uc}$ operates on the orthogonal complement of \mathbf{g}_1 which is spanned by the columns of the $D_p \times (D_p - 1)$ matrix \mathbf{G}^\perp . This is illustrated in Figure 3.9(a) in which \mathbf{w}_{uc} ($D_p - 1$ taps) and \mathbf{w}_s (D_s taps) represent the unconstrained degrees of freedom that can be adaptively updated using any standard adaptative algorithm such as LMS or RLS [31].

Figure 3.9(b) shows a sequential implementation along the lines of Figure 3.1(b) in which the MAI component in \mathbf{z}_p is first estimated from \mathbf{z}_s via a matrix filter \mathbf{C} (or a bank of filters). The primary filter \mathbf{w}_p then acts on the error signal \mathbf{e} to further suppress any residual interference. Note that \mathbf{C} can be adapted unconstrained since the secondary coordinates are signal free. The primary filter \mathbf{w}_p is decomposed as in the parallel scheme to satisfy the constraint. In this case, the \mathbf{w}_{uc} and \mathbf{C} represent the $(D_p - 1) + (D_p \times D_s)$ unconstrained degrees of freedom that can be adaptively updated. A thorough analysis of these adaptive implementations is beyond the scope

of this paper. However, we note that the serial scheme in Figure 3.9(b) is particularly suited for blind estimation of \mathbf{g}_1 , as discussed in the next section. Under certain conditions, the dominant eigenvector of $\mathbf{R}_{\mathbf{e},\mathbf{e}}$ yields an accurate estimate of \mathbf{g}_1 .

3.6.2. Channel Estimation

If \mathbf{h}_1 is not known *a priori*, we can extend the LCMV formulation analogous to the use of Capon's method in [22, 33] to estimate the channel coefficients. We outline an approach for estimating $\mathbf{g}_1 = \mathbf{Q}_{11}\mathbf{h}_1$ from which \mathbf{h}_1 can be obtained since \mathbf{Q}_{11}^{-1} exists. It is based on the serial adaptive receiver in Figure 3.9(b).

We start by noting that the constraint in the LCMV approach is based on \mathbf{g}_1 . In the extended formulation we replace \mathbf{g}_1 with an arbitrary constraint vector \mathbf{f}_1 . This yields the corresponding LCMV solution in (3.44)-(3.45) in terms of \mathbf{f}_1 . Then, the optimum (unit-norm) \mathbf{f}_1 is defined as one which *maximizes* the parameterized minimum output variance:

$$\begin{aligned} \mathbf{f}_{1,o} &= \arg \max_{\|\mathbf{f}_1\|=1} \min_{\mathbf{w}: \mathbf{w}^H \mathbf{f}_1 = \alpha} \mathbf{w}^H \mathbf{R}_{zz} \mathbf{w} \\ &= \arg \min_{\|\mathbf{f}_1\|=1} \mathbf{f}_1^H \mathbf{R}_{\mathbf{e},\mathbf{e}}^{-1} \mathbf{f}_1 \end{aligned} \quad (3.46)$$

where we have used (3.45) in the last equality. The solution to (3.46) is given by the eigenvector corresponding to the smallest eigenvalue of $\mathbf{R}_{\mathbf{e},\mathbf{e}}^{-1}$ (or largest eigenvalue of $\mathbf{R}_{\mathbf{e},\mathbf{e}}$).¹⁶ This solution yields an estimate of \mathbf{h}_1 as $\hat{\mathbf{h}}_1 = \mathbf{Q}_{11}^{-1} \mathbf{f}_{1,o}$. Furthermore, the corresponding MMSE/LCMV solution is given by $\mathbf{w}_{mv}(\mathbf{f}_{1,o})$ in (3.44).

Note that $\mathbf{e} = \mathbf{g}_1 + \Delta \mathbf{i}_p + \Delta \mathbf{v}_p$ where $\Delta \mathbf{i}_p$ and $\Delta \mathbf{v}_p$ represent the residual MAI and noise after the first stage of MAI suppression effected by \mathbf{C} , as illustrated in Figure 3.9(b).

¹⁶Assuming that the largest eigenvalue of $\mathbf{R}_{\mathbf{e},\mathbf{e}}$ corresponds to a one-dimensional invariant subspace. Otherwise, any vector in the invariant subspace will suffice.

Intuitively, for sufficiently high SNR and for sufficiently many secondary coordinates, we expect the dominant eigenvector of $\mathbf{R}_{e,e}$ to be strongly influenced by \mathbf{g}_1 . It is shown in Appendix A that a necessary condition for

$$\lim_{\sigma^2 \rightarrow 0} \mathbf{f}_{1,o} = \frac{e^{j\phi} \mathbf{g}_1}{\|\mathbf{g}_1\|}, \quad \phi \in \mathbb{R} \text{ (phase ambiguity)}, \quad (3.47)$$

is that $D_s \geq N_i$ (secondary coordinates alone are sufficient to completely suppress the MAI). We note that in our simulations we have found this condition to be sufficient as well. Thus, the dominant eigenvector of $\mathbf{R}_{e,e}$ yields a reliable channel estimate up to a scale factor. A representative plot of $\log(\|\mathbf{f}_{1,o} - e^{j\phi} \mathbf{g}_1 / \|\mathbf{g}_1\|\|^2)$, where $\mathbf{f}_{1,o}$ is computed using (3.46), is shown in Figure 3.10 as a function of SNR for different values of D_s . There are 3 interfering users with $T_{obs} < T_{coh,i}$. It is evident that the estimation error decreases monotonically with SNR for $D_s \geq N_i = 3$.

Recall that the MMSE and LCMV solutions are identical upto a scalar and note from (3.33) that in the limit of high SNR, the optimum primary solution $\mathbf{w}_{p,o} = \mathbf{R}_{e,e}^{-1} \mathbf{g}_1 = c \mathbf{g}_{1,\perp}$. However, in the limit \mathbf{g}_1 is an eigenvector of $\mathbf{R}_{e,e}$. Thus, we expect that in the limit of high SNR the optimum primary solution is identical to \mathbf{g}_1 as long as $D_s \geq N_i$.

3.7. Conclusion

The generic linear multiuser receiver in Figure 3.1(a) typifies our integrated design framework in terms of canonical multipath-Doppler coordinates. The canonical coordinates fully incorporate time-varying channel dispersion effects via the robust and parsimonious signal representation (3.3) and provide a natural subspace approach to exploit dispersion effects for MAI suppression. The primary coordinates facilitate maximal exploitation of channel diversity and limited MAI suppression. Progressively

enhanced MAI suppression can be attained by augmenting the receiver with secondary coordinates. The framework also lends itself easily to blind/adaptive implementations that require knowledge of only the desired user's code.

The natural signal space partitioning in terms of primary and secondary coordinates provides a direct handle on controlling receiver complexity. This is a particularly attractive feature in adaptive implementations in which the desired input statistics have to be estimated directly from data. For example, as reported in [21], existing chip-rate sampled adaptive receiver designs operating in the full-dimensional signal space suffer from poor performance due to unreliable estimation of data covariance matrix in practical time-varying scenarios. Our framework for designing a range of progressively complex (powerful) receivers by incorporating secondary coordinates serves as a useful approach for striking a judicious practical tradeoff between complexity and performance. Furthermore, while our examples focused on slow fading scenarios, the notion of Doppler diversity with appropriate signaling [3, 34] may also be leveraged in fast-fading scenarios to further enhance system performance. Finally, we note that notion of canonical coordinates can be extended to space-time scenarios as well [35, 36, 37].

3.8. Figures

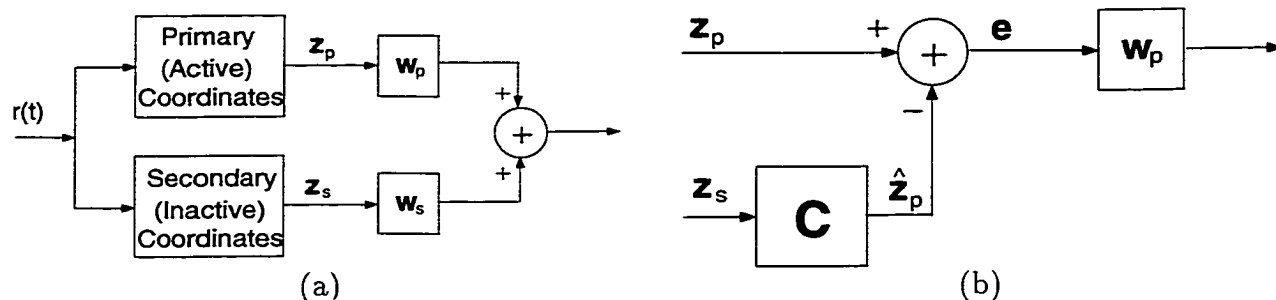


Figure 3.1. (a) Generic linear receiver structure based on canonical multipath-Doppler coordinates. (b) Interpretation of the MMSE receiver in (3.20) and (3.21). The matrix filter C suppresses MAI in the primary coordinates z_p by using the secondary coordinates z_s . The filter w_p further suppresses MAI in the residual e and performs diversity combining.

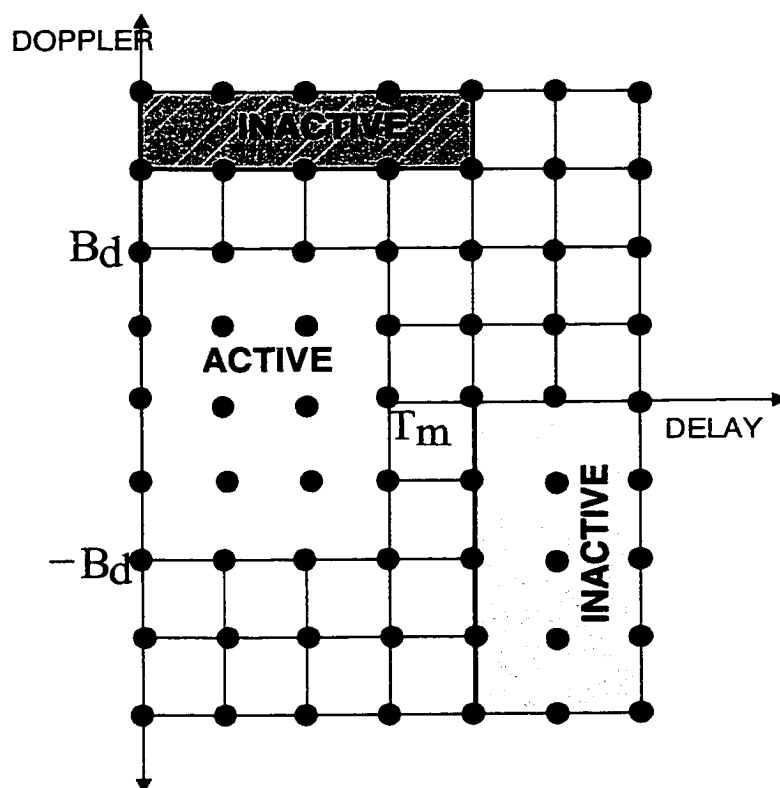


Figure 3.2. A schematic illustrating active and inactive coordinates. Active coordinates correspond to multipath-Doppler basis signals that lie within the channel spread. Inactive coordinates correspond to basis functions outside the channel spread.

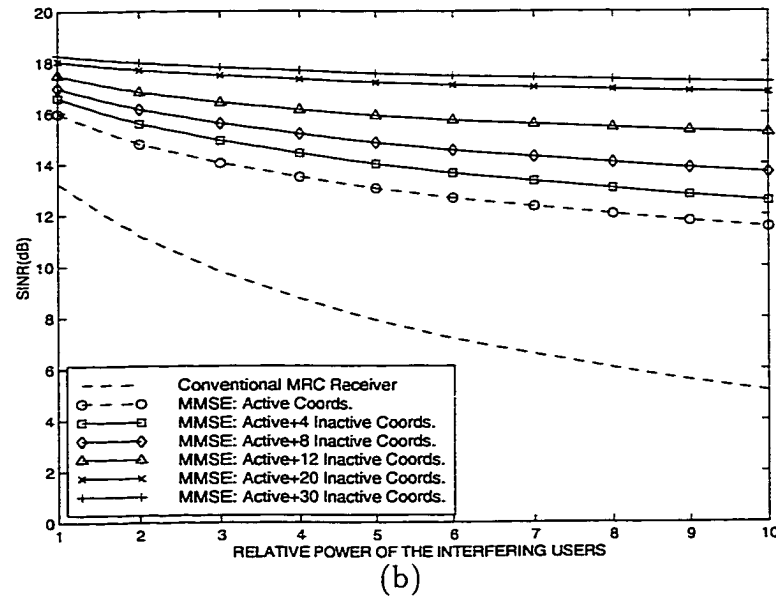
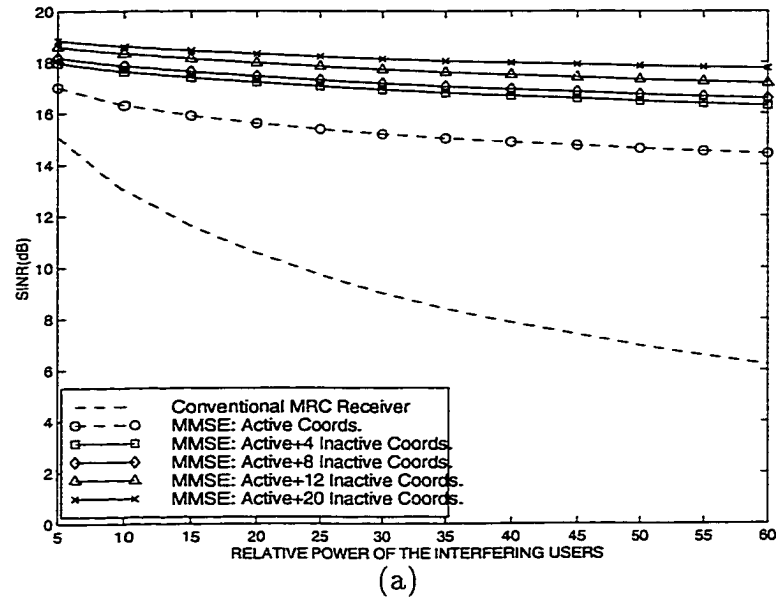


Figure 3.3. Receiver SINR versus relative power of each interfering user for different number of secondary coordinates (D_s). Long times scales with respect to interference coherence time ($T_{obs} \gg T_{coh,i}$). (a) 1 interfering user ($N_i = 9$). (b) 3 interfering users ($N_i = 27$). Notice the saturation of SINR as $N_{tot} = D_p + D_s = 9 + D_s$ increases beyond $N_i + 1$.

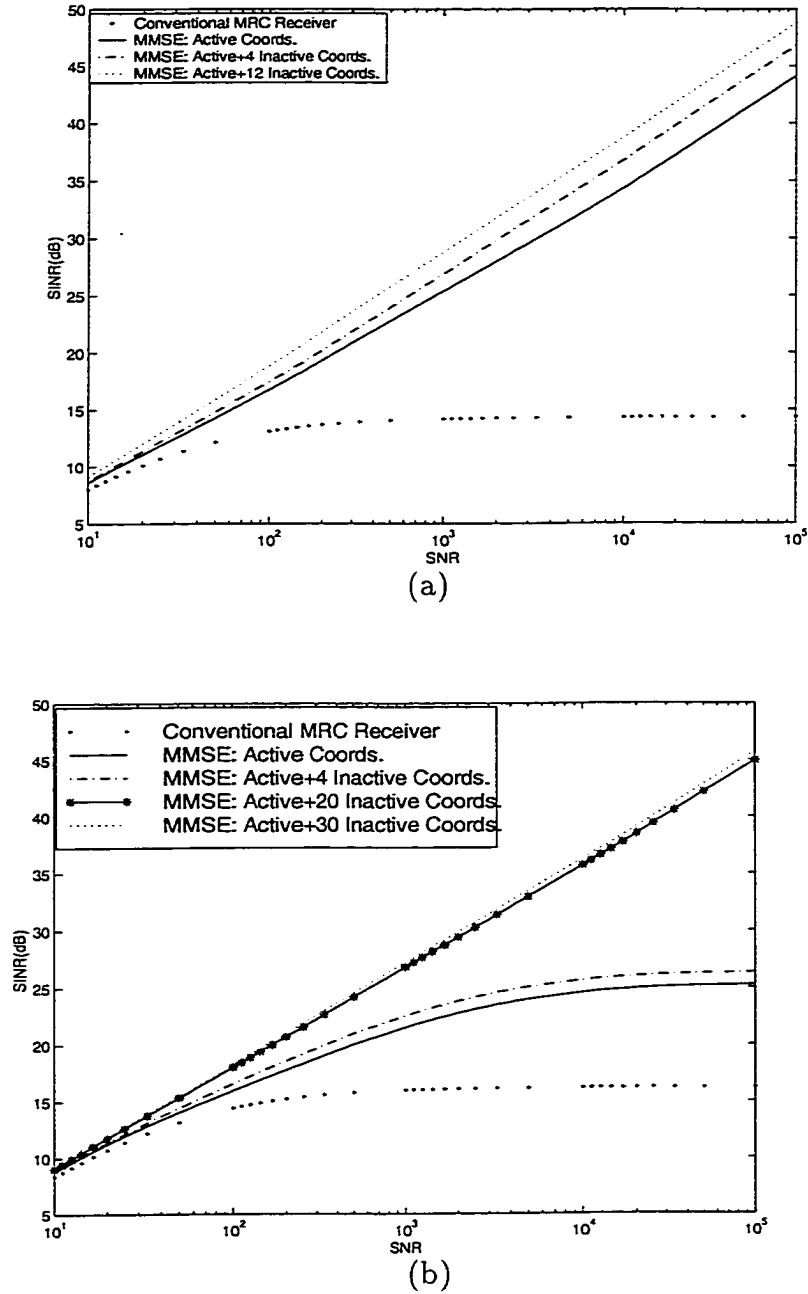


Figure 3.4. Receiver SINR as a function of SNR of desired user for different values of D_s . Three interfering users with the same power as the desired user. (a) $T_{obs} < T_{coh,i}$ ($N_i = 3$). (b) $T_{obs} \gg T_{coh,i}$ ($N_i = 27$). Note that the receiver moves from an MAI-limited regime to a noise-limited regime as D_s increases beyond $N_i + 1 - D_p$ (-5 for (a) and 19 for (b)). SINR saturates in the MAI-limited regime but increases linearly with SNR in the noise-limited regime.

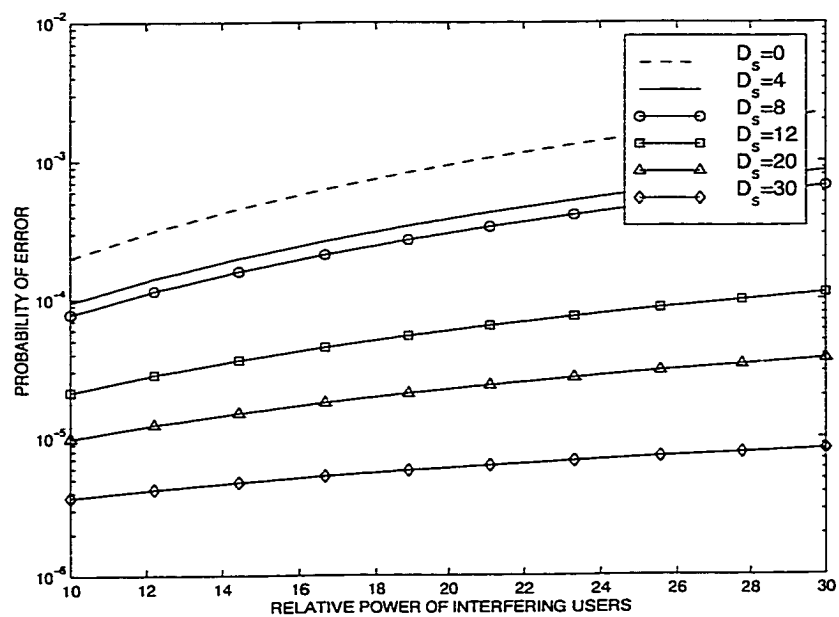


Figure 3.5. Analytically computed P_e (using (3.38)) as a function of the relative power of 3 interfering users ($N_i = 27$) for different values of D_s .

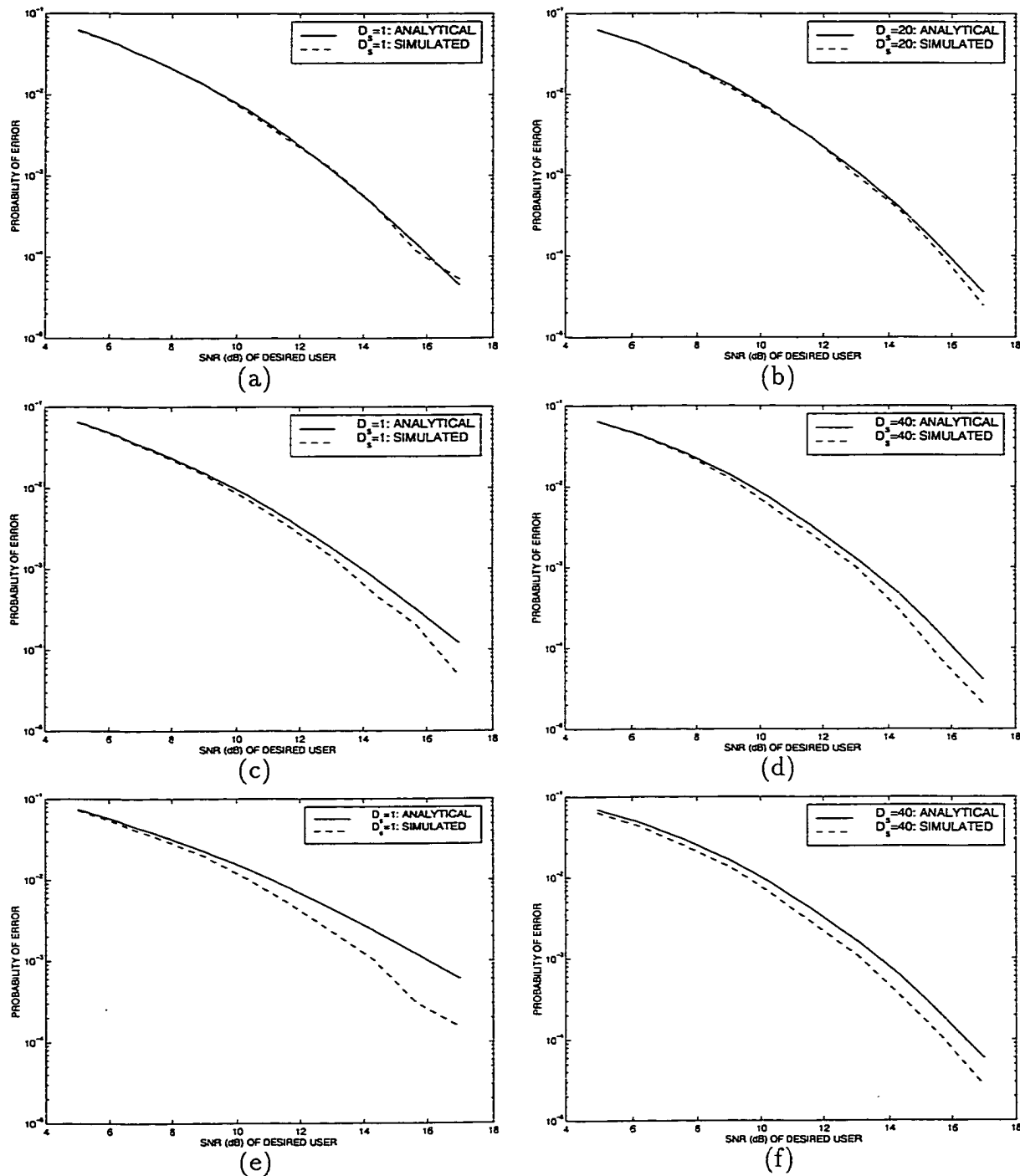


Figure 3.6. Comparison of analytically computed P_e (via (3.38)) versus Monte-Carlo averaging of (3.37) over all \mathbf{h}_k 's for different values of D_s . 3 interfering users. (a) and (b): all users with equal power. (c) and (d): interfering users are 3 times stronger than desired user. (e) and (f): interfering users are 10 times stronger. We note for large D_s the receiver performance is close to that of a single-user (MRC) receiver with 3-level diversity [1] operating in the absence of MAI.

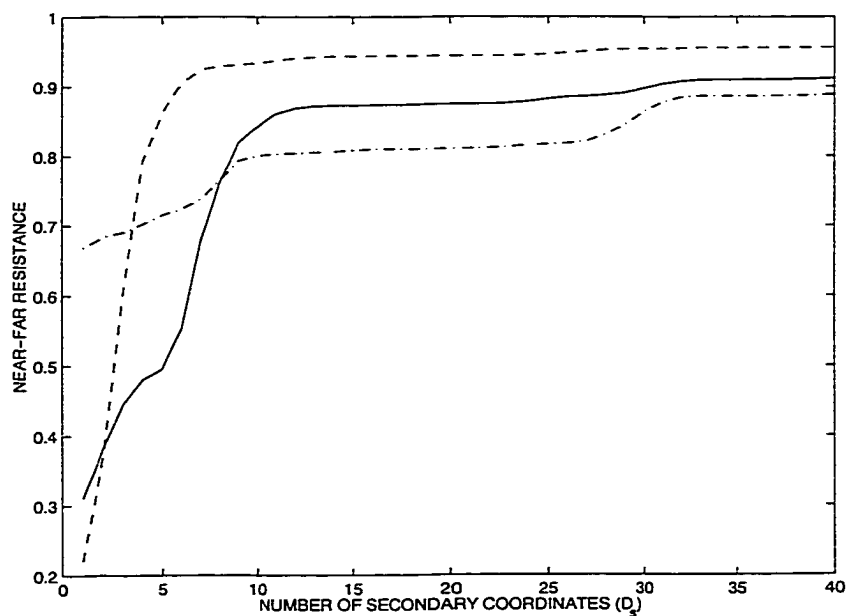
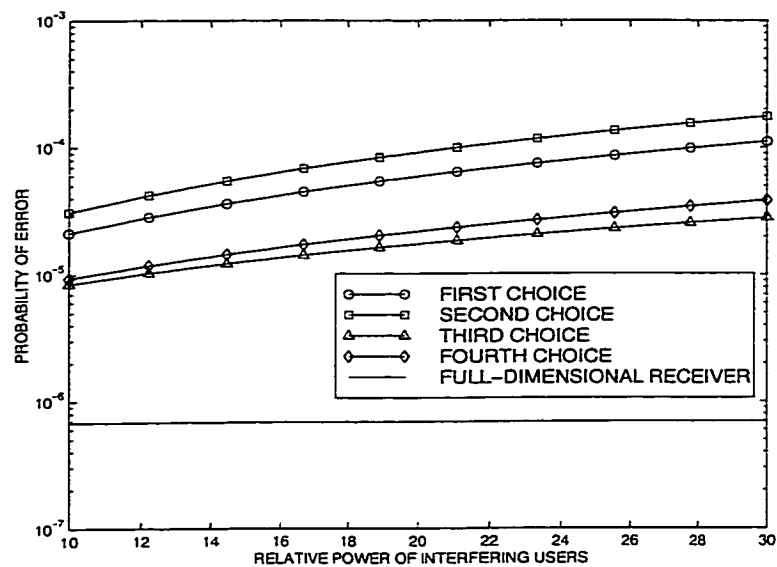
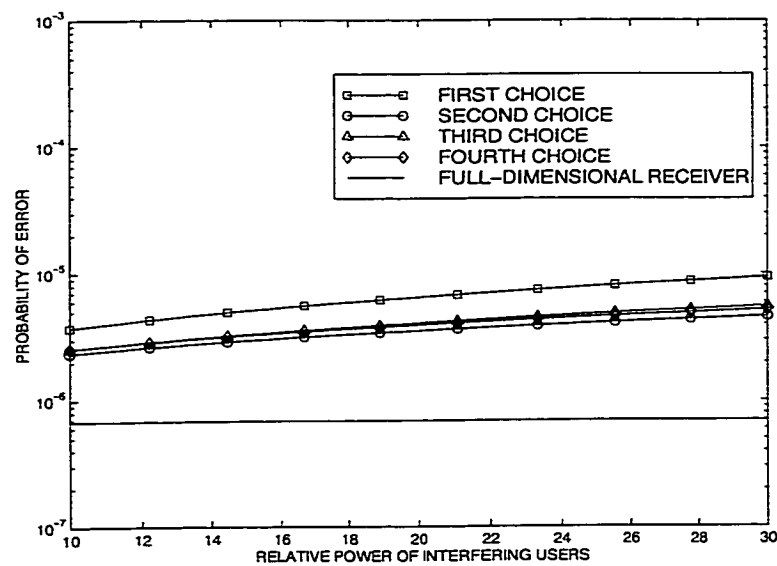


Figure 3.7. Near-far resistance, computed using (3.41) for 3 different realizations of \mathbf{h}_k 's, as a function of D_s . There are 3 interfering users that are 5 times stronger than the desired user.



(a)



(b)

Figure 3.8. Analytically computed P_e for different choices of secondary coordinates as a function of the relative power of 3 interfering users. (a) $D_s = 12$ (b) $D_s = 30$. Notice that the relatively small difference in performance between different choices, especially for larger D_s .

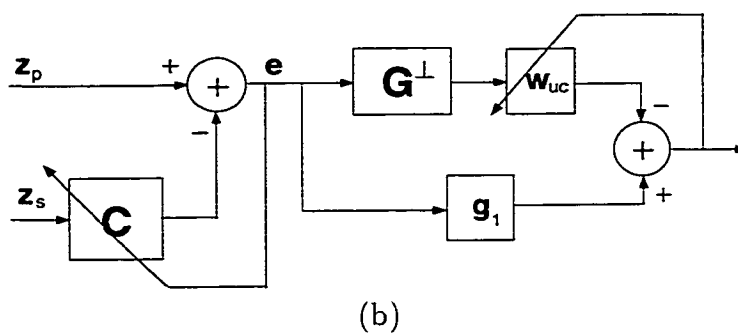
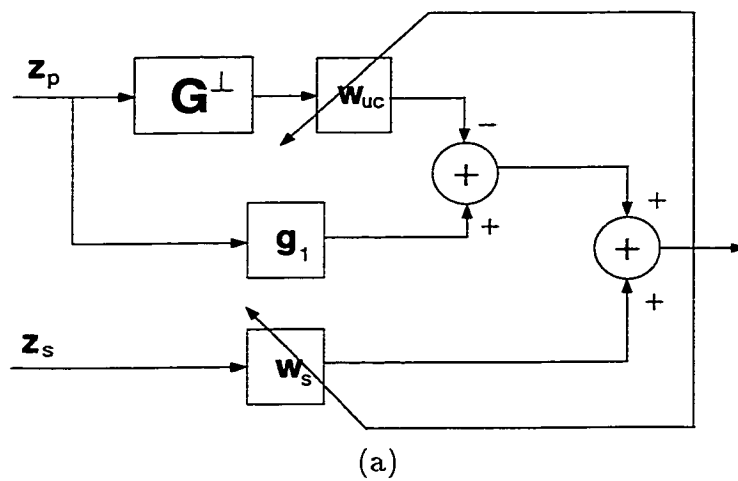


Figure 3.9. Structures for adaptive implementation. (a) Parallel structure, and (b) Serial structure. The serial structure is particularly suited to blind channel estimation from the eigenstructure of \mathbf{e} .

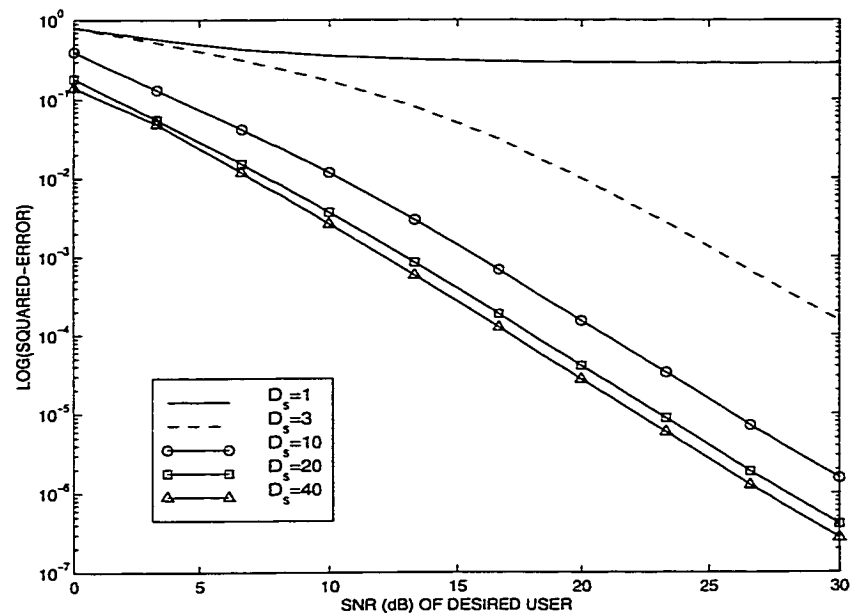


Figure 3.10. A representative plot of the channel estimation error as a function of SNR of desired user for different value of D_s . 3 interfering users that are 10 times stronger than desired user. Notice the monotonic decrease in error for $D_s \geq N_i = 3$.

CHAPTER 4

A NOVEL FRAMEWORK FOR MC-CDMA RECEPTION IN THE PRESENCE OF IMPERFECTIONS

4.1. Introduction

Future wireless personal communication services will require high bandwidth to support multimedia formats. Direct-Sequence (DS)-CDMA has emerged as a core wireless technology in the third generation and emerging standards. However, conventional CDMA systems are fundamentally limited in their ability to deliver high data rates due to implementational issues associated with higher chip rates and complexity issues related to higher Inter Symbol Interference (ISI). These impairments put severe constraints on the data rate supportable by single carrier (SC)-CDMA systems [38]. Multi-Carrier (MC) modulation, often called Orthogonal Frequency-Division Multiplexing (OFDM), has drawn a lot of attention due to its ability to support high rates while ameliorating ISI and fading. In OFDM, the high rate stream is split into a number of parallel lower rate ones that are transmitted over narrowband orthogonal subcarriers. The longer symbol duration of lower rate streams in conjunction with a guard time (cyclic prefix), significantly reduces the effects of ISI. An attractive aspect of OFDM is that modulation and demodulation can be implemented efficiently by a Discrete Fourier Transform (DFT).

MC-CDMA, a combination of CDMA and OFDM, has been proposed to support high data rates in CDMA systems [7, 6, 8]. The lower data rate supported by each subcarrier is manifested in longer symbol and chip durations. In a properly designed MC-CDMA system, each single subchannel encounters flat fading, thereby eliminat-

ing the need for channel equalization. Furthermore, the system exploits frequency selectivity for diversity via the different subcarriers. MC-CDMA also requires a lower-speed parallel-type processing compared to fast serial-type processing in a SC-CDMA system. These important features make MC-CDMA a strong candidate for high-rate wireless communications.

Though OFDM is robust to ISI, its performance and ease of implementation critically depend on orthogonality between subcarriers, a property that is destroyed by non-ideal system characteristics encountered in practice. These non-idealities include frequency offsets and phase noise, that are due to the inefficiency of the local oscillator at the transmitter and/or receiver, as well as Doppler effects due to fast fading. MC-CDMA systems are more sensitive to these imperfections than SC-CDMA systems due to longer symbol durations. For example, the channel may appear almost constant over one (short) symbol duration in a SC-CDMA system while it may exhibit faster variation over the longer MC-CDMA symbol. The loss of orthogonality between subcarriers is due to the dispersion of signal power from a particular subcarrier into adjacent frequencies which results in Inter Carrier Interference (ICI). Since existing MC-CDMA receivers process each sub-channel separately, they collect only part of the transmitted power in each subcarrier in addition to suffering from ICI. These imperfections severely limit the performance of existing MC-CDMA systems [39, 40, 41, 42, 43, 44].

This chapter addresses the design and analysis of MC-CDMA systems in the presence of frequency offset, phase noise and fast fading. We assume sufficiently large number of carriers so that ISI is negligible in each subcarrier. We introduce an integrated receiver structure for combating these imperfections based on a canonical model for

the received signal that efficiently captures the effects of the non-idealities. In essence, each subcarrier is decoded by processing a subset of adjacent subcarriers. Our results demonstrate that, with slightly higher complexity, the degradation due to imperfections can be virtually eliminated. Furthermore, in contrast to existing designs, the proposed receiver exploits Doppler diversity [3] to deliver improved performance under fast fading.

The next section reviews the channel model and receiver structure in conventional MC-CDMA systems. Section 4.3 presents the proposed receiver structure as well as an analysis of its performance. Sections 4.4, 4.5 and 4.6 assess the performance of the proposed receiver in the presence of frequency offsets, fast fading, and phase noise, respectively. Section 4.7 provides some numerical results depicting a variety of scenarios. Section 4.8 an alternative but equivalent representation to the proposed receiver. Section 4.9 presents some concluding remarks.

4.2. System Model

We adopt the Wide Sense Stationary Uncorrelated Scattering (WSSUS) channel model described in Section 2.2. We assume a symbol duration T and essential double-sided bandwidth B . In this section, we review a typical MC-CDMA system. We first introduce a typical MC-CDMA transmitter. We also describe a modified MC-CDMA transmitter that employs longer symbol duration (and a larger number of subcarriers) to reduce ISI. Then, a typical MC-CDMA receiver is discussed.

4.2.1. MC-CDMA Transmitter

In DS-CDMA, the transmitted spread spectrum signal occupies the entire bandwidth B . The idea behind MC-CDMA is to transmit the data on parallel channels, each occupying a fraction of the bandwidth of the original CDMA signal. In a typical MC-CDMA system, shown in Figure 4.1, the signature code $\{\tilde{a}_p, p = 1, 2, \dots, P\}$ is spread among a set of P orthogonal subcarriers each carrying the same information bit b_1 . Thus, each chip modulates one of P orthogonal subcarriers. This process is done by the P -point DFT block. A guard time is then added to reduce the effects of ISI. The subcarriers are separated by $\frac{1}{T}$ and the bandwidth associated with each subcarrier is $B_o = \frac{2}{T}$. Figures 4.2(a) and (b) show the spectrum of a SC-CDMA signal and that of a MC-CDMA signal, respectively. The objective is to make B_o smaller than Δf_c so that each subcarrier encounters flat fading.

For very high data rates, it is desirable to further increase the symbol duration over each subcarrier to make $T \gg T_m$ so that ISI is negligible [7, 38, 45]. The signal is first serial-to-parallel converted before spreading over the frequency domain. In particular, to increase the symbol duration J times, J lower rate streams need to be transmitted in parallel. Each stream is transmitted through a MC-CDMA transmitter similar to the one described in Figure 4.1 with T replaced by JT . Using this technique, the data rate of the parallel streams can be made arbitrary low to alleviate the effects of ISI without affecting the overall data rate. However, increasing the symbol duration on each subcarrier makes the system more susceptible to frequency offset, phase noise and fast fading [38, 45, 41, 40, 39, 46]. The proposed receiver can then be employed in the modified MC-CDMA system to restore the performance loss due to these imperfections and exploit Doppler diversity.

For simplicity of exposition, we limit our development to a conventional MC-CDMA system (the one described in Figure 4.1). The proposed system can be readily extended to the modified MC-CDMA system. Let $P = 2N - 1$. Define the set of *active* subcarriers to be $\{f_n = \frac{2n-1}{T}, n = 1, 2, \dots, N\}$ corresponding to the solid spectra in Figure 4.2(b). Define the set of *inactive* subcarriers as $\{\tilde{f}_n = \frac{2n}{T}, n = 1, 2, \dots, N-1\}$ corresponding to the dotted spectra in Figure 4.2(b). For simplicity of exposition, we assume that only the active set is used for data transmission. The results presented can be readily extended to the case where information is transmitted on all subcarriers. A signature code $\{a_n\}$ of length $N = \frac{P+1}{2}$ is employed to modulate the active subcarriers. In the context of Figure 4.1, $\tilde{a}_p = \begin{cases} a_{\frac{p+1}{2}} & p \text{ odd} \\ 0 & p \text{ even} \end{cases}, p = 1, 2, \dots, P$. The inactive subcarriers may be used at the receiver as will be clarified later. We also focus on a single user system where a single bit is transmitted on all active subcarriers. The transmitted signal can be written as

$$s(t) = b_1 \sum_{n=1}^N a_n q(t) e^{j2\pi f_n t} \quad (4.1)$$

where $q(t) = \frac{1}{\sqrt{T}}, 0 \leq t \leq T$ is the normalized symbol waveform.

4.2.2. Conventional MC-CDMA Receiver

Consider a conventional MC-CDMA system with no imperfections in a slowly fading channel. At the receiver, the guard time (cyclic prefix) is discarded and the signal is fed to a P -point DFT block to separate the subcarriers. The received signal for one symbol can be written as

$$r(t) = b_1 \sum_{n=1}^N a_n \tilde{h}(n) q(t) e^{j2\pi f_n t} + n(t) \quad (4.2)$$

where $\tilde{h}(n)$ is the channel coefficient of the n^{th} subcarrier and $n(t)$ is complex Additive White Gaussian Noise (AWGN) with power spectral density σ^2 . The test static z_n resulting from projecting $r(t)$ onto the n^{th} active subcarrier is

$$z_n = \frac{1}{\sqrt{T}} \int_0^T r(t) e^{-j2\pi f_n t} dt = b_1 a_n \tilde{h}(n) + v_n \quad (4.3)$$

where $\{v_n\}$ are independent with variance σ^2 . With perfect channel estimates, the bit decision is given by

$$\hat{b}_1 = \text{sign} \left[\text{real} \left\{ \sum_{n=1}^N a_n^* \tilde{h}^*(n) z_n \right\} \right]. \quad (4.4)$$

We note that this receiver provides $L + 1$ -fold diversity where $L = \lceil T_m B \rceil$ is the number of resolvable multipaths [1].

4.3. The Proposed Framework

In the presence of fast fading, Doppler shifts, frequency offset and/or phase noise, the orthogonality between subcarriers is destroyed. The matched filter output (4.3) will suffer from *leakage* from the other active subcarriers [41, 40, 39, 46]. This leakage disperses the energy of a particular subcarrier over the adjacent subcarriers. Thus, it is necessary to jointly process the test statistics from different subcarriers. We introduce a receiver structure that combats all these impairments in an integrated fashion. It fully eliminates the performance loss due to frequency offsets and phase noise. Moreover, in contrast to existing receivers, it exploits temporal channel variations for improved performance via Doppler diversity.

4.3.1. General Receiver Structure

The information bearing signal in (4.2) in the ideal channel is a linear combination of the fixed basis functions, $u_n(t) = q(t)e^{j2\pi f_n t}$, $n = 1, 2, \dots, N$, with $\tilde{h}(n)$ as the corresponding expansion coefficients. In the presence of imperfections, the received signal can be represented as

$$r(t) = b_1 \sum_{n=1}^N a_n w(t, f_n) q(t) e^{j2\pi f_n t} + n(t) \quad (4.5)$$

$$w(t, f_n) = \tilde{c}(t, f_n) e^{j2\pi f_{off} t} e^{j\varrho(t)} \quad (4.6)$$

where $\tilde{c}(t, f_n)$ accounts for the channel and is defined in (2.1) (the index k is removed for simplicity since this chapter deals with a single user scenario), the term $e^{j2\pi f_{off} t}$ accounts for frequency offset between the transmitter and receiver oscillators, and $e^{j\varrho(t)}$ accounts for phase noise.¹ Compared to the ideal system (4.2), the channel coefficients in (4.5) are no longer constant over a symbol duration. Temporal variations are manifested as spectral dispersion — each subcarrier exhibits a spectral spread around the subcarrier frequency. However, due to the finite symbol duration, any arbitrary spectral spreading around each subcarrier can be represented in terms of a finite number of discrete frequencies [14, 3]. More specifically, let $\tilde{w}(t, f_n) = w(t, f_n) I_{[0, T]}(t)$ denote the part of $w(t, f_n)$ affecting the symbol, where $I_{[x, y]}(t)$ is the indicator function of the interval $[x, y]$. $\tilde{w}(t, f_n)$ admits the following Fourier series representation

$$\tilde{w}(t, f_n) = \sum_{m=-\infty}^{\infty} \tilde{h}(m, n) e^{j\frac{2\pi m t}{T}}, \quad \tilde{h}(m, n) = \frac{1}{T} \int_0^T \tilde{w}(t, f_n) e^{-j\frac{2\pi m t}{T}} dt \quad (4.7)$$

¹This model corresponds to phase noise at the transmitter. Our development can be easily extended to the case of having the phase noise at the receiver or at both the transmitter and the receiver.

where $\{\tilde{h}(m, n)\}$ are random variables characterizing the effect of $\tilde{w}(t, f_n)$. Using (4.7), the received signal in (4.5) can be written as

$$r(t) = b_1 \sum_{n=1}^N \sum_{m=-M_l}^{M_u} a_n \tilde{h}(m, n) q(t) e^{\frac{j2\pi m t}{T}} e^{j2\pi f_n t} + n(t) \quad (4.8)$$

where M_l and M_u are integers determined by the type of imperfections (discussed later). Note that $M_l = M_u = 0$ is an ideal system. In the presence of imperfections, more than one channel coefficients $\{\tilde{h}(m, n)\}$ are associated with each subcarrier. We also note that in general a relatively small number $(M_u + M_l + 1)$ of subcarriers captures most of the energy in the dispersed subcarrier. The key idea of the paper is to restore the loss in performance and exploit diversity for each subcarrier by jointly processing adjacent subcarriers corresponding to significant $\{\tilde{h}(m, n)\}$.

For convenience, we rewrite (4.8) in terms of the active and inactive subcarriers

$$r(t) = b_1 \sum_{n=1}^N p_a(n) q(t) e^{j2\pi \frac{2n-1}{T} t} + b_1 \sum_{n=1}^{N-1} p_{ia}(n) q(t) e^{j2\pi \frac{2n}{T} t} + n(t) \quad (4.9)$$

where

$$p_a(n) = \sum_{m=-M_{1,l}}^{M_{1,u}} \tilde{h}(2m, n-m) a_{n-m} \quad \text{and} \quad p_{ia}(n) = \sum_{m=-(M_{2,l}+1)}^{M_{2,u}} \tilde{h}(2m+1, n-m) a_{n-m} \quad (4.10)$$

represent the coefficients modulating the active and inactive subcarriers, respectively.

Here, $M_{1,l} = \kappa(M_l)$, $M_{1,u} = \kappa(M_u)$, $M_{2,l} = \mu(M_l)$, $M_{2,u} = \mu(M_u)$, and $\kappa(M)$ and $\mu(M)$

are defined as $\kappa(M) = \left\{ \begin{array}{l} \frac{M}{2}, \quad M \text{ is even} \\ \frac{M-1}{2}, \quad M \text{ is odd} \end{array} \right\}$ and $\mu(M) = \left\{ \begin{array}{l} \frac{M}{2} - 1, \quad M \text{ is even} \\ \frac{M-1}{2}, \quad M \text{ is odd} \end{array} \right\}$.

The representation in (4.9) and (4.10) captures the leakage of information between the different subcarriers and is illustrated in Figure 4.3 for $M_l = M_u = 2$.

It can be readily shown that the general expression for $\tilde{h}(m, n)$ in the presence of

frequency offset, phase noise and fast fading is

$$\tilde{h}(m, n) = \frac{1}{T} \int_{-B_d}^{B_d} \tilde{C}(\theta, f_n) G\left(\frac{k}{T} - f_{off} - \theta\right) d\theta \quad (4.11)$$

where

$$\tilde{C}(\theta, f_n) = \int_0^T \tilde{c}(t, f_n) e^{-j2\pi\theta t} dt \quad (4.12)$$

and

$$G(\theta) = \int_0^T e^{je(t)} e^{-j2\pi\theta t} dt. \quad (4.13)$$

The statistics of the coefficients $\{\tilde{h}(m, n)\}$ vary with the type of imperfection. In most cases the correlation function of $\{\tilde{h}(m, n)\}$ determines the receiver performance. Since $\tilde{C}(\theta, f_n)$ and $G(\theta)$ in (4.11) are statistically independent, and $\tilde{C}(\theta, f_n)$ is uncorrelated for different of θ [1],

$$\begin{aligned} \rho(m_1, n_1; m_2, n_2) &= E[\tilde{h}(m_1, n_1)\tilde{h}(m_2, n_2)^*] = \frac{1}{T^2} \int_{-B_d}^{B_d} \int_{-B_d}^{B_d} E[\tilde{C}(\theta, f_{n_1})\tilde{C}^*(\theta', f_{n_2})] \\ &\times E\left[G\left(\frac{m_1}{T} - f_{off} - \theta\right) G^*\left(\frac{m_2}{T} - f_{off} - \theta'\right)\right] d\theta d\theta' \\ &= \frac{1}{T^2} \int_{-B_d}^{B_d} \psi(\theta, f_{n_1} - f_{n_2}) \varphi(m_1 - \theta T - f_{off}T, m_2 - \theta T - f_{off}T) d\theta \end{aligned} \quad (4.14)$$

where

$$\begin{aligned} E[\tilde{C}(\theta, f_{n_1})\tilde{C}^*(\theta', f_{n_2})] &= \psi(\theta, f_{n_1} - f_{n_2})\delta(\theta - \theta'), \\ \psi(\theta, \Delta f) &= \int \phi(\Delta t, \Delta f) e^{-j2\pi\theta\Delta t} d\Delta t \\ &= \Phi_\theta(\theta)\psi_{\Delta f}(\Delta f) \end{aligned} \quad (4.15)$$

and

$$\varphi(\theta_1, \theta_2) = E\left[G\left(\frac{\theta_1}{T}\right) G^*\left(\frac{\theta_2}{T}\right)\right]. \quad (4.16)$$

$\phi(\Delta t, \Delta f)$ is defined in Section 2.2 and $\varphi(\theta_1, \theta_2)$ depends on phase noise statistics and is discussed in more detail in Section 4.6.

4.3.2. Receiver Performance

In this section we analyze the performance of a coherent receiver employing Maximal Ratio Combining (MRC) based on the proposed signal model in (4.9) and (4.10). Define the active and inactive test statistics to be the projection of the received signal on the active and inactive subcarriers, respectively. The n^{th} active and inactive test statistics are

$$\begin{aligned} z_n &= \frac{1}{\sqrt{T}} \int_0^T r(t) e^{-j2\pi \frac{2n-1}{T} t} dt = b_1 p_a(n) + v_n \\ &= b_1 a_n \tilde{h}(0, n) + b_1 \sum_{m=-M_{l,i}, m \neq 0}^{M_{1,u}} \tilde{h}(2m, n-m) a_{n-m} + v_n, \end{aligned} \quad (4.17)$$

$$\tilde{z}_n = \frac{1}{\sqrt{T}} \int_0^T r(t) e^{-j2\pi \frac{2n}{T} t} dt = b_1 p_{ia}(n) + \tilde{v}_n \quad (4.18)$$

where $\{\tilde{v}_n\}$ are uncorrelated Gaussian random variables with zero mean and variance σ^2 , and are independent of $\{v_n\}$. We analyze three different receiver structures.

R1: This is the conventional receiver that ignores the effect of imperfections. It employs bit detection based only on the first term in the right hand side of (4.17). Note that the first term is the desired signal component while the second term is the ICI due to imperfections.

R2: This is one of the proposed receivers that jointly processes only the *active* subcarriers.

R3: This is another proposed receiver structure that jointly processes both the *active* and *inactive* subcarriers.²

Notice that in absence of imperfections (i.e. $M_l = M_u = 0$), $z_n = b_1 a_n \tilde{h}(0, n) + v_n$ and $\tilde{z}_n = \tilde{v}_n$. The receiver structure **R1** is optimal in this case. It is convenient to express

²Note that if both active and inactive subcarriers are used at the transmitter, **R2** and **R3** become identical.

the test statistics (4.17) and (4.18) in matrix form

$$z_n = b_1 \left(\mathbf{a}_{a,n}^T \tilde{\mathbf{h}}_{a,n} + a_n \tilde{h}(0, n) \right) + v_n \quad (4.19)$$

$$\tilde{z}_n = b_1 \mathbf{a}_{ia,n}^T \tilde{\mathbf{h}}_{ia,n} + \tilde{v}_n \quad (4.20)$$

where

$$\begin{aligned} \mathbf{a}_{a,n} &= \left[a_{n+K_{1,u}}, a_{n+K_{1,u}-1}, \dots, a_{n+1}, a_{n-1}, \dots, a_{n-K_{1,l}} \right]^T, \\ \tilde{\mathbf{h}}_{a,n} &= \left[\tilde{h}(-2K_{1,u}, n + K_{1,u}), \dots, \tilde{h}(-2, n + 1), \tilde{h}(2, n - 1), \dots, \tilde{h}(2K_{1,l}, n - K_{1,l}) \right]^T, \\ \mathbf{a}_{ia,n} &= \left[a_{n+K_{2,u}}, a_{n+K_{2,u}-1}, \dots, a_{n+1}, a_n, a_{n-1}, \dots, a_{n-K_{2,l}} \right]^T \text{ and} \\ \tilde{\mathbf{h}}_{ia,n} &= \left[\tilde{h}(-2K_{2,u}, n + K_{2,u}), \dots, \tilde{h}(-1, n + 1), \dots, \tilde{h}(2K_{2,l} + 1, n - K_{2,l}) \right]^T. \end{aligned}$$

Note that in the above definitions $a_i = 0$ if $i < 1$ or $i > N$. Stacking the active and inactive test statistics in one vector we have

$$\mathbf{z} = \begin{bmatrix} \mathbf{z}_a \\ \mathbf{z}_{ia} \end{bmatrix} = b_1 \mathbf{g} + \mathbf{v} = b_1 \begin{bmatrix} \mathbf{g}_a \\ \mathbf{g}_{ia} \end{bmatrix} + \mathbf{v} = b_1 \begin{bmatrix} \mathbf{g}_{a,o} \\ \mathbf{0} \end{bmatrix} + b_1 \begin{bmatrix} \tilde{\mathbf{g}}_a \\ \mathbf{g}_{ia} \end{bmatrix} + \mathbf{v} \quad (4.21)$$

where \mathbf{z}_a and \mathbf{z}_{ia} are the active and inactive test statistic vectors, respectively. $\mathbf{g}_a = \mathbf{g}_{a,o} + \tilde{\mathbf{g}}_a$ are active noise-free test statistics, where $\mathbf{g}_{a,o} = \mathbf{A}_o \tilde{\mathbf{h}}_o$ denotes the part of \mathbf{g}_a corresponding to $m = 0$ coefficients, and $\tilde{\mathbf{g}}_a = \mathbf{A}_a \tilde{\mathbf{h}}_a$ corresponds to $m \neq 0$. In these definitions

$$\begin{aligned} \mathbf{A}_o &= \text{diag}(a_1, a_2, \dots, a_N), & \tilde{\mathbf{h}}_o &= \left[\tilde{h}(0, 1), \tilde{h}(0, 2), \dots, \tilde{h}(0, N) \right]^T \quad (4.22) \\ \mathbf{A}_a &= \begin{bmatrix} \mathbf{a}_{a,1}^T & \mathbf{0} & \dots & \mathbf{0} \\ \mathbf{0} & \mathbf{a}_{a,2}^T & \dots & \mathbf{0} \\ \vdots & \ddots & \ddots & \vdots \\ \mathbf{0} & \dots & \mathbf{0} & \mathbf{a}_{a,N}^T \end{bmatrix} & \text{and } \tilde{\mathbf{h}}_a &= \left[\tilde{\mathbf{h}}_{a,1}^T, \tilde{\mathbf{h}}_{a,2}^T, \dots, \tilde{\mathbf{h}}_{a,N}^T \right]^T. \end{aligned} \quad (4.23)$$

Meanwhile, $\mathbf{g}_{ia} = \mathbf{A}_{ia} \tilde{\mathbf{h}}_{ia}$ are the inactive noise-free test statistics where

$$\mathbf{A}_{ia} = \begin{bmatrix} \mathbf{a}_{ia,1}^T & \mathbf{0} & \cdots & \mathbf{0} \\ \mathbf{0} & \mathbf{a}_{ia,2}^T & \cdots & \mathbf{0} \\ \vdots & \ddots & \ddots & \vdots \\ \mathbf{0} & \cdots & \mathbf{0} & \mathbf{a}_{ia,N-1}^T \end{bmatrix} \quad \text{and} \quad \tilde{\mathbf{h}}_{ia} = \left[\tilde{\mathbf{h}}_{ia,1}^T, \tilde{\mathbf{h}}_{ia,2}^T, \cdots, \tilde{\mathbf{h}}_{ia,N-1}^T \right]^T. \quad (4.24)$$

The bit decision based on MRC is given by

$$\hat{b}_1 = \text{sign} \left\{ \text{real} \left[\mathbf{f}^H \mathbf{z} \right] \right\} \quad (4.25)$$

$$\mathbf{f} = \left\{ \begin{array}{l} \left[\begin{array}{l} \mathbf{g}_{a,o} \\ \mathbf{0} \end{array} \right], \quad \mathbf{R1} \\ \left[\begin{array}{l} \mathbf{g}_a \\ \mathbf{0} \end{array} \right], \quad \mathbf{R2} \\ \mathbf{g} = \left[\begin{array}{l} \mathbf{g}_a \\ \mathbf{g}_{ia} \end{array} \right], \quad \mathbf{R3} \end{array} \right\}. \quad (4.26)$$

We now compute the probability of error (P_e) for the three receivers assuming perfect knowledge of \mathbf{f} at the receiver. In computing P_e for **R1**, the second term on the right hand side of (4.17) is taken to be zero, i.e. the ICI term is not considered. This provides an upper bound on **R1** performance.³ The conditional P_e given \mathbf{f} is

$$P_e(\mathbf{f}) = Q \left(\sqrt{2 \frac{\mathbf{f}^H \mathbf{f}}{\sigma^2}} \right) \quad (4.27)$$

where $Q(x) = \frac{1}{\sqrt{2\pi}} \int_x^\infty e^{-\frac{x^2}{2}} dx$. The unconditional P_e is obtained by averaging the expression in (6.38) over the distribution of \mathbf{f} . If \mathbf{f} is a complex Gaussian vector, P_e

³The ICI term in (4.17) will be included for **R1** in the case of phase noise.

is given by [1]

$$P_e = \sum_{l=1}^D \frac{\pi_l}{2} \left[1 - \sqrt{\frac{\mu_l}{1 + \mu_l}} \right], \quad \pi_l = \prod_{i=1, i \neq l}^D \frac{\mu_l}{\mu_l - \mu_i} \quad (4.28)$$

where μ_l , $l = 1, 2, \dots, D$ are the nonzero eigenvalues of $\frac{1}{\sigma^2} \mathbf{R}_{\mathbf{f}, \mathbf{f}}$. $\mathbf{R}_{\mathbf{f}, \mathbf{f}}$ depends on the correlation function $\rho(k, n; m, q)$ defined in (4.14). Using (4.26), these eigenvalues correspond to the nonzero eigenvalues of $\mathbf{R}_{\mathbf{g}_{\alpha, \alpha}, \mathbf{g}_{\alpha, \alpha}}$ for **R1**, $\mathbf{R}_{\mathbf{g}_{\alpha}, \mathbf{g}_{\alpha}}$ for **R2**, and $\mathbf{R}_{\mathbf{g}, \mathbf{g}}$ for **R3**. The number of nonzero eigenvalues reflects the diversity order. Note that \mathbf{f} is not Gaussian when phase noise is present. We will rely on simulations to assess system performance in the presence of phase noise.

We note that the constants M_l and M_u determine the number of subcarriers to be jointly processed for decoding a particular subcarrier. Accurate values for M_l and M_u are useful in the context of noisy channel estimation so that the coefficients $\{\tilde{h}(m, n)\}$ other than the expected $M_l + M_u + 1$ nonzero components are explicitly set to zero. This is akin to finger management in RAKE receivers [1]. Including subcarriers outside the $[-M_l, M_u]$ range only picks up noise and degrades system performance. In subsequent sections we compute the relevant statistics for the three receivers for the different imperfections. We also provide estimates for M_l and M_u .

4.4. Reception in the Presence of Fast Fading

When only fast fading is present, $w(t, f_n) = \tilde{c}(t, f_n)$, $f_{off} = 0$ and $\varrho(t) = 0$ in (4.6).

The $\{\tilde{h}(m, n)\}$ in (4.8) are given by [14, 3]

$$\tilde{h}(m, n) = \int_{-B_d}^{B_d} \tilde{C}(\theta, f_n) \text{sinc} \left(\left(\frac{m}{T} - \theta \right) T \right) e^{-j\pi T \left(\frac{k}{T} - \theta \right)} d\theta. \quad (4.29)$$

The correlation function that determines $\mathbf{R}_{f,f}$ is given by

$$\rho(m_1, n_1; m_2, n_2) = e^{-j\pi(m_1 - m_2)} \int_{-B_d}^{B_d} \psi(\theta, \Delta f) \times \text{sinc}\left(\left(\frac{m_1}{T} - \theta\right)T\right) \text{sinc}\left(\left(\frac{m_2}{T} - \theta\right)T\right) d\theta \quad (4.30)$$

where $\Delta f = f_{n_1} - f_{n_2}$ and $\psi(\theta, \Delta f)$ is defined in (4.15). Notice that for a particular subcarrier n , the power captured by the coefficients, $\rho(m, n; m, n)$, is symmetric in m . Thus, $M_l = M_u = M$. Figure 4.4(a) shows the power in $\{\tilde{h}(m, n)\}$, for any given n , and $B_d T = 2$. It is evident that most of the energy (and diversity) is captured by $|m| \leq M = 2$. The expression in (4.29) is a smoothing of $\tilde{C}(\theta, f_n)$ over θ with a sinc function having a null-to-null bandwidth $\frac{1}{T}$. It follows that for any n , $M = \lceil B_d T \rceil$ is a good upper bound on the number of significant subcarriers [14, 3]. For each n , as long as $\{\tilde{h}(m, n), m = -M, \dots, M\}$ are weakly correlated, the proposed receivers **R2** and **R3** would exploit Doppler diversity due to the increase in the rank of $\mathbf{R}_{f,f}$ in **R2** and **R3** over that in **R1**. Thus, **R2** and **R3** provide better performance compared to **R1** by collecting the dispersed energy as well as exploiting Doppler diversity.

Since the level of diversity increases with $B_d T$, the modified MC scheme described in Section 4.2.1 can be used to increase the effective T and hence $B_d T$. However, at higher $B_d T$, the number of strong coefficients M increases as well, thereby, increasing receiver complexity.

4.5. Reception in the Presence of Frequency Offset

We now consider the case when there exists a frequency offset f_{off} between the transmitter and receiver local oscillators (no phase noise). Subcarrier frequency offset causes severe attenuation in each subcarrier as well as ICI between the different subcarriers

(see, e.g., [47]). We consider both slow and fast fading channels.

4.5.1. Frequency Offset Correction in Slow Fading Channels

In this case, $w(t, f_n) = \tilde{c}(f_n)e^{j2\pi f_{off}t}$ in (4.5) and the $\{\tilde{h}(m, n)\}$ in (4.8) are given by

$$\tilde{h}(m, n) = \tilde{c}(f_n)\text{sinc}(m - f_{off}T) e^{-j\pi(m - f_{off}T)}. \quad (4.31)$$

Since most of the dominant coefficients in (4.31) lie in the main lobe of the sinc function, we have

$$M_l = \lceil -f_{off}T \rceil \text{ and } M_u = \lceil f_{off}T \rceil. \quad (4.32)$$

From (4.31), the correlation function of the coefficients is given by

$$\rho(m_1, n_1; m_2, n_2) = e^{-j\pi(m_1 - m_2)} \psi_{\Delta f}(\Delta f) \text{sinc}(m_1 - f_{off}T) \text{sinc}(m_2 - f_{off}T) \quad (4.33)$$

where $\Delta f = f_{n_1} - f_{n_2}$. Figures 4.4(b) shows the energy captured by the m^{th} coefficient at $f_{off}T = 0.8$. It is evident that (4.32) provides a good estimate for the range of dominant coefficients.

We note from (4.33) that in this case, the covariance matrix $\mathbf{R}_{f,f}$ has the same rank for **R1**, **R2** and **R3**. This is because the statistics depend on $\psi_{\Delta f}(\Delta f)$ which does not depend on f_{off} . For any n there is essentially a single dominant coefficient $\tilde{h}(m, n)$ — the frequency offset simply shifts the location of this coefficient. Hence, no additional diversity is available in this case. However, **R2** and **R3** restore the loss in performance encountered by **R1** by collecting the dispersed energy.

4.5.2. Frequency Offset Correction in Fast Fading Channels

In this case $w(t, f_n) = \tilde{c}(t, f_n)e^{j2\pi f_{off}t}$ in (4.5) and

$$\tilde{h}(m, n) = \int_{-B_d}^{B_d} \tilde{C}(\theta, f_n) \text{sinc} \left(\left(\frac{m}{T} - f_{off} - \theta \right) T \right) e^{-j\pi T \left(\frac{m}{T} - f_{off} - \theta \right)} d\theta. \quad (4.34)$$

Following the same argument as in Sections 4.4 and 4.5.1, $M_l = \lceil B_d T - f_{off} T \rceil$ and $M_u = \lceil B_d T + f_{off} T \rceil$. The correlation function of the coefficients is given by

$$\begin{aligned} \rho(m_1, n_1; m_2, n_2) &= e^{-j\pi(m_1 - m_2)} \int_{-B_d}^{B_d} \psi(\theta, \Delta f) \text{sinc} \left(\left(\frac{m_1}{T} - f_{off} - \theta \right) T \right) \\ &\quad \times \text{sinc} \left(\left(\frac{m_2}{T} - f_{off} - \theta \right) T \right) d\theta. \end{aligned} \quad (4.35)$$

Figures 4.4(c) show the distribution of energy over k for $B_d T = 2$ and $f_{off} T = 0.8$. In this case, the proposed receiver **R2** and **R3** not only restore the loss in performance due to frequency offset, but yield further improvement due to Doppler diversity.

4.6. Reception in the Presence of Phase Noise

We consider slow fading for simplicity in this case. As reported in many papers (see, e.g., [39, 40, 41, 42]), the performance of OFDM systems degrades severely in the presence of phase noise and frequency offsets. Phase noise is particularly serious problem when relatively low-cost tuners are employed at the receiver.

In this case, the received signal can be expressed as

$$r(t) = b_1 \sum_{n=1}^N a_n \tilde{c}(f_n) q(t) e^{j2\pi f_n t} e^{j\varrho(t)} + n(t) = b_1 x(t) e^{j\varrho(t)} + n(t) \quad (4.36)$$

where $\varrho(t)$ is modeled as Brownian motion (or Wiener-Lévy) process with zero mean and variance $2\pi B_o t$ [41, 48, 49]. If the phase noise realization is known at the receiver along with the channel coefficients $\{\tilde{c}(f_n)\}$, the optimal decision statistic is

$$\zeta = \int_0^T x^*(t) e^{-j\varrho(t)} r(t) dt = b_1 \int_0^T |x(t)|^2 dt + \int_0^T x^*(t) n(t) dt, \quad (4.37)$$

which cancels phase noise and there is no loss in performance. In our framework $w(t, f_n) = \tilde{c}(f_n)e^{je(t)}$ in (4.5) and the coefficients $\{\tilde{h}(m, n)\}$ in the model (4.11) are given by

$$\tilde{h}(m, n) = \frac{1}{T}\tilde{c}(f_n)G(m/T) = \frac{1}{T}\tilde{c}(f_n) \int_0^T e^{je(t)} e^{-j\frac{2\pi mt}{T}} dt. \quad (4.38)$$

The performance can be restored by processing the discrete frequencies in (4.38) as opposed to the continuous processing in (4.37).

We note that \mathbf{f} in (4.26) is no longer Gaussian in this case. Hence, the system performance does not only depend on $\mathbf{R}_{\mathbf{f}, \mathbf{f}}$ but rather on higher order statistics as well. However, the correlation function $\rho(m_1, n_1; m_2, n_2)$ can be used to determine the number of coefficients $\{\tilde{h}(m, n)\}$ needed to capture the dispersed energy.

The correlation function of $\{\tilde{h}(m, n)\}$ given in (4.38) is given by

$$\rho(m_1, n_1; m_2, n_2) = \frac{1}{T^2} \psi_{\Delta f}(\Delta f) \varphi(m_1, m_2) \quad (4.39)$$

where $\Delta f = f_{n_1} - f_{n_2}$, $\psi_{\Delta f}(f_{n_1} - f_{n_2})$ is defined in Section 2.2 and

$$\begin{aligned} \varphi(x, y) &= \mathbb{E} \left[G\left(\frac{x}{T}\right) G^*\left(\frac{y}{T}\right) \right] = \mathbb{E} \left[\int_0^T \int_0^T e^{j(\varrho(t) - \varrho(u))} e^{-j\frac{2\pi(xt - yu)}{T}} dt du \right] \quad (4.40) \\ &= \frac{T^2}{\pi^2} \frac{\gamma (e^{j2\pi(y-x)} - 1)}{j(\gamma^2 + 4x^2)(y-x)} \\ &\quad + \frac{T^2}{\pi^2} \frac{(\gamma^2 - 4xy) (e^{-\pi(\gamma - j2y)} - e^{-j2\pi(y-x)} + e^{-\pi(\gamma + j2x)} - 1)}{(\gamma^2 + 4x^2)(\gamma^2 + 4y^2)} \\ &\quad + \frac{T^2}{\pi^2} \frac{j2\gamma(x+y) (e^{-\pi(\gamma - j2y)} + e^{-j2\pi(y-x)} - e^{-\pi(\gamma + j2x)} - 1)}{(\gamma^2 + 4x^2)(\gamma^2 + 4y^2)} \quad (4.41) \end{aligned}$$

where $\gamma = B_o T$. We have used (4.13) and (4.16) in (4.40). The expression in (4.41) is derived as follows. For a particular t, u , $\varrho(t) - \varrho(u)$ is a Gaussian random variable with zero mean and variance $2\pi B_o |t - u|$. It can be shown that

$$\mathbb{E} \left[e^{j(\varrho(t) - \varrho(u))} \right] = e^{-\pi B_o |t - u|}, \quad (4.42)$$

that is, the characteristic function of $\varrho(t) - \varrho(u)$ evaluated at a particular point. Substituting (4.42) in (4.40), and after some algebraic manipulations we reach the expression in (4.41).

We use $\rho(m_1, n_1; m_2, n_2)$ to estimate M_l and M_u . The power in the coefficients is proportional to

$$\varphi(x, x) = \frac{2T^2}{\pi} \left\{ \frac{\gamma}{\gamma^2 + 4x^2} - \frac{(\gamma^2 - 4x^2)}{\pi(\gamma^2 + 4x^2)^2} + \frac{e^{-\pi\gamma}}{\pi} \left[\frac{(\gamma^2 - 4x^2) \cos(2\pi\gamma) - 4\gamma x \sin(2\pi\gamma)}{(\gamma^2 + 4x^2)^2} \right] \right\}. \quad (4.43)$$

Special case of (4.41) for integer variables m_1, m_2 is

$$\varphi(m_1, m_2) = \frac{2T^2}{\pi^2} \frac{(\gamma^2 - 4m_1 m_2) (e^{-\pi\gamma} - 1)}{(\gamma^2 + 4m_1^2) (\gamma^2 + 4m_2^2)} \quad (4.44)$$

and the corresponding power at $m_1 = m_2 = m$ is

$$\varphi(m, m) = \frac{2T^2}{\pi} \left[\frac{\gamma}{(\gamma^2 + 4m^2)} - \frac{(\gamma^2 - 4m^2)(1 - e^{-\pi\gamma})}{\pi(\gamma^2 + 4m^2)^2} \right]. \quad (4.45)$$

Figure 4.5(a) shows the normalized energy captured by the coefficients on a symbol duration T as a function of the coefficient index m . As evident, the energy of the coefficients is symmetric around $m = 0$. Hence, $M_l = M_u = M$. The function $\varphi(m, m)$ in (4.45) does not have a zero for any finite m , but it is monotonically decreasing with m . One way to choose M is so that only those $\{\tilde{h}(m, n)\}$ are included whose normalized power is above some preset threshold $\epsilon > 0$. Figure 4.5(b) shows M as a function of $B_o T$ for different threshold values.

As mentioned earlier, due to non-Gaussianity of phase noise, the expression of P_e in (4.28) is no longer valid. In this case we assess system performance via simulations.

4.7. Numerical Results

We now compare the performance of the proposed receiver **R2** and **R3** relative to conventional receiver **R1** via various examples emphasizing different types of imperfections. Examples 1,2,3 and 4 are based on a system with a signature code of length $N = 64$ (only active subcarriers are used for transmission). In Example 5, all the subcarriers are used for transmission corresponding to a signature code of length $P = 127$. We consider a WSSUS channel model with $L = 6$ resolvable paths. All the results correspond to BPSK signaling and we assume perfect knowledge of \mathbf{f} at the receiver. System performance is compared in terms of P_e as a function of the parameters, B_dT , $f_{off}T$ and B_oT . The separability assumption in (2.2) is used in Examples 1 and 3. In Examples 1,2 and 3 (based on analytical results), the P_e computation for **R1** ignores ICI and is thus a lower bound on the P_e of the conventional receiver operating in the presence of imperfections. In Examples 4 and 5, Monte-Carlo simulations are used to assess system performance in the presence of phase noise. In these examples, the effects of ICI are included in **R1** as well.

EXAMPLE 1

We compare the three receivers in fast fading channels ($B_dT > 0$, $f_{off}T = 0$ and $B_oT = 0$), $SNR = 10dB$, and $M = 5$ which is sufficient to capture the signal energy. Perfect knowledge of \mathbf{f} automatically takes care of insignificant coefficient in the range $-M, M$. The coefficients corresponding to the n^{th} active subcarrier are $\{\tilde{h}(n-2,4), \tilde{h}(n-1,2), \tilde{h}(n,0), \tilde{h}(n+1,-2), \tilde{h}(n+2,-4)\}$, whereas those corresponding to the n^{th} inactive subcarrier are $\{\tilde{h}(n-2,5), \tilde{h}(n-1,3), \tilde{h}(n,1), \tilde{h}(n+1,-1), \tilde{h}(n+2,-3), \tilde{h}(n+3,-5)\}$. Figure 4.6(a) shows the performance of the three receivers as a function of B_dT . The P_e of the conventional receiver **R1** increases monotonically with increasing B_dT . The

performance of **R2** shows modest improvement up to $B_dT \approx 1$, but then considerable improvement beyond $B_dT = 1$. This because **R2** only uses the active subcarriers. The performance of **R3** which uses both the active and inactive subcarriers is the best. Note that both **R2** and **R3** show improved performance relative to the conventional receiver under slow fading ($B_dT = 0$). This is due Doppler diversity. The gains due to Doppler diversity becomes significant for $B_dT > 0.05$ which may not be directly attainable in existing systems. However, the modified MC-CDMA system can be used to exploit Doppler diversity by effectively increasing B_dT , analogous to the schemes in [3, 34].

EXAMPLE 2

This example compares the performance of the receivers in the presence of frequency offset in a slowly fading channel (i.e. $B_dT = 0$, $f_{off}T > 0$ and $B_oT = 0$), $SNR = 10dB$ and $M_l = M_u = 5$. Figure 4.6(b) shows the performance as a function of $f_{off}T$. The degradation in the performance of the conventional receiver **R1** with increasing in $f_{off}T$ is evident. The performance based on **R2** shows a severe degradation as well up to $f_{off}T = 1$, beyond within the receiver shows significant improvement. The reason is that for $1 < f_{off}T < 2$, most of the energy lost in the n^{th} subcarrier due to frequency offset is dispersed into the $\{n + 1^{th}, n + 2^{th}\}^4$ subcarriers. Since, **R2** collects energy for $n \pm 2$ and not for $n \pm 1$, it does not collect the dispersed energy until $f_{off}T > 1$. Note also that the P_e for **R2** is maximum at $f_{off}T = 1$ because **R2** only processes the active subcarriers and, thus, if the received signal is offset by $\frac{1}{T}$, it will be orthogonal to all active subcarriers. The performance of **R3** is constant, unaffected by the increase of $f_{off}T$, since it processes both the active and inactive subcarriers. Thus, **R3** fully

⁴If $f_{off} < 0$ the energy will be dispersed on $\{n - 1^{th}, n - 2^{th}\}$ subcarriers.

restores the performance to the offset-free case. However, there is no diversity gain in this case.

EXAMPLE 3

This example considers effects of frequency offset in a fast fading channel (i.e. $B_dT > 0$, $f_{off}T > 0$ and $B_oT = 0$), $SNR = 10dB$ and $M_l = M_u = 5$. Figure 4.7(a) shows the performance as a function of B_dT for fixed $f_{off}T = 0.3$. Comparing the figure to Figure 4.6(a), it is clear that the performance of **R2** and **R3** show a similar trend with **R2** showing some loss due to frequency offset. Figure 4.7(b) shows the performance as a function of $f_{off}T$ at $B_dT = 0.3$. Comparing with Figure 4.6(b), it is clear that in addition to correcting for the frequency offset, **R3** delivers improved performance due to Doppler diversity.

EXAMPLE 4

This example compares the receivers in the presence of phase noise in a slowly fading channel (i.e. $B_dT = 0$, $f_{off}T = 0$ and $B_oT > 0$), $SNR = 10dB$, and $M = 10$. The results are based on Monte-Carlo simulations over 50,000 iterations. Figure 4.8(a) shows the system performance as a function of B_oT . The severe deterioration in performance of **R1** is evident. **R2** performs better than **R1**. However, since **R2** collects only part of the energy, there is a degradation in performance compared to the ideal case with no phase noise ($B_oT = 0$). The performance of **R3** is almost unaffected even at higher values of B_oT because **R3** collects all the dispersed energy ($M = 10$ is sufficiently large for the considered values of B_oT).

Figure 4.8(b) assesses receiver performance as a function of M at $B_oT = 0.8$ for **R2** and **R3**. We see that the performance almost saturates after $M = 2$. This approximation corresponds to a threshold $\epsilon = 0.08$. This suggests that a relatively small subset of M

subcarriers in (4.38) is sufficient to restore the loss in performance due to moderate phase noise.

EXAMPLE 5

This example is an extension of Example 4 when all the subcarriers are used for transmission. As mentioned before, in this case, **R2** and **R3** become identical since all the subcarriers are active. In Figure 4.8(c), the performance of the proposed receiver is compared to **R1** as a function of B_oT . Similar to the results in Figure 4.8(a), the proposed receiver is almost unaffected by phase noise.

4.8. Alternative Representation

In this section we revisit the receiver structure presented in this paper from a different but equivalent point of view. We only focus on fast fading imperfection, similar arguments follow for other types of imperfections as well.

We start by introducing the concept of Block Fading (BF) for MC-CDMA systems. First assume a frequency selective slowly fading channel. The BF assumption relies on the fact that if the frequency selective channel exhibits L multipaths, then the channel has only that many degrees of freedom. That is, the covariance matrix of the different channel coefficients has a rank L . In other words, the channel coefficients can be divided into L groups, where those coefficients in the same group are highly correlated. The BF assumption goes beyond the statistic correlation to assume that if we group the coefficients into N_1 groups sufficiently larger than L , then those $N_2 = \lceil \frac{N}{N_1} \rceil$ coefficients in the same group are faded similarly. Similar argument holds for MC-CDMA system in frequency selective fast fading channels at a given time instant t or equivalently at a given Doppler shift m . More precisely, if the set of indices of subcarriers in the

i^{th} sub-band is Ω_i , $i = 0, 1, \dots, N_1 - 1$, then under BF assumption (recall (4.29)), $\tilde{h}(m, n) \approx \tilde{h}(m, i) \forall n \in \Omega_i$. Now recall (4.8), under BF, the received signal can be alternatively written as

$$r(t) = b_1 \sum_{i=1}^{N_1} \sum_{m=-M_i}^{M_u} \tilde{h}(m, i) \varrho_i(t) e^{\frac{j2\pi mt}{T}} + n(t) \quad (4.46)$$

where $\varrho_i(t) = \sum_{n \in \Omega_i} a_n q(t) e^{j2\pi f_n t}$. In view of (4.46), it is clear that Doppler dispersion is manifested in MC-CDMA systems over time and frequency selective channel as multiple Doppler components per sub-band. This is analogous to DS-CDMA system in frequency selective slow fading channel that encounters multipath components in the time domain except for having positive and negative Doppler shifts as oppose to multipaths shift which are only positive.

It is known [1] that the optimal receiver in DS-CDMA system over frequency selective channel is a Rake receiver that captures the energy dispersed in the different multipaths and exploits Doppler diversity. Building on the analogy explained above, we can see that the optimal receiver in MC-CDMA system over time and frequency selective channel is a Rake receiver per sub-band in the frequency domain that captures the energy dispersed in the different Doppler components and exploits Doppler diversity. In fact, the receiver introduced in this chapter under BF is equivalently a Rake receiver per sub-band in the frequency domain.

In Chapter 6, we revisit the analogy shown in this section when we introduce a general framework that includes a class of CDMA systems operating over different types of channels.

4.9. Conclusion

We have proposed an integrated receiver for MC-CDMA system operating in the presence of commonly encountered imperfections — frequency offsets, fast fading and phase noise. The receiver structure is based on a canonical model for the received signal in terms of subcarrier basis functions that capture the effect of all imperfections. In the case of frequency offset and phase noise, the proposed receiver fully restores the loss in performance of the conventional receivers. The proposed receiver also eliminates the need to estimate the frequency offset, an approach often proposed in existing alternatives. In the presence of fast fading, the proposed receiver actually delivers improved performance by exploiting Doppler diversity. Our results demonstrate that significant gains in performance can be attained with little increase in complexity. The receiver structure proposed in this paper can be easily extended to different MC systems including the modified MC-CDMA system and the MC-TDMA system [50].

4.10. Figures

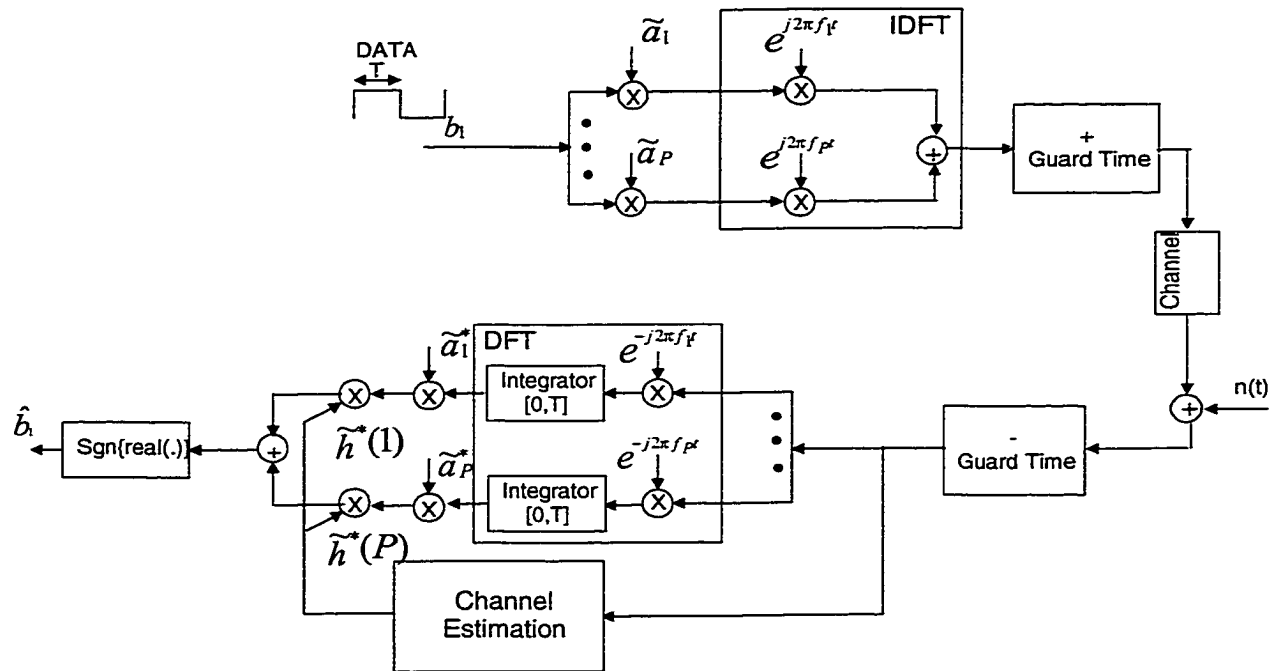


Figure 4.1. The MC-CDMA transmitter.

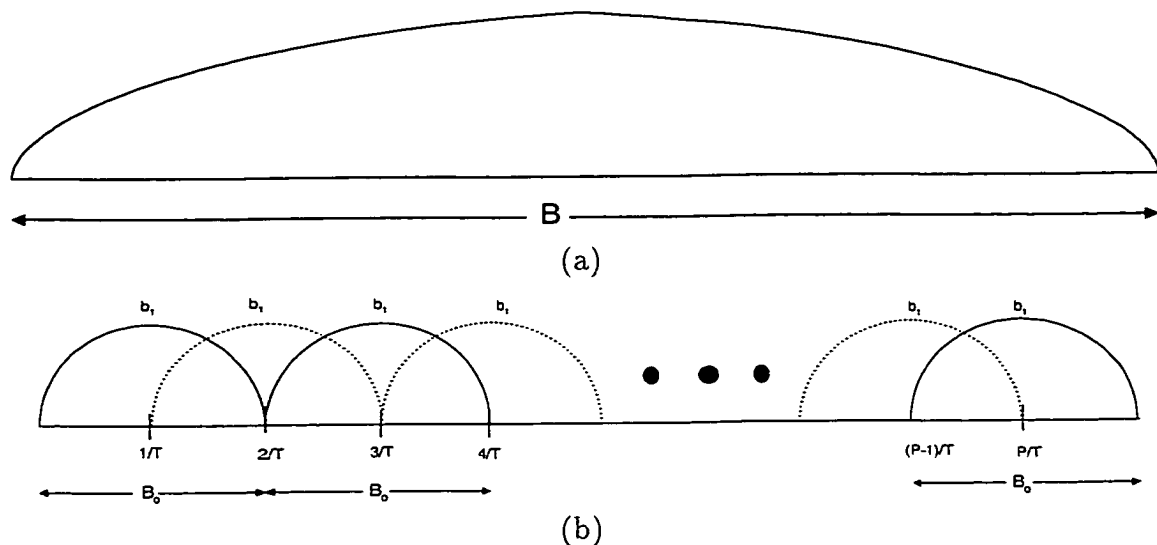


Figure 4.2. (a) The spectrum of SC-CDMA signal. (b) The spectrum of a MC-CDMA signal.

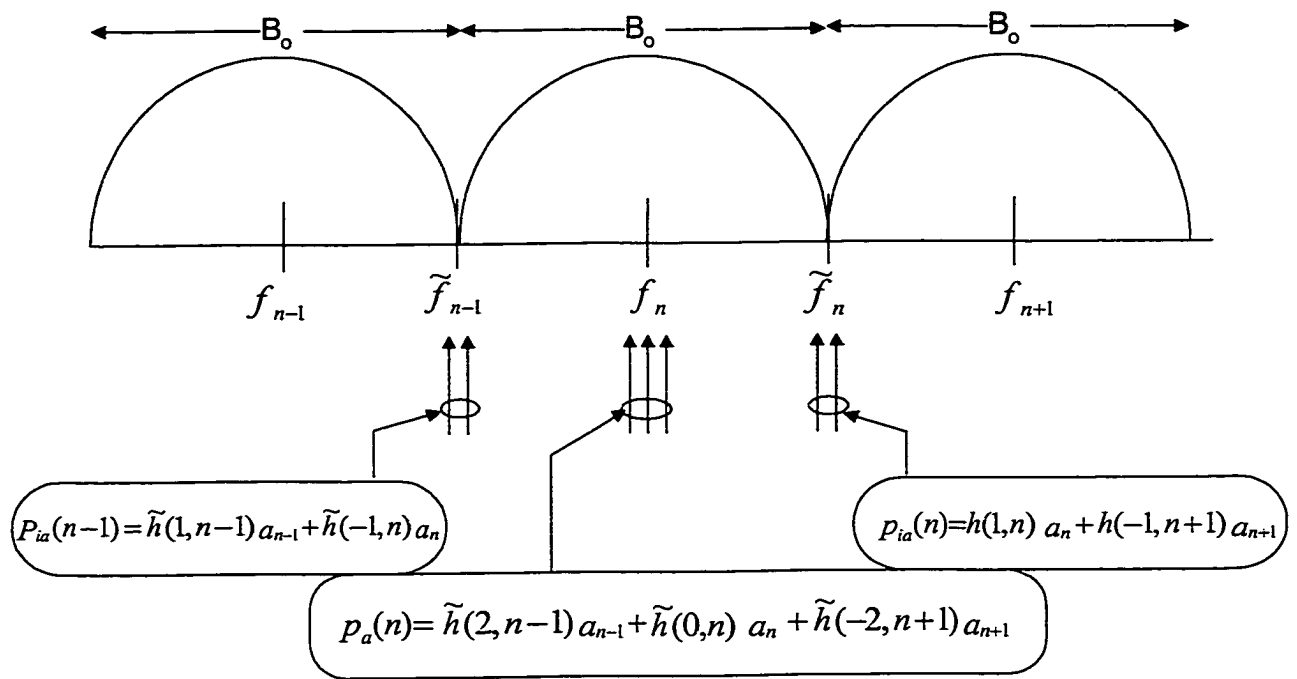


Figure 4.3. Coefficients associated with the the active and inactive subcarriers at the receiver for $M_l = M_u = 2$.

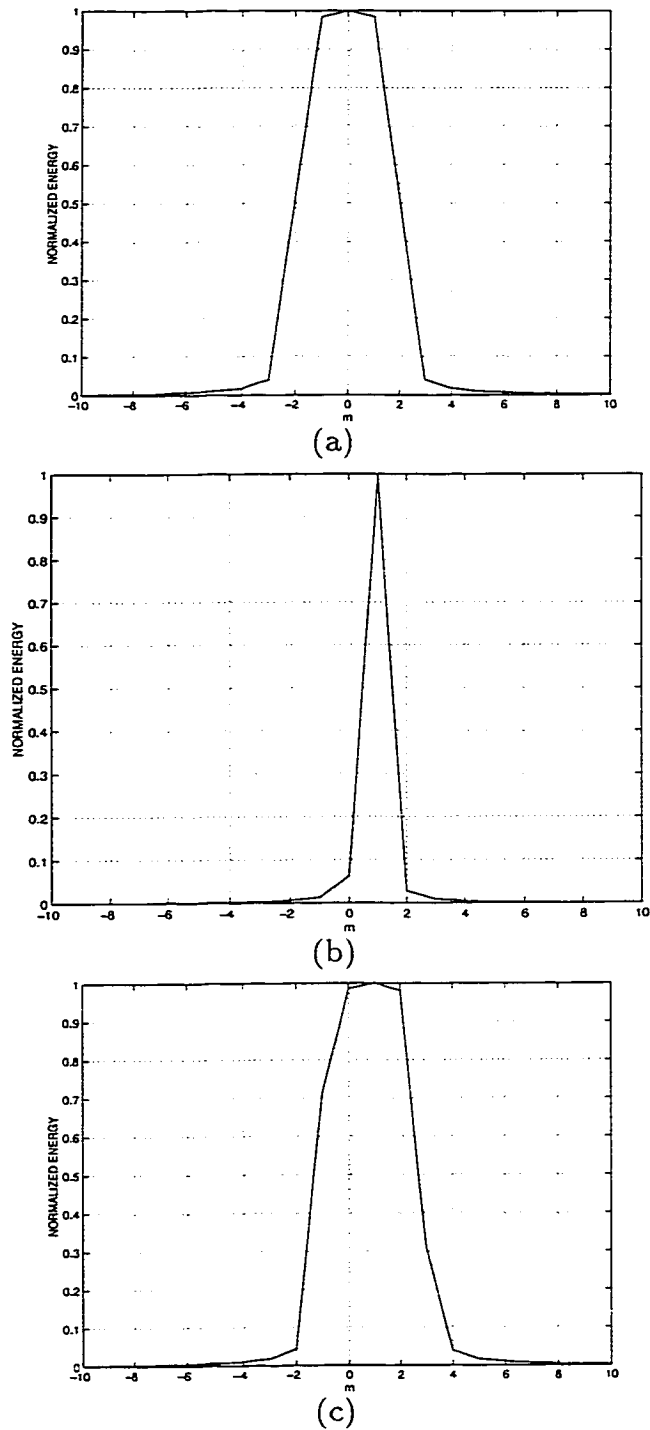
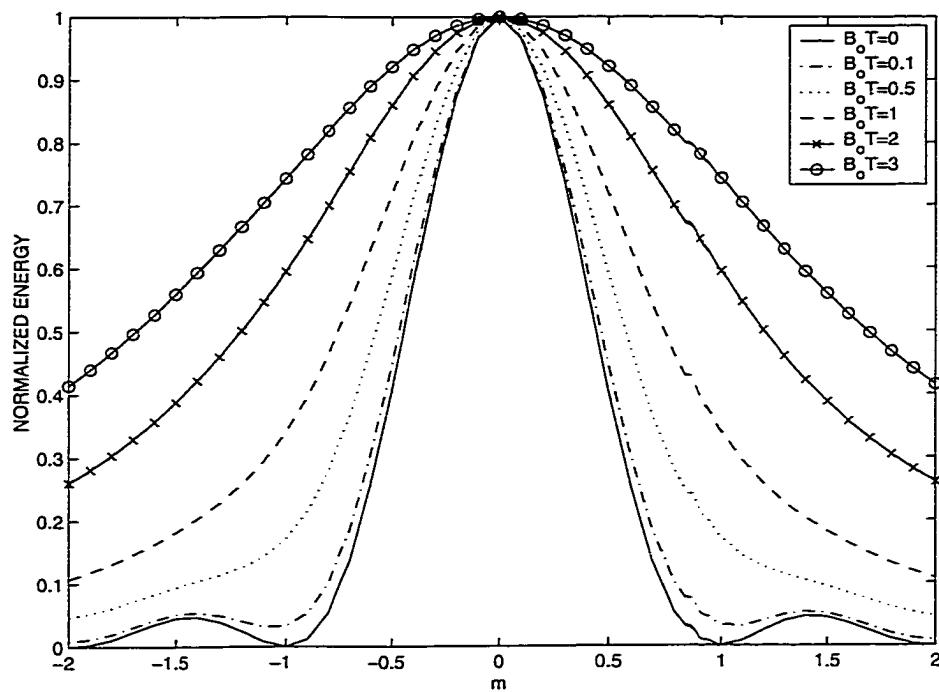
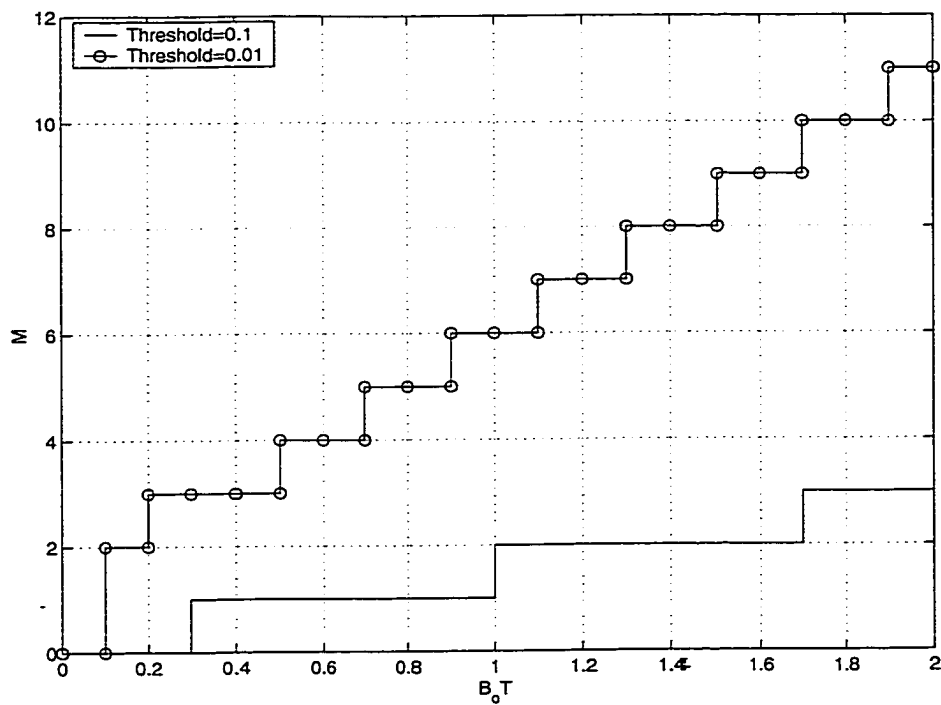


Figure 4.4. The normalized energy captured by the m^{th} coefficient. (a) Fast fading channels with $B_d T = 2$. (b) Slowly fading channel in the presence of frequency offset with $f_{off} T = 0.8$. (c) $B_d T = 2$, $f_{off} T = 0.8$.



(a)



(b)

Figure 4.5. (a) Normalized energy captured by the m^{th} coefficient in the presence of phase noise. (b) The number of coefficients M whose normalized power exceeds a threshold $\epsilon = 0.1, 0.01$ as a function of $B_o T$.

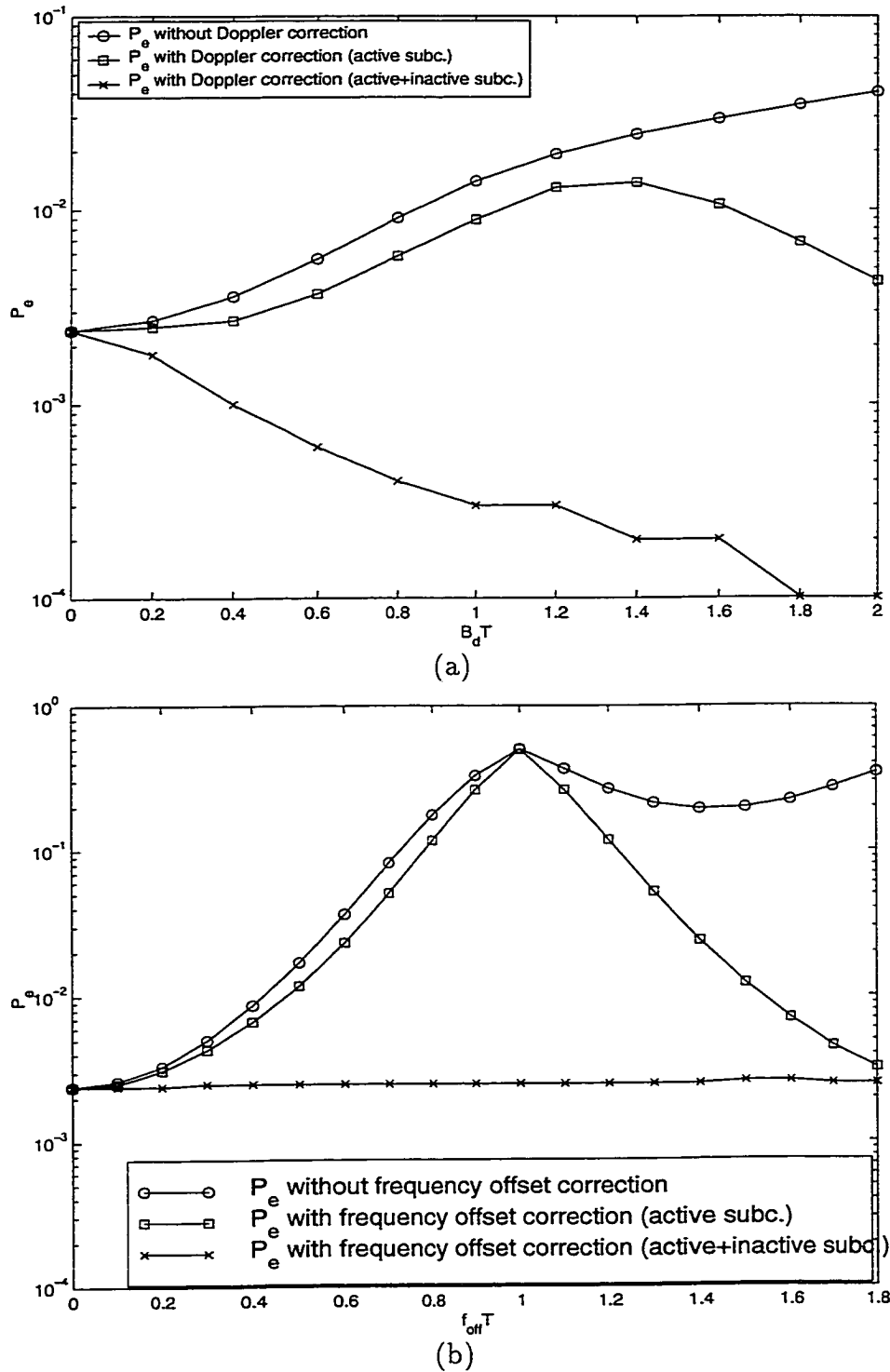


Figure 4.6. (a) System performance as a function of fast fading parameter $B_d T$ at $SNR = 10dB$. (b) System performance as a function of frequency offset parameter $f_{off} T$ at $SNR = 10dB$.

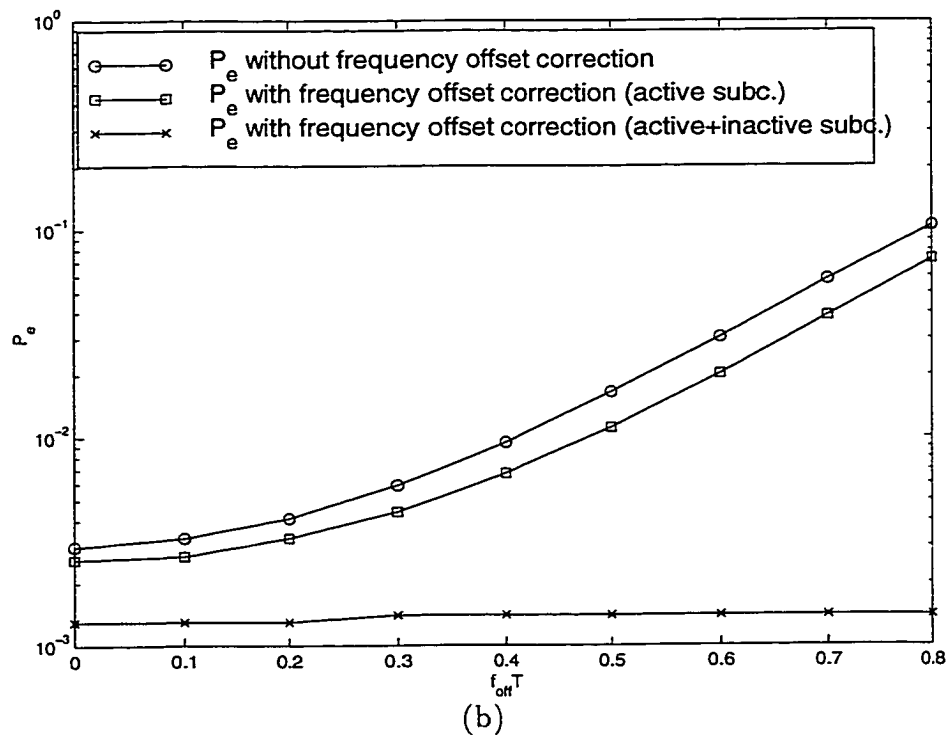
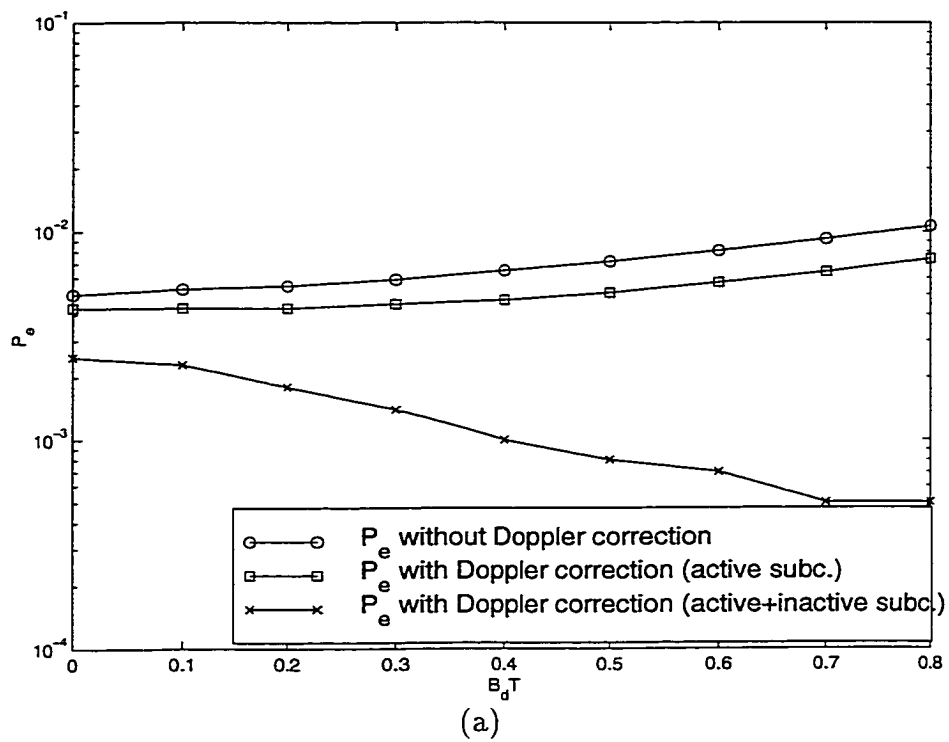
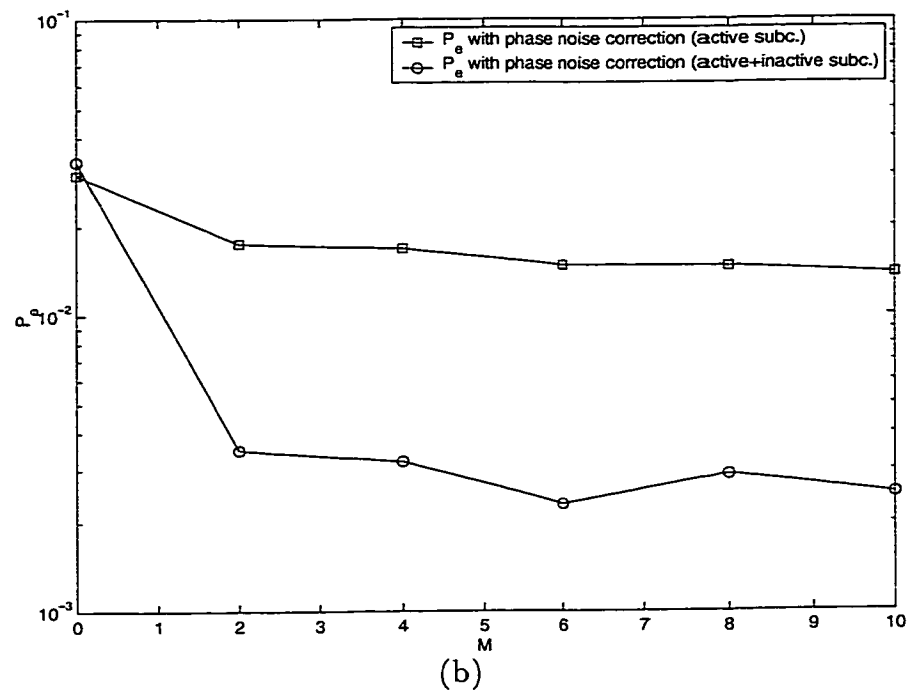
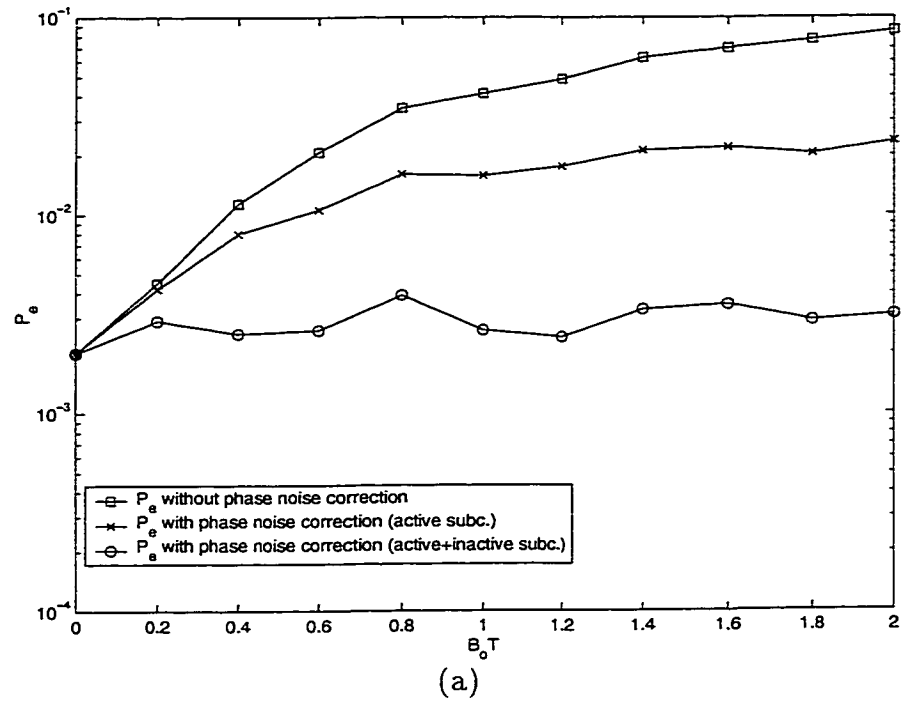


Figure 4.7. (a) System performance as a function of $B_d T$ at $SNR = 10dB$ and $f_{off} T = 0.3$.
 (b) System performance as a function of $f_{off} T$ at $SNR = 10dB$ and $B_d T = 0.3$.



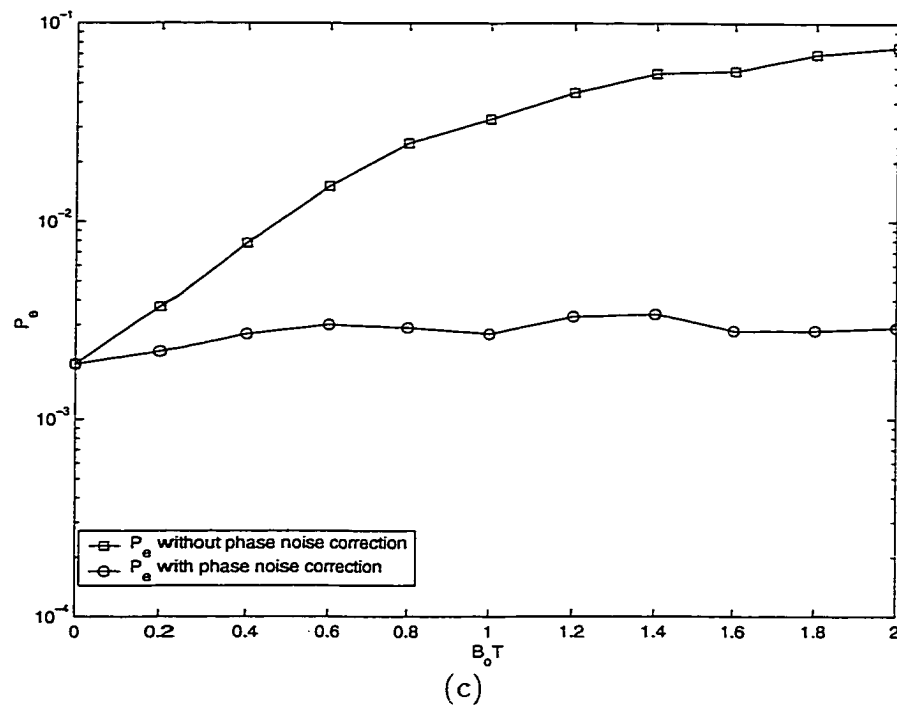


Figure 4.8. Receiver performance in the presence of phase noise at $SNR = 10dB$. (a) P_e as a function of B_oT for $M=10$. (b) P_e as a function of M for $B_oT = 0.8$. (c) Same as (a) when all subcarriers are used for transmission.

CHAPTER 5

A NEW SIGNALING SCHEME FOR TIME AND FREQUENCY DISPERSIVE CHANNELS

5.1. Introduction

Multicarrier (MC)- Code Division Multiple Access (CDMA) systems operating over slowly time-varying frequency selective channels transmit information over a set of orthogonal subcarriers (Fourier basis functions), each supporting a low rate stream and encountering flat fading. Since Fourier basis functions are eigenfunctions of time-invariant channels, MC signaling diagonalizes the channel and converts the slow fading frequency selective channel into parallel flat fading channels. This reduces the effect of inter symbol interference (ISI) and, in conjunction with a cyclic prefix, eliminates the need for equalization. It is advantageous to increase the symbol duration in each subcarrier as much as possible to reduce the effects of ISI, particularly in high rate applications. However, as the symbol duration increases, the system becomes more prone to temporal distortions in time-varying (fast fading) situations. The subcarriers encounter spectral dispersion under fast fading channels that destroys the orthogonality between the subcarriers and significantly degrades performance [44].

In the previous chapter, we introduced a reception model and a receiver structure in time-varying channels that captures the loss in performance due to imperfections and exploits diversity. The underlying signaling scheme used in the previous chapter was the MC-CDMA system that adopts the Fourier basis waveforms for transmission. Since the Fourier basis are not the eigenfunctions for time-varying channels, the channel matrix (i.e. the matrix that relates the input to the output of the channel) is not

diagonal and the introduced receiver in Chapter 4 is an equalizer that mitigates the effects of imperfections and exploit Doppler diversity. In this chapter, we focus on fast fading channels (we assume no frequency offset or phase noise) and introduce a second scheme for time and frequency selective channels. In particular, we introduce a new signaling scheme based on time-frequency basis functions that approximately diagonalize time-varying frequency selective channels — the basis functions serve as approximate eigenfunctions of the channel and each basis function encounters non-selective fading. The signaling scheme uses time-frequency basis functions whose time-frequency support is matched to the coherence time and bandwidth of the channel. We discuss the necessary conditions for such channel diagonalization to be possible and derive optimal basis parameters that yield the most accurate diagonalization for given multipath and Doppler spreads of the channel. The proposed scheme thus facilitates optimal exploitation of the diversity afforded by the channel. We denote this scheme by the Time (T) Frequency (F)- CDMA system. At the end of the chapter, we show an intuitive connection between the MC-CDMA system introduced in Chapter 4 and that introduced in this chapter. In particular, we show that under Block Fading (BF) (as defined in Chapter 4) and per sub-band, the MC-CDMA and TF-CDMA systems over fast fading frequency selective channels resemble Direct Sequence (DS)-CDMA and MC-CDMA systems over slow fading frequency selective channel respectively.

The next section describes the proposed time-frequency signaling scheme. Optimal choice of basis parameters is derived in Section 5.3. Section 5.4 analyzes the performance of a coherent receiver for the proposed signaling scheme. Section 5.5 provides an intuitive mapping between the MC-CDMA and TF-CDMA systems over fast fading channels, and, the DS-CDMA and MC-CDMA systems over slow fading channels

respectively. Concluding remarks are provided in Section 5.6.

5.2. Time-Frequency Signaling

Let T denote the symbol duration and B the essential two-sided bandwidth occupied by each symbol waveform. The dimension of the signal space is approximately equal to the time-bandwidth product: $N = BT$. We consider a wide sense stationary uncorrelated scattering (WSSUS) channel model with multipath spread, T_m , and the one-sided Doppler spread, B_d defined in Section 2.2. The level of multipath diversity is $L+1$ where $L = \lceil T_m B \rceil$ and level of Doppler diversity is $2M+1$, where $M = \lceil B_d T \rceil$. Consider signaling with N basis functions spanning the signal space. All basis functions have the same support in time and frequency: T_o and B_o respectively. Figure 5.2 illustrates the conventional MC-CDMA (Fourier) signaling for slow fading channels and the proposed time-frequency signaling for fast fading channels. In slowly fading scenarios, the channel response is constant over the symbol duration T . Thus, in conventional MC-CDMA signaling, $T_o = T$ and the information is transmitted over N orthogonal subcarriers in parallel, each with bandwidth $B_o = B/N = 1/T$. Together, the N Fourier basis functions cover the entire bandwidth, as illustrated in Figure 5.2(a). The symbol duration $T = T_o$ is chosen long enough so that $B_o = 1/T \ll \Delta f_c$ and each carrier encounters flat fading. The transmitted signal in conventional MC-CDMA systems can be written as

$$\tilde{s}(t) = b \sum_{n=0}^{N-1} a_n q_T(t) e^{j \frac{2\pi n}{T} t} \quad (5.1)$$

where b is the transmitted bit, $\{a_n\}$ is the CDMA signature code, and $q_T(t)$ is the normalized pulse shape of duration T , assumed rectangular for simplicity: $q_T(t) =$

$$\frac{1}{\sqrt{T}}, \quad -T/2 \leq t \leq T/2.$$

In rapidly time-varying situations, the channel response is no longer constant over the symbol duration and the temporal distortion destroys the orthogonality between subcarriers and degrades performance [44]. We propose signaling with time-frequency basis functions that avoids distortion in both time and frequency by appropriately choosing T_o and B_o according to Δt_c and Δf_c . The TF-CDMA transmitter is shown in Figure 5.1 and the transmitted signal using the time-frequency basis functions is

$$s(t) = b \sum_{n=0}^{N_f-1} \sum_{p=0}^{N_t-1} a_{n,p} u_{n,p}(t) \quad (5.2)$$

where $\{a_{n,p}\}$ is the length N signature code distributed over the $N = N_t N_f$ basis functions

$$u_{n,p}(t) = q_{T_o}(t - pT_o) e^{j2\pi n B_o t}. \quad (5.3)$$

As illustrated in Figure 5.2(b), $N = N_t N_f$ time-frequency basis functions in (5.3) are generated by N_t time shifts and N_f frequency shifts of the prototype signal $q_{T_o}(t)$ of duration $T_o = T/N_t$ and bandwidth $B_o = B/N_f$.

The choice of T_o and B_o is made so that each basis function (5.3) encounters approximately flat fading. Essentially, T_o has to be sufficiently small compared to Δt_c and B_o has to be sufficiently small compared to Δf_c . More precisely, T_o and B_o need to satisfy the following symmetric conditions:

$$\begin{aligned} \mathbf{C1} : \max\left(\frac{1}{B}, T_m\right) &\ll T_o \ll \min\left(\frac{1}{2B_d}, T\right) \quad \text{or, equivalently} \\ &\max(2TB_d, 1) \ll N_t = \frac{T}{T_o} \ll \min\left(\frac{T}{T_m}, N\right) \\ \mathbf{C2} : \max\left(\frac{1}{T}, 2B_d\right) &\ll B_o \ll \min\left(\frac{1}{T_m}, B\right) \quad \text{or, equivalently} \\ &\max(T_m B, 1) \ll N_f = \frac{B}{B_o} \ll \min\left(\frac{B}{2B_d}, N\right) \end{aligned} \quad (5.4)$$

Note that the above conditions imply

$$\max\left(\frac{1}{N}, 2T_m B_d\right) \ll T_o B_o \ll \min\left(\frac{1}{2T_m B_d}, N\right) \quad (5.5)$$

which can be satisfied only for *underspread* channels [51] for which $2T_m B_d < 1$. For most practical channels, $2T_m B_d \ll 1$. In this paper, we focus on the case where $T_o B_o = 1 \Leftrightarrow N = N_t N_f$, for which **C1** and **C2** become equivalent.

We note that the proposed time-frequency signaling can be efficiently implemented digitally by dividing the N samples in each symbol into N_t segments, each containing N_f samples, and applying an N_f -point discrete Fourier transform to each segment. A digital implementation for the system is shown in Figure 5.3. One can see that the transceiver structure is basically a MC-CDMA one accompanied with a sort of pre-processing at the transmitter and post-processing at the receiver. In particular, recalling Figure 5.3, in the MC-CDMA transceiver, the data frame of length N samples pass by Inverse Discrete Fourier Transform (IDFT) operation then a cyclic prefix Cp_t is added to correct for multipath dispersion. Cp_t should be longer than L . The transmitted signal then passes by the channel and at the receiver the Cp_t is removed and a DFT operation is performed to extract the data. For slow fading channels, the extracted data after the DFT operation is the transmitted data point-wise multiplied by a fading coefficient due to channel in addition to the Additive White Gaussian Noise (AWGN) term (i.e. the channel matrix is diagonal). On the other hand, in fast fading channels, the received data per subcarrier after the DFT operation suffers interference from the other subcarriers due to time selectivity. Now, the TF-CDMA transceiver restores the diagonal nature of the system by pre-processing the data fed to the MC-CDMA transmitter. The N samples of a data symbol is divided into N_t groups each contains N_f samples and an N_f -point DFT operation is performed per

group. A cyclic prefix Cp_f is added to correct for Doppler dispersion which should be longer than $2M + 1$. The N_t groups are stacked together to form the data frame to be fed to the MC-CDMA transceiver.¹ At the receiver, a counter process takes place and the overall channel is now diagonal.

5.3. Near-Optimal Choice of T_o and B_o

For given pulse shape, the time-frequency basis functions (5.3) are completely determined by T_o and B_o . In this section, we discuss the optimal choice of T_o and B_o for the case $T_o B_o = 1$ so that the time-frequency basis functions yield the most accurate approximate diagonalization of the channel with each basis function encountering approximately flat fading. The problem boils down to finding the optimal T_o subject to the condition C1. We first discuss some assumptions on channel statistics and then derive a representation for the received signal in terms of the time-frequency basis functions which is then used to derive optimal T_o and B_o .

The received signal can be written as

$$r(t) = \int \tilde{c}(t, f) S(f) e^{j2\pi ft} df + n(t) \quad (5.6)$$

where $S(f)$ is the Fourier transform of the transmitted signal, $\tilde{c}(t, f)$ is defined in (2.1) and $n(t)$ is AWGN with power spectral density σ^2 . Under the WSSUS assumption, the correlation function of $\tilde{c}(t, f)$ is given by $\phi(\Delta t, \Delta f)$ which is defined in Section 2.2 and as seen in (2.2) is separable if all multipaths have the same *spaced-time* correlation function $\phi_{\Delta t}(\Delta t)$ (also defined in Section 2.2) [15]. We also assume a flat Doppler and multipath power profile: $\Phi_{\theta}(\theta) = \frac{1}{2B_d}$, $-B_d \leq \theta \leq B_d$ and $\Psi_{\tau}(\tau) = \frac{1}{T_m}$, $0 \leq \tau \leq T_m$,

¹One can see that this process basically transmits the data over short-time Fourier basis.

under this assumption

$$\phi_{\Delta t}(\Delta t) = \text{sinc}(2B_d\Delta t) \quad , \quad \psi_{\Delta f}(\Delta f) = \text{sinc}(T_m\Delta f) e^{-j\pi T_m\Delta f}. \quad (5.7)$$

For the proposed signaling scheme (5.2), the received signal in (5.6) can be expressed as

$$r(t) = b \sum_{n=0}^{N_f-1} \sum_{p=0}^{N_t-1} a_{n,p} \int_{(n-1/2)B_o}^{(n+1/2)B_o} \tilde{c}_{n,p}(t, f) U_{n,p}(f) e^{j2\pi ft} df + n(t) \quad (5.8)$$

where $U_{n,p}(f) = \int_{-\infty}^{\infty} u_{n,p}(t) e^{-j2\pi ft} dt$ and

$$\tilde{c}_{n,p}(t, f) = \tilde{c}(t, f) I_{[(p-1/2)T_o, (p+1/2)T_o]}(t) I_{[(n-1/2)B_o, (n+1/2)B_o]}(f) \quad (5.9)$$

denotes the part of $\tilde{c}(t, f)$ affecting $u_{n,p}(t) = q(t - pT_o) e^{j2\pi n B_o t}$ and $I_{[x,y]}(t)$ is the indicator function of the interval $[x, y]$. $\tilde{c}_{n,p}(t, f)$ admits the Fourier series

$$\tilde{c}_{n,p}(t, f) \approx \sum_{m=-M_o}^{M_o} \sum_{l=0}^{L_o} \hat{h}^{(m,l)}(p, n) e^{j\frac{2\pi mt}{T_o}} e^{-j\frac{2\pi lf}{B_o}} \quad (5.10)$$

$$\hat{h}^{(m,l)}(p, n) = \frac{1}{T_o B_o} \int_{(p-1/2)T_o}^{(p+1/2)T_o} \int_{(n-1/2)B_o}^{(n+1/2)B_o} \tilde{c}_{n,p}(t, f) e^{-j\frac{2\pi mt}{T_o}} e^{j\frac{2\pi lf}{B_o}} df dt \quad (5.11)$$

where $M_o \approx \lceil B_d T_o \rceil$ and $L_o \approx \lceil T_m B_o \rceil$. Substituting (5.10) in (5.8), we get

$$r(t) \approx b \sum_{n=0}^{N_f-1} \sum_{p=0}^{N_t-1} a_{n,p} \sum_{m=-M_o}^{M_o} \sum_{l=0}^{L_o} \hat{h}^{(m,l)}(p, n) u_{n,p} \left(t - \frac{l}{B_o} \right) e^{j\frac{2\pi mt}{T_o}} + n(t) \quad (5.12)$$

If **C1** and **C2** are satisfied then $\tilde{c}(t, f)$ is approximately constant over any time-frequency region with support $T_o \times B_o$. Thus, $\hat{h}^{(m,l)}(p, n) \approx 0$ for $l \neq 0$ or $m \neq 0$ in (5.11). This reduces (5.12) to

$$r(t) \approx b \sum_{n=0}^{N_f-1} \sum_{p=0}^{N_t-1} a_{n,p} \hat{h}(p, n) u_{n,p}(t) + n(t) \quad (5.13)$$

where $\hat{h}(p, n) = \hat{h}^{(0,0)}(p, n)$ and we have dropped the superscript $(0, 0)$ for convenience of notation. The approximate diagonalization of the channel by the time-frequency basis functions is evident from (5.13).

The main source of error in the diagonal approximation (5.13) is the contribution due to the $\hat{h}^{(m,l)}(p,n)$'s in (5.12) corresponding to the $m \neq 0$ and $l \neq 0$ terms. We now discuss the optimal choice of T_o (and $B_o = 1/T_o$) that minimizes this contribution. Under the WSSUS assumption, the statistics of $\hat{h}^{(m,l)}(p,n)$ are independent of n or p . Hence, without loss of generality, we derive optimum T_o for $n = p = 0$. We define the approximation error ρ to be the ratio of the energy in $\tilde{c}_{0,0}(t,f)$ not captured by $\hat{h}(0,0)$ to the total energy²

$$\rho = \frac{\mathbb{E} \left[\int_{-T_o/2}^{T_o/2} \int_{-B_o/2}^{B_o/2} |\tilde{c}(t,f)|^2 dt df \right] - \mathbb{E}[|\hat{h}(0,0)|^2]}{\mathbb{E} \left[\int_{-T_o/2}^{T_o/2} \int_{-B_o/2}^{B_o/2} |\tilde{c}(t,f)|^2 dt df \right]}. \quad (5.14)$$

Proposition 1: Given a flat multipath and Doppler power profile, ρ in (5.14) is minimized when $\frac{T_o}{B_o} = \frac{T_m}{B_d}$.

Proof: See Appendix B.

Hence, under the assumption $T_o B_o = 1$, the optimal choice of T_o is $T_o = \sqrt{T_m/B_d}$.

5.4. Signal Reception and Performance

Let $z_{n,p}$ denote the projection of the received signal in (5.13) onto $u_{n,p}(t)$

$$z_{n,p} = \int r(t) q_{T_o}^*(t - pT_o) e^{-j2\pi n B_o t} dt = b_1 a_{n,p} \hat{h}(p,n) + v_{n,p} \quad (5.15)$$

where $\{v_{n,p}\}$ are independent Gaussian random variables with variance σ^2 . For convenience of notation, we stack the test statistics in one vector, that is

$$\mathbf{z} = \mathbf{b} \mathbf{A} \hat{\mathbf{h}} + \mathbf{v} \quad (5.16)$$

where \mathbf{A} is a diagonal matrix whose entries are the signature code, $\hat{\mathbf{h}}$ is the Gaussian vector of channel coefficients $\{\hat{h}(p,n)\}$, and \mathbf{v} is the noise vector. Given the knowledge

²For a general treatment, see [52].

of $\hat{\mathbf{h}}$ at the receiver, the optimum coherent bit decision is given by

$$\hat{b} = \text{sign}[\text{real}(\hat{\mathbf{h}}^H \mathbf{A}^H \mathbf{z})]. \quad (5.17)$$

The bit error probability conditioned on $\hat{\mathbf{h}}$ is

$$P_e(\mathbf{c}) = Q(\sqrt{2\hat{\mathbf{h}}^H \hat{\mathbf{h}}/\sigma^2}) \quad (5.18)$$

where $Q(x) = \frac{1}{\sqrt{2\pi}} \int_x^\infty e^{-\frac{x^2}{2}} dx$. The unconditional $P_e = E[P_e(\hat{\mathbf{h}})]$ where the averaging is over the distribution of $\hat{\mathbf{h}}$. Since $\hat{\mathbf{h}}$ is complex Gaussian random vector, P_e is determined by the eigenvalues $\{\mu_i, i = 1, 2, \dots, (L+1)(2M+1)\}$ of $\mathbf{R}_{\hat{\mathbf{h}}, \hat{\mathbf{h}}}$ where $\mathbf{R}_{\hat{\mathbf{h}}, \hat{\mathbf{h}}}$ is the correlation matrix of the channel coefficients $\{\hat{h}(p, n) = \hat{h}^{(0,0)}(p, n)\}$ in (5.11).

A convenient closed form expression for P_e is given by [53]

$$P_e = \frac{1}{\pi} \int_0^{\pi/2} \prod_{i=1}^{(L+1)(2M+1)} \left(1 + \frac{\mu_i}{\sigma^2 \sin^2(\theta)}\right)^{-1} d\theta. \quad (5.19)$$

Since the channel is almost constant over each region of support $T_o \times B_o$, we have $\hat{h}(p, n) \approx \tilde{c}(pT_o, nB_o)$ and

$$E[\hat{h}(p, n)\hat{h}(m, l)^*] = \phi((p-l)T_o, (n-m)B_o) = \phi_{\Delta t}((p-l)T_o) \psi_{\Delta f}((n-m)B_o). \quad (5.20)$$

We note that for a given frequency index n , the different time samples of the channel have a covariance matrix of rank $2M+1$ — the Doppler diversity in the channel. Similarly, for a given time slot p , the different frequency samples of the channel have a covariance matrix of rank $L+1$ — the multipath diversity in the channel. Consequently, the rank of $\mathbf{R}_{\hat{\mathbf{h}}, \hat{\mathbf{h}}}$ is $(L+1)(2M+1)$ and the proposed system exploits full $(L+1)(2M+1)$ -fold diversity.

Figure 5.4(a) compares the performance of the conventional MC-CDMA system, the MC-CDMA system proposed in Chapter 4, and the TF-CDMA system. The SNR is

10dB and the underlying channel has 2 resolvable paths ($L = 2$). The figure shows the P_e of the three systems as a function of the fast fading parameter $T B_d$. Perfect channel estimates are available at the receiver. $T_o B_d$ is kept fixed corresponding to the optimum choice of T_o which results in $T_o B_d = \sqrt{T_m B_d} = 0.2$ in this case. $T B_d$ is increased by increasing T from T_o to $9T_o$ which corresponds to increasing N from 10 to 90 in this case. This is akin to using longer symbol duration for given bandwidth and thus increasing the signal space dimension. The simulation results are generated via Monte-Carlo simulation of 50,000 symbols using Jakes Model. The channel estimates for the simulation results are generated via a noise-free pilot signal. The analytical P_e computation for the TF-CDMA system uses the separability assumption (2.2) and assumes uniform multipath and Doppler power profiles. Furthermore, the interference between different time-frequency basis functions is ignored in the analytical computation. The close agreement between the analytical and simulated results for the TF-CDMA system demonstrates the accuracy of the diagonalization at optimum choice of T_o . The performance of the MC-CDMA system proposed in Chapter 4 and the TF-CDMA system are almost the same.

Figure 5.4(a) clearly shows the significant degradation in the performance of conventional MC-CDMA systems under fast fading, consistent with results reported by other authors (see, e.g., [44]). On the other hand, the performance of the proposed time-frequency signaling scheme improves significantly under faster fading due to Doppler diversity. Thus, the proposed scheme not only facilitates longer symbol durations to reduce the effects of ISI but also yields improved performance with longer symbols.

Figure 5.4(b) shows the analytically computed P_e of the proposed system as a function of SNR for different values of $T B_d$. As evident, the gain in performance with increasing

TB_d is more pronounced at higher SNRs. Furthermore, the slope of the P_e curve gets sharper with increasing TB_d due to Doppler diversity.

5.5. Intuitive Mapping Between MC-CDMA and TF-CDMA Systems

In Chapter 4 we showed that MC-CDMA system over time-varying channels suffers energy dispersion and inter carrier interference. The reason is that even though each subcarrier encounters flat fading in the frequency domain, it does encounter time selective fading in the time domain which creates the energy dispersion and interference. We also showed in Section 4.8 that under Block Fading (BF) assumption, if the bandwidth is divided into N_f sub-bands chosen such that each N_t subcarriers in the same sub-band encounter the same channel fading, then per sub-band, the dispersion is manifested into the generation of multiple Doppler components that resemble the multipath components encountered by the DS-CDMA system in time. We then argued that, per sub-band, the MC-CDMA system over fast fading channels resembles the DS-CDMA system over slow fading channels.

Now, considering the analogy stated above, we note that the TF-CDMA system diagonalizes the fast fading channel in the same manner the MC-CDMA system diagonalizes the slow fading channels. In particular, starting with a MC-CDMA system, to diagonalize the channel, instead of using the whole symbol duration for transmission, we rather use basis waveforms with shorter time support so that each encounters flat fading in time. The decrease of the time support will imply an expansion in the frequency support, however, if N_f is properly chosen, then after expansion the basis waveform

will still occupy the same sub-band and hence encountering flat fading in frequency as well. This is precisely the idea behind TF-CDMA system. In other words, the TF-CDMA system in fast fading channels resemble the MC-CDMA system in slow fading channels.

5.6. Conclusion

We have introduced a novel signaling scheme for CDMA communication systems operating over time-and frequency-selective channels denoted by TF-CDMA system. Information is transmitted over time-frequency basis functions whose time-frequency support is matched to the coherence time and bandwidth of the channel. The time-frequency basis functions serve as approximate eigenfunctions of underspread channels with each basis signal encountering flat fading. We derive a near-optimum duration and bandwidth of the basis functions that yields the most accurate diagonalization for given channel spread parameters. The proposed TF-CDMA system fully exploits channel diversity and our results demonstrate that it delivers significantly improved performance under fast fading by exploiting Doppler diversity. This is in stark contrast to existing systems whose performance deteriorates under fast fading. We also drew an intuitive mapping between MC-CDMA and TF-CDMA systems operating over time and frequency selective channels.

5.7. Figures

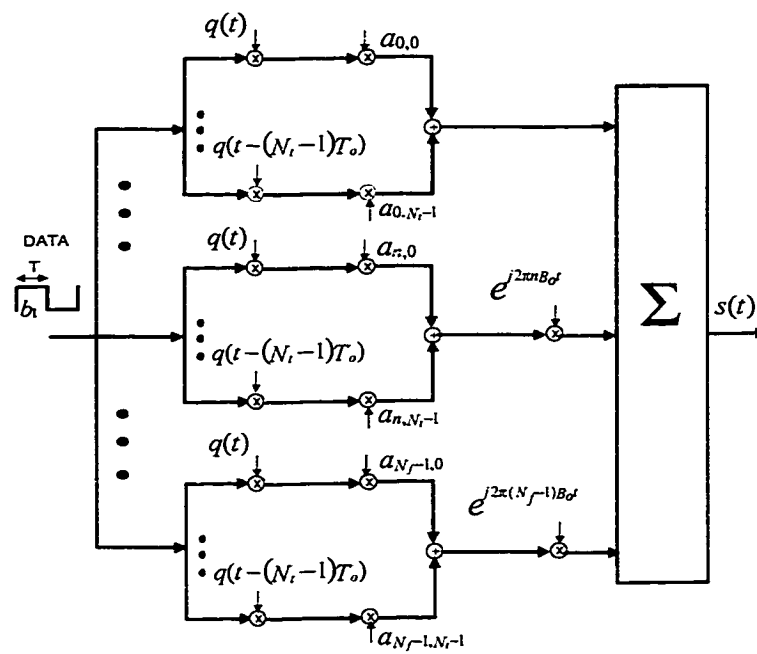


Figure 5.1. The TF-CDMA transmitter.

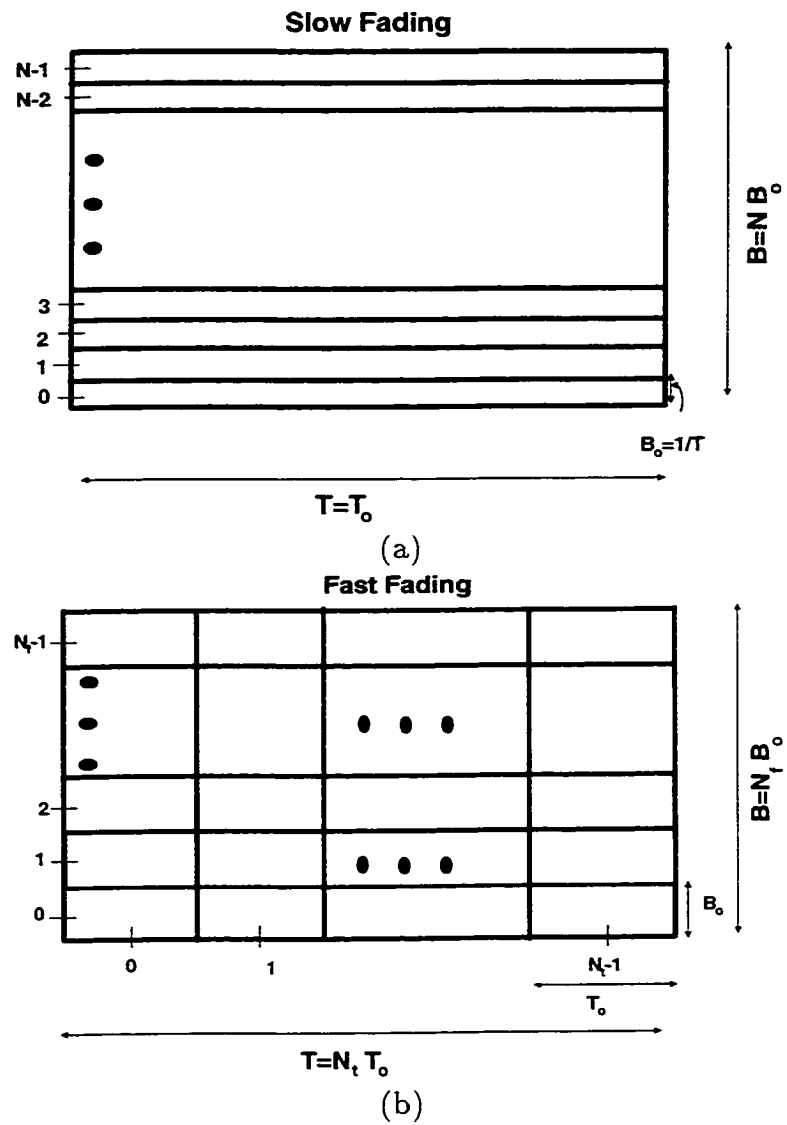


Figure 5.2. Time-frequency support of basis signals. (a) Fourier basis used in multicarrier systems in slow fading channels. (b) The proposed short-time Fourier basis in fast fading channels.

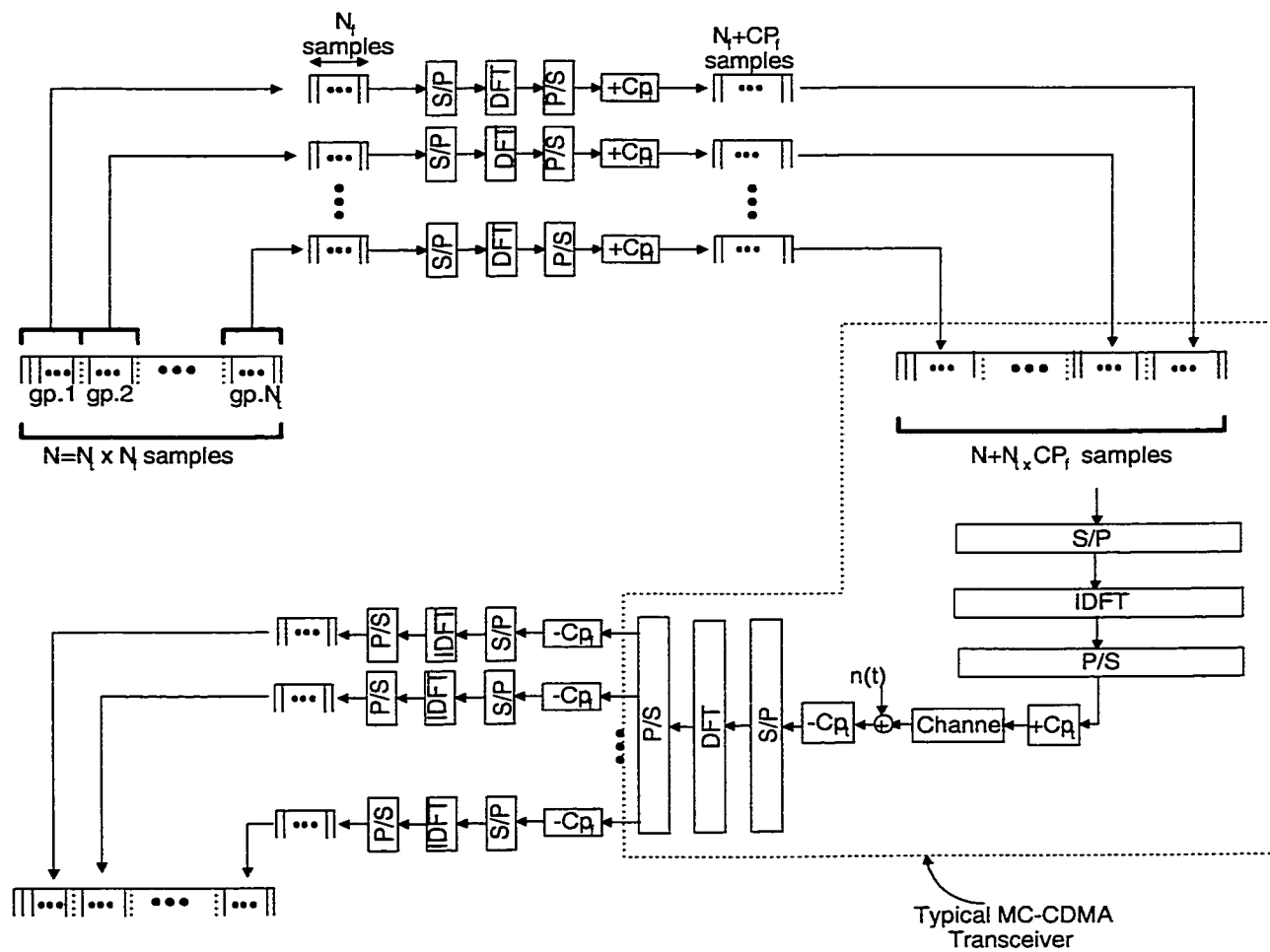


Figure 5.3. A digital implementation for the TF-CDMA transceiver.

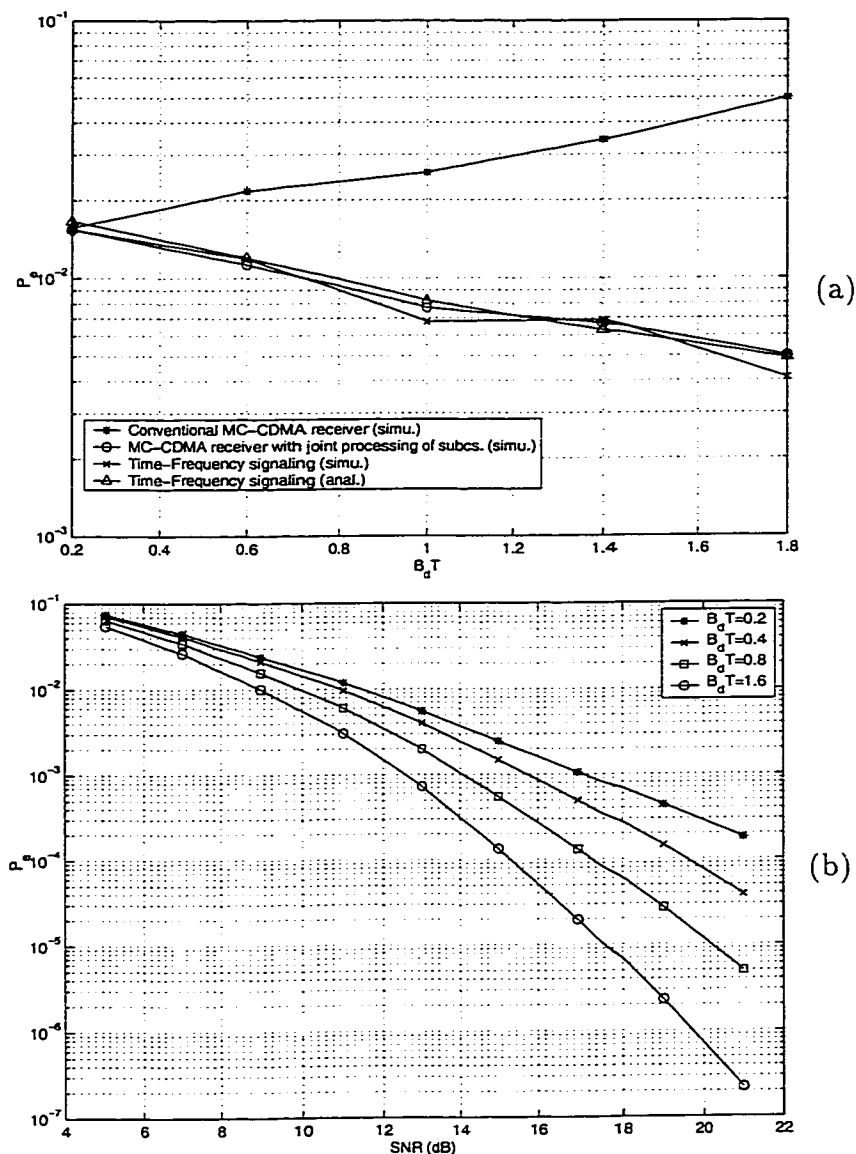


Figure 5.4. (a) Comparison between the P_e of a conventional MC-CDMA system, the proposed TF-CDMA system and the MC-CDMA system introduced in Chapter 4 as a function of TB_d . There are two resolvable multipaths ($L = 2$) and $\text{SNR}=10\text{dB}$. The simulation results are based on Monte-Carlo simulation of 50,000 symbols via Jakes Model. The performance of the proposed TF-CDMA and MC-CDMA proposed systems are almost the same and improve with faster fading, in contrast to the degradation in performance of the conventional system. (b) The P_e of the proposed TF-CDMA system as a function of SNR for different values of TB_d ($L = 2$). The increase in the slope of the P_e curve with increasing TB_d (higher Doppler diversity) is evident.

CHAPTER 6

MULTIUSER DETECTION IN TIME AND FREQUENCY DISPERSIVE CHANNELS

6.1. Introduction

Code Division Multiple Access (CDMA) has emerged as a promising wireless technology for meeting the physical layer challenges of modern communication networks. This is partially due to the multiple access capability of CDMA systems as well as the robustness against fading. Many signaling schemes were proposed for CDMA communication systems. The key to reliable communications is how those signaling schemes interact with the channel.

Denote the symbol duration with T and its essential two-sided bandwidth with B . The time-bandwidth product is denoted by $N \approx TB$ which is the dimension of the signal space. A CDMA system with such time-bandwidth product can support up to N users by employing signature codes of length N . In general, the signature code is transmitted over a set of basis waveforms each has a time duration T_o and essential two-sided bandwidth of B_o . The different signaling schemes differ in how we choose T_o and B_o . In Direct Sequence (DS)-CDMA [1], the basis waveforms are generated via time shifts of a *narrow* time pulse with duration $T_o = \frac{T}{N}$ and bandwidth $B_o = B$. In MultiCarrier (MC)-CDMA [5, 6, 7], the basis waveforms are generated via frequency shifts of a narrow band pulse with duration $T_o = T$ and bandwidth $B_o = \frac{B}{N}$. The MC-DS-CDMA [8, 5, 9] is the hybrid case where $N_t \times N_f$ basis waveforms ($N = N_t N_f$) are used. The basis functions are generated via the time-frequency shifts of a pulse of duration $T_o = \frac{T}{N_t}$ and bandwidth $B_o = \frac{B}{N_f}$. Notice that the DS-CDMA (MC-

CDMA) system is a special case of the MC-DS-CDMA system when $N_f = 1$, $N_t = N$ ($N_f = N$, $N_t = 1$).

As mentioned before in Chapter 1, whether or not the channel is selective and/or dispersive depends on the interaction between T_o , B_o , with Δt_c , Δf_c . In this chapter, we study the purely Frequency Selective channel (denoted in this chapter by FS channel), the purely Time Selective channel (denoted in this chapter by TS channel), and the general Time and Frequency Selective channel (denoted in this chapter by TFS channel). The different CDMA signaling schemes serve as eigenfunctions for certain types of channels. The DS-CDMA basis waveforms are the eigenfunctions, and hence diagonalize, TS channels. On the other hand, the MC-CDMA basis waveforms are the eigenfunctions, and hence diagonalize, FS channels. We also showed in Chapter 5, that for proper choice of T_o and B_o , the MC-DS-CDMA basis waveforms diagonalize TFS channels. The performance of those signaling schemes for single user scenario has been analyzed in several papers. However, the behaviour of these systems in the presence of multiuser detection and for different types of channels is not clear.

In this Chapter, we compare the performance of these systems in the context of multiuser detection. The comparison is based on linear Minimum Mean Square Error (MMSE) receivers. We show that, for a given channel conditions, the different systems can perform in a near-identical fashion via appropriate choice of signature codes. To show these results, we first develop a general framework that includes the three considered CDMA systems as special cases. Furthermore, we use the notion of duality between time and frequency domains to develop equivalences between the different systems.

In Section 6.2, we discuss CDMA systems in TFS channel as well as the effect of

channel selectivity on the received signal. In Section 6.3, we lay the foundation for the analysis in the following sections by discussing the duality between time and frequency domains. In Section 6.4, we derive expressions for Signal to Interference and Noise Ratio (SINR)¹ and probability of error (P_e) which will be used later in the section to derive the sufficient conditions for the different systems to perform equivalently in FS, TS, and TFS channels. In Section 6.5, we illustrate our results through some numerical examples. Concluding remarks are provided in Section 6.6.

6.2. CDMA Systems

In this section we briefly describe the DS-CDMA, MC-CDMA, and the MC-DS-CDMA systems in a general TFS channel (the different systems in FS and TS channels are special cases) with the assumption of synchronous reception. We note that, in the analysis to come, we use many of the notation stated in Section 2.1.

6.2.1. DS-CDMA System

In DS-CDMA systems, the prototype basis waveform is a the chip $v_{T_c}(t) = \frac{1}{\sqrt{T_c}}$, $0 \leq t \leq T_c$ (assumed rectangular for simplicity) which has a duration $T_c = T_o = \frac{T}{N}$ and a bandwidth $B_o = B = \frac{1}{T_c}$. Each user is assigned a signature waveform that is generated from time shifts of the prototype basis waveform as

$$q_k(t) = \sum_{p=0}^{N-1} q_k[p]u_p(t) = \sum_{p=0}^{N-1} q_k[p]v_{T_c}(t - pT_c) \quad (6.1)$$

where $\{u_p(t) = v_{T_c}(t - pT_c), p = 0, 1, \dots, N - 1\}$ are the set of basis functions used in transmission and $q_k[p]$ is the length N signature code of user k as the coupling

¹The SINR is defined to be the ratio between the energy in the desired signal to the energy in noise plus interference.

coefficients. The transmitted signal for user k can be written as

$$s_k(t) = \sum_{i=-\infty}^{\infty} b_{k,i} q_k(t - iT) \quad (6.2)$$

where $b_{k,i}$ is the i^{th} bit corresponding to user k . We assume negligible Inter Symbol Interference (ISI) so that a one shot detector suffices. Hence, without loss of generality, we will focus on the detection of $b_{1,0}$ (0^{th} bit for user 1) and drop the index 0 for simplicity.

We now derive the form for the sampled received signal for a TFS channel. The FS and TS cases are special cases. The noise-free received signal for user k in TFS channel can be written as

$$x_k(t) = b_k \sum_{p=0}^{N-1} \sum_{l=0}^L h_k[p, l] q_k[p] v_{T_c}(t - pT_c - lT_c) \quad (6.3)$$

where

$$h_k[p, l] = \int_0^{T_m} c((p + 1/2)T_c, \tau) \text{sinc}(l - B\tau) e^{j\pi(l - B\tau)} d\tau \quad (6.4)$$

is the channel coefficient corresponding to the l^{th} path and p^{th} chip of the k^{th} user, and $c(t, \tau)$ is defined in Section 2.2. In (6.3), the k^{th} user transmitted power is absorbed in $h_k[p, l]$, a convention that is used throughout the chapter. The overall multiuser received signal is

$$r(t) = \sum_{k=1}^K x_k(t) + v(t) \quad (6.5)$$

where $v(t)$ is the complex Additive White Gaussian Noise (AWGN) with power spectral density σ^2 . Front-end processing at the receiver corresponds to projecting onto the basis waveforms. Assuming the receiver to be synchronized to the first path ($l = 0$) in (6.3), projecting over $u_p(t)$, we get

$$r[p] = \langle r(t), u_p(t) \rangle = \frac{1}{\sqrt{T_c}} \int_{pT_c}^{(p+1)T_c} r(t) dt$$

$$= \sum_{k=1}^K b_k \sum_{l=0}^L h_k[p-l, l] q_k[p-l] + v[p] \quad (6.6)$$

where $\langle r(t), u_p(t) \rangle = \int r(t) u_p^*(t) dt$ and $v[p]$ is the p^{th} noise sample. For convenience of notation, we express $\{r[p]\}$ in a vector form as

$$\begin{aligned} \mathbf{r} &= \begin{bmatrix} r[0] & r[1] & \cdots & r[N-1] \end{bmatrix}^T \\ &= b_1 \mathbf{Q}_1 \mathbf{h}_1 + \sum_{k=2}^K b_k \mathbf{Q}_k \mathbf{h}_k + \mathbf{v} \end{aligned} \quad (6.7)$$

$$= b_1 \mathbf{g}_1 + \sum_{k=2}^K b_k \mathbf{g}_k + \mathbf{v} \quad (6.8)$$

where $\mathbf{Q}_k = \begin{bmatrix} \mathbf{Q}_k(0), & \cdots, & \mathbf{Q}_k(L) \end{bmatrix}$, $\mathbf{Q}_k(l) = \text{diag}\{\mathbf{q}_k(l)\}$, \mathbf{q}_k is the $N \times 1$ vector corresponding to k^{th} user's signature code, $\mathbf{h}_k = \begin{bmatrix} \mathbf{h}_{k,0}^T & \cdots & \mathbf{h}_{k,L}^T \end{bmatrix}^T$, $\mathbf{h}_{k,l} = \begin{bmatrix} h_k[-l, l], & \cdots, & h_k[N-1-l, l] \end{bmatrix}^T$ ², \mathbf{v} is zero mean N -dimensional Gaussian noise vector with covariance matrix $\sigma^2 \mathbf{I}_N$, and $\mathbf{g}_k = \mathbf{Q}_k \mathbf{h}_k$. Notice that due to the time-varying channel, for a given path l , each chip is faded differently. One can easily deduce this from the expression in (6.7) since for a given path l , the sampled vector after projecting over the basis waveforms is $\mathbf{Q}_k(l) \mathbf{h}_{k,l}$.

For FS channels (in absence of channel time variation), $h_k[p, l]$ is constant over p within a symbol duration, i.e. $h_k[p, l] \approx h_k[0, l]$, $p = 0, 1, \dots, N-1$. Hence, $\mathbf{Q}_k(l) \mathbf{h}_{k,l} = h_k[0, l] \mathbf{Q}_k(l) \mathbf{1}_N = h_k[0, l] \mathbf{q}_k(l)$. Now, we can rewrite (6.7) with replacing $\mathbf{Q}_k(l)$ by $\mathbf{q}_k(l)$ in the definition of \mathbf{Q}_k , and $\mathbf{h}_{k,l}$ with $h_k[0, l]$ in the definition of \mathbf{h}_k . Notice that in this case \mathbf{Q}_k is Toeplitz due to multipath dispersion. On the other hand, for TS channels, $L = 0$. Hence, \mathbf{Q}_k reduces to $\mathbf{Q}_k(0)$ and \mathbf{h}_k reduces to $\mathbf{h}_{k,0}$. The diagonal

²Negative l indices correspond to those channel coefficients from previous symbols due to ISI. These samples are ignored in the analysis since typically $N \gg L$, hence, the symbol encounters negligible ISI.

structure of the system is evident in this case.³

6.2.2. MC-CDMA System

In a MC-CDMA system, the prototype basis waveform is a the complex exponential $v_T(t)e^{j\frac{2\pi(n+1/2)t}{T}}$ which has a duration $T_o = T$ and bandwidth $B_o = \frac{B}{N} = \frac{1}{T}$. Each user is assigned a signature waveform that is generated from frequency shifts of the prototype basis waveform as

$$\tilde{q}_k(t) = \sum_{n=0}^{N-1} \tilde{q}_k[n] \tilde{u}_n(t) \quad (6.9)$$

where $\left\{ \tilde{u}_n(t) = v_T(t)e^{j\frac{2\pi(n+1/2)t}{T}} \right\}$ are the set of basis functions used in transmission and $\tilde{q}_k[n]$ is the n^{th} entry of the k^{th} user signature code. The transmitted signal for user k is

$$\tilde{s}_k(t) = b_k \sum_{n=0}^{N-1} \tilde{q}_k[n] v_T(t) e^{j\frac{2\pi(n+1/2)t}{T}}. \quad (6.10)$$

Using the model in Chapter 4, the noise-free received signal for user k in a TFS channel can be written as (recall (4.8))

$$\tilde{x}_k(t) = b_k \sum_{n=0}^{N-1} \sum_{m=-M}^M \tilde{q}_k[n] \tilde{h}_k[m, n] v_T(t) e^{j\frac{2\pi mt}{T}} e^{j\frac{2\pi(n+1/2)t}{T}} \quad (6.11)$$

where $M = \lceil B_d T \rceil$. We note that in (6.11), due to the time-varying channel response affecting each subcarrier, the information transmitted over a particular basis waveform is dispersed into the adjacent $2M + 1$ basis waveforms. We denote this frequency dispersion by Doppler dispersion. In (6.11),

$$\tilde{h}_k[m, n] = \int_{-B_d}^{B_d} \tilde{C}_k(\theta, (n + 1/2)/T) \text{sinc}(m - \theta T) e^{-j\pi(m - \theta T)} d\theta \quad (6.12)$$

³Recall that DS-CDMA system diagonalizes TS channels.

is the channel coefficient corresponding to the n^{th} subcarrier and m^{th} Doppler shift of the k^{th} user, and $\tilde{C}_k(\theta, f) = \int \tilde{c}_k(t, f) e^{-j2\pi\theta t} dt$ where $\tilde{c}_k(t, f)$ is defined in (2.1). The overall received signal for all users is

$$\tilde{r}(t) = \sum_{k=1}^K \tilde{x}_k(t) + v(t). \quad (6.13)$$

Projecting over $\tilde{u}_n(t)$, we get

$$\begin{aligned} \tilde{r}[n] &= \langle \tilde{r}(t), \tilde{u}_n(t) \rangle = \frac{1}{\sqrt{T}} \int_0^T r(t) e^{-j\frac{2\pi(n+1/2)t}{T}} dt \\ &= \sum_{k=1}^K b_k \sum_{m=-M}^M \tilde{h}_k[m, n-m] \tilde{q}_k[n-m] + \tilde{v}[n]. \end{aligned} \quad (6.14)$$

The sampled received vector can be written as

$$\tilde{\mathbf{r}} = b_1 \tilde{\mathbf{Q}}_1 \tilde{\mathbf{h}}_1 + \sum_{k=2}^K b_k \tilde{\mathbf{Q}}_k \tilde{\mathbf{h}}_k + \tilde{\mathbf{v}} \quad (6.15)$$

$$= b_1 \tilde{\mathbf{g}}_1 + \sum_{k=2}^K b_k \tilde{\mathbf{g}}_k + \tilde{\mathbf{v}} \quad (6.16)$$

where $\tilde{\mathbf{Q}}_k = \begin{bmatrix} \tilde{\mathbf{Q}}_k(-M) & \dots & \tilde{\mathbf{Q}}_k(M) \end{bmatrix}$, $\tilde{\mathbf{Q}}_k(m) = \text{diag}\{\tilde{\mathbf{q}}_k(m)\}$, $\tilde{\mathbf{q}}_k$ is the $N \times 1$ vector corresponding to the k^{th} user signature code. $\tilde{\mathbf{h}}_k = \begin{bmatrix} \tilde{h}_{k,-M}^T & \dots & \tilde{h}_{k,M}^T \end{bmatrix}^T$, $\tilde{\mathbf{h}}_{k,m} = \begin{bmatrix} \tilde{h}_k[m, 0] & \dots & \tilde{h}_k[m, N-1] \end{bmatrix}^T$, and $\tilde{\mathbf{g}}_k = \tilde{\mathbf{Q}}_k \tilde{\mathbf{h}}_k$.

In FS channels, $M = 0$. Hence, in this case, $\tilde{\mathbf{Q}}_k$ reduces to $\tilde{\mathbf{Q}}_k(0)$, $\tilde{\mathbf{h}}_k$ reduces to $\tilde{\mathbf{h}}_{k,0}$. The diagonal structure of the system is evident in this case.⁴ On the other hand, in TS channel, $\tilde{h}_k[m, n] \approx \tilde{h}_k[m, 0]$, $n = 0, 1, \dots, N-1$. Parallel to the argument in Section 6.2.1, in this case, $\tilde{\mathbf{h}}_k = \begin{bmatrix} \tilde{h}_k[-M, 0] & \dots & \tilde{h}_k[M, 0] \end{bmatrix}^T$ and $\tilde{\mathbf{Q}}_k(m)$ reduces to $\tilde{\mathbf{q}}_k(m)$ so that $\tilde{\mathbf{Q}}_k$ becomes Toeplitz (due to Doppler dispersion).

⁴Recall that MC-CDMA system diagonalizes FS channels.

6.2.3. MC-DS-CDMA system

In a MC-DS-CDMA system, the prototype basis waveform is $v_{T_o}(t)e^{j\frac{2\pi(1/2)t}{T_o}}$ which has a duration $T_o = \frac{T}{N_t}$ and bandwidth $B_o = \frac{B}{N_f}$. Each user is assigned a signature waveform that is generated from time-frequency shifts of the prototype basis waveform as

$$\hat{q}_k(t) = \sum_{n=0}^{N_f-1} \sum_{p=0}^{N_t-1} \hat{q}_k[p, n] \hat{u}_{p,n}(t) \quad (6.17)$$

where $\left\{ \hat{u}_{p,n}(t) = v_{T_o}(t - pT_o) e^{j\frac{2\pi(n+1/2)t}{T_o}} \right\}$ are the set of basis functions used in transmission and $\hat{q}_k[p, n]$ is the $(p, n)^{th}$ entry of the k^{th} user's spreading code transmitted over $\hat{u}_{p,n}(t)$. The transmitted signal for user k can be written as

$$\hat{s}_k(t) = b_k \sum_{n=0}^{N_f-1} \sum_{p=0}^{N_t-1} \hat{q}_k[p, n] v_{T_o}(t - pT_o) e^{j\frac{2\pi(n+1/2)t}{T_o}} \quad (6.18)$$

where depending on the choice of N_t and N_f , the effect of the channel can be categorized into four cases.

6.2.3.1. Case 1: $B_o > \Delta f_c$, $T_o \ll \Delta t_c$

In this case the channel affects each time-frequency basis function in a FS fashion.

The noise-free received signal is

$$\hat{x}_k(t) = b_k \sum_{n=0}^{N_f-1} \sum_{p=0}^{N_t-1} \sum_{l=0}^{L_o} h_k[p, n; l] \hat{q}_k[p, n] v_{T_o}(t - pT_o - lT_o) e^{j\frac{2\pi(n+1/2)t}{T_o}} \quad (6.19)$$

where $L_o = \lceil T_m B_o \rceil$, and analogous to (6.4),

$$h_k[p, n; l] = \int_0^{T_m} c((p+1/2)T_o, \tau) \text{sinc}(l - B_o\tau) e^{j2\pi(n+1/2)(l-B_o\tau)} d\tau. \quad (6.20)$$

The projection on $\hat{u}_{p,n}(t)$ is

$$\begin{aligned} \hat{r}[p, n] &= \langle \hat{r}(t), \hat{u}_{p,n}(t) \rangle = \frac{1}{\sqrt{T_o}} \int_{pT_o}^{(p+1)T_o} r(t) e^{-j\frac{2\pi(n+1/2)t}{T_o}} dt \\ &= \sum_{k=1}^K \sum_{l=0}^{L_o} h_k[p-l, n; l] \hat{q}_k[p-l, n] + \hat{v}[p, n] \end{aligned} \quad (6.21)$$

and the sampled received vector is

$$\hat{\mathbf{r}} = b_1 \hat{\mathbf{Q}}_1^{(f)} \hat{\mathbf{h}}_1^{(f)} + \sum_{k=2}^K b_k \hat{\mathbf{Q}}_k^{(f)} \hat{\mathbf{h}}_k^{(f)} + \hat{\mathbf{v}} \quad (6.22)$$

$$= b_1 \hat{\mathbf{g}}_1^{(f)} + \sum_{k=2}^K b_k \hat{\mathbf{g}}_k^{(f)} + \hat{\mathbf{v}} \quad (6.23)$$

$$\text{where } \hat{\mathbf{Q}}_k^{(f)} = \begin{bmatrix} \hat{\mathbf{Q}}_k^{(f)}(0) & \mathbf{0} & \cdots & \mathbf{0} \\ \mathbf{0} & \hat{\mathbf{Q}}_k^{(f)}(1) & \cdots & \mathbf{0} \\ \vdots & \ddots & \ddots & \vdots \\ \mathbf{0} & \cdots & \mathbf{0} & \hat{\mathbf{Q}}_k^{(f)}(N_f - 1) \end{bmatrix},$$

$$\hat{\mathbf{Q}}_k^{(f)}(n) = \left[\hat{\mathbf{Q}}_k^{(f)}(n, 0) \quad \cdots \quad \hat{\mathbf{Q}}_k^{(f)}(n, L_o) \right],$$

$$\hat{\mathbf{Q}}_k^{(f)}(n, l) = \text{diag}\{\hat{\mathbf{q}}_{k,n}^{(f)}(l)\}, \quad \hat{\mathbf{q}}_{k,n}^{(f)} = \left[\hat{q}_k[0, n] \quad \cdots \quad \hat{q}_k[N_t - 1, n] \right]^T,$$

$$\hat{\mathbf{h}}_k^{(f)} = \left[\hat{\mathbf{h}}_{k,0}^{(f)T} \quad \cdots \quad \hat{\mathbf{h}}_{k,N_f-1}^{(f)T} \right]^T, \quad \hat{\mathbf{h}}_{k,n}^{(f)} = \left[\hat{\mathbf{h}}_{k,n,0}^{(f)T} \quad \cdots \quad \hat{\mathbf{h}}_{k,n,L_o}^{(f)T} \right]^T,$$

$\hat{\mathbf{h}}_{k,n,l}^{(f)} = \left[h_k[-l, n; l] \quad \cdots \quad h_k[N_t - 1 - l, n; l] \right]^T$, and $\hat{\mathbf{g}}_k^{(f)} = \hat{\mathbf{Q}}_k^{(f)} \hat{\mathbf{h}}_k^{(f)}$. The superscript f stands for frequency domain since $\hat{\mathbf{q}}_{k,n}^{(f)}$ corresponds to part of the signature code corresponding to all time shifts of the n^{th} frequency (n^{th} row in Figure 6.2(c)).

Note that, the DS-CDMA system in TFS channels is a special case of this system when $N_f = 1$ (hence, $N_t = N$ and $L_o = L$).

6.2.3.2. Case 2: $B_o \ll \Delta f_c$, $T_o > \Delta t_c$

In this case the channel affects each time-frequency basis function in a TS fashion.

The noise-free received signal is

$$\hat{x}_k(t) = b_k \sum_{n=0}^{N_f-1} \sum_{p=0}^{N_t-1} \sum_{m=-M_o}^{M_o} \tilde{h}_k[p, n; m] \hat{q}_k[p, n] v_{T_o}(t - pT_o) e^{j \frac{2\pi m t}{T_o}} e^{j \frac{2\pi(n+1/2)t}{T_o}} \quad (6.24)$$

where $M_o = \lceil B_d T_o \rceil$, and

$$\tilde{h}_k[p, n; m] = \int_{-B_d}^{B_d} \tilde{C}_k(\theta, (n+1/2)/T_o) \text{sinc}(m - \theta T_o) e^{-j2\pi(p+1/2)(m-\theta T_o)} d\theta. \quad (6.25)$$

In this case $\hat{r}[p, n]$ becomes

$$\hat{r}[p, n] = \sum_{k=1}^K \sum_{m=-M_o}^{M_o} \tilde{h}_k[p, n - m; m] \hat{q}_k[p, n - m] + \hat{v}[p, n] \quad (6.26)$$

and the received vector is

$$\hat{\mathbf{r}} = b_1 \hat{\mathbf{Q}}_1^{(t)} \hat{\mathbf{h}}_1^{(t)} + \sum_{k=2}^K b_k \hat{\mathbf{Q}}_k^{(t)} \hat{\mathbf{h}}_k^{(t)} + \hat{\mathbf{v}} \quad (6.27)$$

$$= b_1 \hat{\mathbf{g}}_1^{(t)} + \sum_{k=2}^K b_k \hat{\mathbf{g}}_k^{(t)} + \hat{\mathbf{v}} \quad (6.28)$$

$$\text{where } \hat{\mathbf{Q}}_k^{(t)} = \begin{bmatrix} \hat{\mathbf{Q}}_k^{(t)}(0) & \mathbf{0} & \cdots & \mathbf{0} \\ \mathbf{0} & \hat{\mathbf{Q}}_k^{(t)}(1) & \cdots & \mathbf{0} \\ \vdots & \ddots & \ddots & \vdots \\ \mathbf{0} & \cdots & \mathbf{0} & \hat{\mathbf{Q}}_k^{(t)}(N_t - 1) \end{bmatrix},$$

$$\hat{\mathbf{Q}}_k^{(t)}(p) = \left[\hat{\mathbf{Q}}_k^{(t)}(p, -M_o) \cdots \hat{\mathbf{Q}}_k^{(t)}(p, M_o) \right],$$

$$\hat{\mathbf{Q}}_k^{(t)}(p, m) = \text{diag}\{\hat{\mathbf{q}}_{k,p}^{(t)}(m)\}, \hat{\mathbf{q}}_{k,p}^{(t)} = \left[\hat{q}_k[p, 0] \cdots \hat{q}_k[p, N_f - 1] \right]^T,$$

$$\hat{\mathbf{h}}_k^{(t)} = \left[\hat{\mathbf{h}}_{k,0}^{(t)T} \cdots \hat{\mathbf{h}}_{k,N_t-1}^{(t)T} \right]^T, \hat{\mathbf{h}}_{k,p}^{(t)} = \left[\hat{\mathbf{h}}_{k,p,-M_o}^{(t)T} \cdots \hat{\mathbf{h}}_{k,p,M_o}^{(t)T} \right]^T,$$

$\hat{\mathbf{h}}_{k,p,m}^{(t)} = \left[\tilde{h}_k[p, 0; m] \cdots \tilde{h}_k[p, N_f - 1; m] \right]^T$, and $\hat{\mathbf{g}}_k^{(t)} = \hat{\mathbf{Q}}_k^{(t)} \hat{\mathbf{h}}_k^{(t)}$. The superscript t stands for time domain since $\hat{\mathbf{q}}_{k,p}^{(t)}$ corresponds to all frequency shifts of the p^{th} time shift (p^{th} column in Figure 6.2(c)).

Note that MC-CDMA system over TFS channel is a special case of this system when $N_t = 1$ (hence, $N_f = N$ and $M_o = M$).

6.2.3.3. Case 3: $B_o \ll \Delta f_c, T_o \ll \Delta t_c$

In this case, the channel affects each time-frequency basis function in a non selective fashion in both time and frequency domains. That is, the effective channel matrix is diagonal in this case. This interesting signaling scheme was discussed in Chapter 5 and

denoted by TF-CDMA system. It was shown that the N_f and N_t conditions necessary for this case to hold can be met for under-spread channels, i.e. $T_m B_d \ll 1$.⁵ From (5.13), the noise-free received signal in this case is given by

$$\hat{x}_k(t) = b_k \sum_{n=0}^{N_f-1} \sum_{p=0}^{N_t-1} \hat{h}_k[p, n] \hat{q}_k[p, n] v_{T_o}(t - pT_o) e^{j \frac{2\pi(n+1/2)t}{T_o}} \quad (6.29)$$

where

$$\hat{h}_k[p, n] = \int_{pT_o}^{(p+1)T_o} \int_{nB_o}^{(n+1)B_o} \tilde{c}_k(t, f) df dt \approx \tilde{c}_k((p+1/2)T_o, (n+1/2)B_o). \quad (6.30)$$

The approximation in (6.30) is due to the fact that for proper choice of T_o and B_o , $\tilde{c}_k(t, f)$ is almost flat over the basis function's time and frequency support. In this case $\hat{r}[p, n]$ in (6.21) is

$$\hat{r}[p, n] = \sum_{k=1}^K \hat{h}_k[p, n] \hat{q}_k[p, n] \quad (6.31)$$

from which the diagonal nature of the system is evident. The received vector is given by (6.22) with the following definitions: $\hat{\mathbf{Q}}_k^{(f)} = \text{diag}\{\hat{\mathbf{q}}_k^{(f)}\}$, $\hat{\mathbf{q}}_k^{(f)} = \left[\hat{q}_{k,0}^{(f)T} \ \cdots \ \hat{q}_{k,N_f-1}^{(f)T} \right]^T$, $\hat{\mathbf{h}}_k^{(f)} = \left[\hat{h}_{k,0}^{(f)T} \ \cdots \ \hat{h}_{k,N_f-1}^{(f)T} \right]^T$ and $\hat{\mathbf{h}}_{k,n}^{(f)} = \left[\hat{h}_k[0, n] \ \cdots \ \hat{h}_k[N_t-1, n] \right]^T$.

The sampled received vector can be also written as (6.27) with the following definitions: $\hat{\mathbf{Q}}_k^{(t)} = \text{diag}\{\hat{\mathbf{q}}_k^{(t)}\}$, $\hat{\mathbf{q}}_k^{(t)} = \left[\hat{q}_{k,0}^{(t)T} \ \cdots \ \hat{q}_{k,N_t-1}^{(t)T} \right]^T$, $\hat{\mathbf{h}}_k^{(t)} = \left[\hat{h}_{k,0}^{(t)T} \ \cdots \ \hat{h}_{k,N_t-1}^{(t)T} \right]^T$ and $\hat{\mathbf{h}}_{k,p}^{(t)} = \left[\hat{h}_k[p, 0] \ \cdots \ \hat{h}_k[p, N_f-1] \right]^T$.

The MC-CDMA system over FS channel is a special case of this system when $N_t = 1$ (hence $N_f = N$) and $B_d = 0$. Also, the DS-CDMA system over TS channel is a special case of this system when $N_f = 1$ (hence $N_t = N$) and $T_m = 0$.

The fourth case in TFS channel is $B_o > \Delta f_c$ and $T_o > \Delta t_c$ so that the channel affects each basis function in a TFS fashion. The conditions above imply that $T_o < T_m$ and

⁵Most communication channels are under-spread [1].

$B_o < B_d \Rightarrow T_m B_d > T_o B_o = 1$. This is the case of over-spread channels and is not addressed in this thesis.

6.2.4. Special Cases

The MC-DS-CDMA system in FS (TS) channel can only have Case 1 in Section 6.2.3.1 (Case 2 in Section 6.2.3.2) where the channel is frequency (time) selective per basis waveform (so that the basis functions encounter multipath (Doppler) dispersion), and Case 3 where the channel is non selective per basis waveform. The system does not have Case 2 (Case 1) in FS (TS) channel due to the absence of time (frequency) selectivity. In the sequel, whenever we address the MC-DS-CDMA system over FS (TS) channel, we only consider Case 1 and 3 (2 and 3). The following special cases hold:

1. Case 1 in the MC-DS-CDMA system over FS channel is a special case of that in Section 6.2.3.1 when $B_d = 0$, i.e. $h_k[p, n; l] \approx h_k[0, n; l]$, $p = 0, 1, \dots, N_t - 1$. In this case, $\hat{\mathbf{Q}}_k^{(f)}(n)$ becomes a Toeplitz matrix built by $\hat{\mathbf{q}}_{k,n}^{(f)}$, and

$$\hat{\mathbf{h}}_{k,n}^{(f)} = \begin{bmatrix} h_k[0, n; 0] & \dots & h_k[0, n; L_o] \end{bmatrix}^T.$$

2. Case 2 in the MC-DS-CDMA system in TS channel is a special case of that in 6.2.3.2 when $T_m = 0$, i.e. $\tilde{h}_k[p, n; m] \approx \tilde{h}_k[p, 0; m]$, $n = 0, 1, \dots, N_f - 1$. In this case, $\hat{\mathbf{Q}}_k(p)$ becomes Toeplitz matrix built by $\hat{\mathbf{q}}_{k,p}$, and $\hat{\mathbf{h}}_{k,p} = \begin{bmatrix} \tilde{h}_k[p, 0, -M_o] & \dots & \tilde{h}_k[p, 0; M_o] \end{bmatrix}^T$.

3. Case 3 in the MC-DS-CDMA system in FS channel is a special case of that in

Section 6.2.3.3 when $B_d = 0$, i.e. $\hat{h}_k[p, n] \approx \hat{h}_k[0, n]$, $p = 0, 1, \dots, N_t - 1$. In this case

$$\hat{\mathbf{Q}}_k^{(f)} = \begin{bmatrix} \hat{\mathbf{q}}_{k,0}^{(f)} & \mathbf{0} & \cdots & \mathbf{0} \\ \mathbf{0} & \hat{\mathbf{q}}_{k,1}^{(f)} & \cdots & \mathbf{0} \\ \vdots & \ddots & \ddots & \vdots \\ \mathbf{0} & \cdots & \mathbf{0} & \hat{\mathbf{q}}_{k,N_f-1}^{(f)} \end{bmatrix} \text{ and } \mathbf{h}_k^{(f)} = \left[\hat{h}_k[0,0] \quad \cdots \quad \hat{h}_k[0, N_f - 1] \right]^T. \quad (6.32)$$

4. Case 3 in the MC-DS-CDMA system in TS channel is a special case of that in Section 6.2.3.3 when $T_m = 0$, i.e. $\hat{h}_k[p, n] \approx \hat{h}_k[p, 0]$, $n = 0, 1, \dots, N_f - 1$. In this case

$$\hat{\mathbf{Q}}_k^{(t)} = \begin{bmatrix} \hat{\mathbf{q}}_{k,0}^{(t)} & \mathbf{0} & \cdots & \mathbf{0} \\ \mathbf{0} & \hat{\mathbf{q}}_{k,1}^{(t)} & \cdots & \mathbf{0} \\ \vdots & \ddots & \ddots & \vdots \\ \mathbf{0} & \cdots & \mathbf{0} & \hat{\mathbf{q}}_{k,N_t-1}^{(t)} \end{bmatrix} \text{ and } \mathbf{h}_k^{(t)} = \left[\hat{h}_k[0,0] \quad \cdots \quad \hat{h}_k[N_t - 1, 0] \right]^T. \quad (6.33)$$

6.3. Time Domain- Frequency Domain Mappings

As shown in the previous section (and is illustrated in Figure 6.3), in FFS channel, each basis function in a DS-CDMA system encounters frequency selective fading since it occupies the whole bandwidth which is greater than Δf_c . Consequently, the transmitted signal encounters multipath dispersion and a Rake receiver is needed for multipath combining. To avoid multipath dispersion, the MC-CDMA system uses basis waveforms that are narrowband subcarriers with $B_o \ll \Delta f_c$. Hence, each basis function encounters non selective fading and the resultant channel matrix is diagonal. The diversity due to frequency selectivity is exploited via $L + 1$ multipath in DS-CDMA system, and via $L + 1$ subcarriers separated by Δf_c in the MC-CDMA system. The

diversity order in both systems is $L + 1$ which equals to the rank of the channel matrix for both systems, i.e. $\text{rank}(\mathbf{R}_{\mathbf{h}_k, \mathbf{h}_k}) = \text{rank}(\mathbf{R}_{\tilde{\mathbf{h}}_k, \tilde{\mathbf{h}}_k}) = L + 1$.

The behaviour of the two systems in TS channels is totally analogous to that discussed above for FS channels except for interchanging time and frequency domains, and DS-CDMA and MC-CDMA systems. In particular, in a DS-CDMA system in TS channel, the channel matrix is diagonal as long as $T_o \ll \Delta t_c$ – each basis function (chip) encounters non selective fading. On the other hand, each MC-CDMA system basis function suffers time selective fading since $T_o = T > \Delta t_c$. This is manifested as multiple Doppler components, as illustrated in Figure 6.4, analogous to multipath components in a DS-CDMA system in FS channel. Consequently, the MC-CDMA system over a TS channel requires a frequency domain Rake receiver to do multiple Doppler combining. The order of diversity in both systems is the same and is equal to $2M + 1$ – the channel covariance matrix for both systems has a rank of $2M + 1$. This duality between MC-CDMA and DS-CDMA as well as between TS and FS channels will be used in Section 6.4 to derive equivalences between different systems.

Using the previous discussion, we can deduce intuitive insights about diagonalizing the TFS channel in Section 6.2.3.3. We redefine the notion of Block Fading (BF) (previously defined in Chapter 4) for a MC-CDMA system in a FS channel and a DS-CDMA system in TS channel. For a MC-CDMA system, if the whole bandwidth is divided into N_f sub-bands, where N_f is chosen sufficiently larger than L , then under BF assumption, the N_t subcarriers in the same sub-band encounter identical fading coefficients. More precisely, if the set of indices of subcarriers in the i^{th} sub-band is $\Omega_i^{(f)}$, $i = 0, 1, \dots, N_f - 1$, then under BF assumption (recall (6.12)), $\tilde{h}_k[m, n_1] \approx \tilde{h}_k[m, n_2] \forall n_1, n_2 \in \Omega_i^{(f)}$. A similar definition holds for a DS-CDMA system in a TS

channel. If the whole symbol duration is divided into N_t time slots, where N_t is chosen sufficiently larger than $2M + 1$, then under BF assumption, the N_f chips in the same time slot encounter identical fading coefficients. That is, if the set of indices of chips in the i^{th} time slot is $\Omega_i^{(t)}$, $i = 0, 1, \dots, N_t - 1$, then under BF assumption (recall (6.4)), $h_k[p_1, l] \approx h_k[p_2, l] \forall p_1, p_2 \in \Omega_i^{(t)}$.

Consider a MC-CDMA system in a TFS channel. Divide the bandwidth into N_f sub-bands such that BF holds for the N_t subcarriers per sub-band. Now, per sub-band, the channel is frequency non-selective but may be time selective. That is, each sub-band resembles a TS channel and multiple Doppler components are generated. Hence, to diagonalize the system (analogous to DS-CDMA system over TS channel), we need to choose basis waveforms that are narrower in time so that each encounters non selective fading. This is precisely the case with the basis waveforms in Section 6.2.3.3 which are the basis functions for the TF-CDMA system in Chapter 5. Compared to a MC-CDMA system, the symbol duration is decreased by a factor of N_t i.e. $T_o = \frac{T}{N_t}$ and consequently the bandwidth increases N_t times to $B_o = \frac{BN_t}{N} = \frac{B}{N_f}$. Since B_o equals the sub-band bandwidth, flat fading in the frequency domain is still preserved. A dual way of looking at the TF-CDMA system in Section 6.2.3.3 is via a DS-CDMA systems in a TFS channel. In this case, T is divided into well-chosen N_t slots such that BF holds in time. Per time slot, the N_f time samples encounter frequency selective but time non selective fading. To diagonalize the system, we need to decrease the bandwidth of each basis waveform by a factor of N_f , increase the time duration by the same factor to achieve non selective fading. This idea is illustrated in Figures 6.5 and 6.6.

6.4. Equivalences

In this section, we derive the sufficient conditions for the CDMA systems in Section 6.2 to be equivalent. We say that two systems are equivalent if both attain the same SINR for any given set of channel realizations for all users. One can easily deduce that if two systems are equivalent, then both also attain the same P_e . Before introducing the equivalence results, we derive the linear MMSE detector, the expression for SINR, and the expression for P_e .

One can notice from (6.8), (6.16), and (6.23), that the sampled received vector for a given system x is

$$\begin{aligned} \mathbf{r}_x &= b_1 \mathbf{g}_1^{(x)} + \sum_{k=2}^K b_k \mathbf{g}_k^{(x)} + \mathbf{v}_x \\ &= b_1 \mathbf{g}_1^{(x)} + \mathbf{i}_x + \mathbf{v}_x = \mathbf{g}_1^{(x)} + \epsilon_x \end{aligned} \quad (6.34)$$

where $\mathbf{g}_k^{(x)} = \mathbf{Q}_k^{(x)} \mathbf{h}_k^{(x)}$, $\mathbf{Q}_k^{(x)}$ is a matrix that is a function of the k^{th} user signature code for system x , $\mathbf{h}_k^{(x)}$ is the corresponding channel coefficient vector, \mathbf{i}_x is the MAI vector affecting the desired signal component, \mathbf{v}_x is the noise vector, and ϵ_x is the noise plus interference vector. The linear detector for user 1 takes the form $\hat{b}_1 = \text{sign} \left\{ \text{real} \left[\mathbf{w}^{MMSEH} \mathbf{r}_x \right] \right\}$ and \mathbf{w}^{MMSE} is chosen to solve

$$\mathbf{w}_x^{MMSE} = \min_{\mathbf{w}} E \left[|\mathbf{w}^H \mathbf{r}_x - b_1|^2 \right]. \quad (6.35)$$

The solution is the well-known Wiener filter

$$\mathbf{w}_x^{MMSE} = \mathbf{R}_{\mathbf{r}_x, \mathbf{r}_x}^{-1} \mathbf{g}_1^{(x)}. \quad (6.36)$$

The SINR can be written as [17]

$$\text{SINR}^{(x)} = \mathbf{g}_1^{(x)H} \mathbf{R}_{\epsilon_x, \epsilon_x}^{-1} \mathbf{g}_1^{(x)} \quad (6.37)$$

where $\mathbf{R}_{\epsilon_x, \epsilon_x} = \sum_{k=2}^K \mathbf{g}_k^{(x)} \mathbf{g}_k^{(x)H} + \sigma^2 \mathbf{I}_N$. There is no closed form expression for the receiver P_e in the presence of MAI. However, parallel to the discussion in [30], we note that for sufficiently large N , the Gaussian approximation of the interference at the output of the MMSE is fairly accurate. In this case, the conditional P_e given $\mathbf{h}_1^{(x)}, \dots, \mathbf{h}_K^{(x)}$ can be approximated as

$$P_e^{(x)}(\mathbf{h}_1^{(x)}, \dots, \mathbf{h}_K^{(x)}) = Q\left(\sqrt{2 \frac{\mathbf{g}_1^{(x)H} \mathbf{R}_{\epsilon_x, \epsilon_x}^{-1} \mathbf{g}_1^{(x)}}{\sigma^2}}\right) \quad (6.38)$$

where $Q(x) = \frac{1}{\sqrt{2\pi}} \int_x^\infty e^{-\frac{x^2}{2}} dx$. To find the average P_e , we need to average (6.38) over the distribution of $\mathbf{h}_1^{(x)}, \dots, \mathbf{h}_K^{(x)}$. However, under the assumption of treating the MAI term after the MMSE detector as Gaussian noise, we only need to average (6.38) over $\mathbf{h}_1^{(x)}$ (or equivalently over $\mathbf{g}_1^{(x)}$). Recalling that $\mathbf{g}_1^{(x)}$ is a complex Gaussian vector, the average $P_e^{(x)}$ over the distribution of $\mathbf{g}_1^{(x)}$ is [1]

$$\begin{aligned} P_e^{(x)} &= \mathbb{E}\left[P_e(\mathbf{h}_1^{(x)})\right] \\ &= \sum_{l=1}^D \frac{\pi_l}{2} \left[1 - \sqrt{\frac{\mu_l}{1 + \mu_l}}\right] \text{ and } \pi_l = \prod_{i=1, i \neq l}^D \frac{\mu_l}{\mu_l - \mu_i} \end{aligned} \quad (6.39)$$

where μ_l , $l = 1, 2, \dots, D$ are the nonzero eigenvalues of $\mathbf{R}_{\epsilon_x, \epsilon_x}^{-1} \mathbf{R}_{\mathbf{g}_1^{(x)}, \mathbf{g}_1^{(x)}}$. For the numerical results in Section 6.5, we adopt this Gaussian approximation and use the SINR and P_e expressions in (6.37) and (6.39), respectively.

Recalling that two systems are equivalent if both attain the same SINR, from the expression in (6.37), we note that a sufficient condition for systems x and y to be equivalent is to have

$$\mathbf{g}_k^{(y)} = \mathbf{F} \mathbf{g}_k^{(x)}, \quad k = 1, 2, \dots, K \quad (6.40)$$

where \mathbf{F} is a unitary transformation, i.e. $\mathbf{F} \mathbf{F}^H = \mathbf{F}^H \mathbf{F} = \mathbf{I}_N$. From (6.8), (6.16), and

(6.23) or (6.28), one can note that we can always write $\mathbf{g}_k^{(x)}$ as

$$\mathbf{g}_k^{(x)} = \mathbf{H}_k^{(x)} \mathbf{q}_k^{(x)} \quad (6.41)$$

where $\mathbf{H}_k^{(x)}$ is the channel matrix for system x that relates the signature $\mathbf{q}_k^{(x)}$ to the output. Now (6.40) becomes

$$\mathbf{H}_k^{(y)} \mathbf{q}_k^{(y)} = \mathbf{F} \mathbf{H}_k^{(x)} \mathbf{q}_k^{(x)}. \quad (6.42)$$

If $\mathbf{q}_k^{(y)} = \mathbf{F} \mathbf{q}_k^{(x)}$, then condition (6.42) for equivalence becomes

$$\mathbf{H}_k^{(x)} = \mathbf{F}^H \mathbf{H}_k^{(y)} \mathbf{F} \quad (6.43)$$

In the next section we implicitly solve the following problem: Given $\mathbf{q}_k^{(x)}$, $\mathbf{H}_k^{(x)}$ and $\mathbf{H}_k^{(y)}$, find an \mathbf{F} such that $\mathbf{q}_k^{(y)} = \mathbf{F} \mathbf{q}_k^{(x)}$ and (6.43) is satisfied. In other words, for the same channel realization systems x and y have identical performance when $\mathbf{q}_k^{(x)}$, $\mathbf{q}_k^{(y)}$ are chosen as the signature codes.

In the next section, we prove the sufficient conditions for the different CDMA systems to be equivalent for FS channel. Using the duality relations described in Section 6.3, in conjunction with necessary additional proofs, we show that similar conditions for TS and TFS channels follow.

6.4.1. Equivalences in FS Channel

We first recall from Section 6.2.4, that in FS channel, The MC-DS-CDMA system only have Case 1 in (6.2.3.1) and Case 3 in (6.2.3.3). In this section, in Proposition 1, we derive the sufficient conditions for a DS-CDMA system to be equivalent to a MC-CDMA system. In Proposition 2, we derive the conditions for a MC-CDMA system and a MC-DS-CDMA Case 1 system to be equivalent. In Proposition 3, we derive

the conditions for a MC-CDMA system and a MC-DS-CDMA Case 3 system to be equivalent. The conditions for a MC-DS-CDMA system Cases 1 and 3 to be equivalent to a DS-CDMA system will then follow.

Proposition 1:

The DS-CDMA system is equivalent to the MC-CDMA system provided that the following condition is satisfied:

$$\tilde{\mathbf{q}}_k = \mathbf{D}_N \mathbf{q}_k \quad (6.44)$$

where \mathbf{D}_N is the $N \times N$ DFT matrix whose $(n, m)^{th}$ entry is defined to be $D_{n,m} = e^{-j\frac{2\pi nm}{N}}$.

Proof:

Recall \mathbf{Q}_k and \mathbf{h}_k are the signature code matrix and channel vector for the DS-CDMA system and $\tilde{\mathbf{Q}}_k$ and $\tilde{\mathbf{h}}_k$ are the corresponding quantities in MC-CDMA system. As discussed in Section 6.2.1, \mathbf{Q}_k is a Toeplitz matrix in FS channel. In Appendix C we show that

$$\tilde{\mathbf{h}}_k = \mathbf{D}_N(1 : L + 1)\mathbf{h}_k \quad (6.45)$$

so that $\mathbf{D}(L + 2 : N)^H \tilde{\mathbf{h}}_k = \mathbf{0}$. Hence, using (6.8),

$$\mathbf{g}_k = \mathbf{Q}_k \mathbf{D}_N(1 : L + 1)^H \tilde{\mathbf{h}}_k = \tilde{\mathbf{Q}}_k \mathbf{D}_N^H \tilde{\mathbf{h}}_k \quad (6.46)$$

where $\tilde{\mathbf{Q}}_k = \begin{bmatrix} \mathbf{Q}_k & \mathbf{X} \end{bmatrix}$ for any appropriately sized matrix \mathbf{X} . We note that in general $L \ll N$, so that $\mathbf{q}_k(l)$ in (6.8) can be approximated with an l -order cyclic shift of \mathbf{q}_k . Then, we can choose \mathbf{X} so that $\tilde{\mathbf{Q}}_k$ is circulant and multiply \mathbf{g}_k by \mathbf{D}_N to get

$$\mathbf{D}_N \mathbf{g}_k \approx \mathbf{D}_N \tilde{\mathbf{Q}}_k \mathbf{D}_N^H \tilde{\mathbf{h}}_k = \tilde{\tilde{\mathbf{Q}}}_k \tilde{\mathbf{h}}_k = \tilde{\tilde{\mathbf{g}}}_k \quad (6.47)$$

where $\bar{\bar{\mathbf{Q}}}_k = \text{diag} \{ \mathbf{D}_N \mathbf{q}_k \}$ since the DFT matrix diagonalizes circulant matrices. One can see that $\bar{\mathbf{g}}_k$ in (6.16) for the FS channel is equal to $\bar{\bar{\mathbf{g}}}_k$ in (6.47) provided that $\bar{\mathbf{q}}_k = \mathbf{D}_N \mathbf{q}_k$. Recall (6.40), the proof then follows. \square

Proposition 2:

The MC-DS-CDMA system Case 1 is equivalent to a MC-CDMA system provided that the following condition is satisfied:

$$\bar{\mathbf{q}}_k = \bar{\mathbf{D}}_{N_t} \hat{\mathbf{q}}_k^{(f)} \quad (6.48)$$

where $\bar{\mathbf{D}}_{N_t} = \begin{bmatrix} \mathbf{D}_{N_t} & \mathbf{0} & \cdots & \mathbf{0} \\ \mathbf{0} & \mathbf{D}_{N_t} & \cdots & \mathbf{0} \\ \vdots & \ddots & \ddots & \vdots \\ \mathbf{0} & \cdots & \mathbf{0} & \mathbf{D}_{N_t} \end{bmatrix}$ and $\hat{\mathbf{q}}_k^{(f)} = \begin{bmatrix} \hat{\mathbf{q}}_{k,0}^{(f)T} & \cdots & \hat{\mathbf{q}}_{k,N_f-1}^{(f)T} \end{bmatrix}$.

Proof:

We first recall that in FS channel, each sub-band n in the MC-DS-CDMA system Case 1 encounters multipath components. The proof to this proposition is then obtained by applying the proof of Proposition 1 per sub-band n . We start by writing $\hat{\mathbf{g}}_k^{(f)}$ in (6.23) as

$$\hat{\mathbf{g}}_k^{(f)} = \begin{bmatrix} \hat{\mathbf{g}}_{k,0}^{(f)T} & \cdots & \hat{\mathbf{g}}_{k,N_f-1}^{(f)T} \end{bmatrix}^T \quad (6.49)$$

where $\hat{\mathbf{g}}_{k,n}^{(f)} = \hat{\mathbf{Q}}_k^{(f)}(n) \hat{\mathbf{h}}_{k,n}^{(f)}$. Following the proof in Appendix A, one can show that

$$\tilde{\mathbf{h}}_{k,n} = \mathbf{D}_{N_t}(1 : L_o + 1) \hat{\mathbf{h}}_{k,n}^{(f)} \quad (6.50)$$

where $\tilde{\mathbf{h}}_{k,n} = \begin{bmatrix} \tilde{h}_k[0, nN_t] & \cdots & \tilde{h}_k[0, (n+1)N_t - 1] \end{bmatrix}$ is the n^{th} segment of $\tilde{\mathbf{h}}_k$ of length $N_t \times 1$. Recall from Section 6.2.4 that in FS channel, $\hat{\mathbf{Q}}_k^{(f)}(n)$ is Toeplitz built by $\hat{\mathbf{q}}_{k,n}^{(f)}$. hence, using (6.50), and following the proof of Proposition 1, one can

show that

$$\begin{aligned} \mathbf{D}_{N_t} \hat{\mathbf{g}}_{k,n}^{(f)} &\approx \mathbf{D}_{N_t} \hat{\mathbf{Q}}_k^{(f)}(n) \mathbf{D}_{N_t} (1 : L_o + 1)^H \tilde{\mathbf{h}}_{k,n} \\ &= \tilde{\tilde{\mathbf{Q}}}_{k,n} \tilde{\mathbf{h}}_{k,n} \end{aligned} \quad (6.51)$$

where $\tilde{\tilde{\mathbf{Q}}}_{k,n} = \text{diag} \{ \mathbf{D}_{N_t} \hat{\mathbf{q}}_{k,n}^{(f)} \}$. That is

$$\bar{\mathbf{D}}_{N_t} \hat{\mathbf{g}}^{(f)} \approx \tilde{\tilde{\mathbf{Q}}}_k \tilde{\mathbf{h}}_k = \tilde{\tilde{\mathbf{g}}}_k \quad (6.52)$$

where $\tilde{\tilde{\mathbf{Q}}}_k = \text{diag} \{ \bar{\mathbf{D}}_{N_t} \hat{\mathbf{q}}_k^{(f)} \}$. One can see that $\tilde{\mathbf{g}}_k$ in (6.16) for the FS channel is equal to $\tilde{\tilde{\mathbf{g}}}_k$ in (6.52) provided that $\tilde{\mathbf{q}}_k = \bar{\mathbf{D}}_{N_t} \hat{\mathbf{q}}_k^{(f)}$. The proof then follows. \square

Proposition 3:

Under the BF assumption, a MC-DS-CDMA system Case 3 is equivalent to a MC-CDMA system provided that the condition in (6.48) is satisfied.

Proof:

This proof is basically a special case from the proof of Proposition 2 when $L_o = 0$ (so that each sub-band encounters frequency non-selective fading and the BF assumption is valid). We recall from Section 6.3, that under BF assumption $\tilde{\mathbf{h}}_k$ can be written as

$$\tilde{\mathbf{h}}_k \approx \left[\tilde{h}_k[0,0] \mathbf{1}_{N_t}^T \quad \cdots \quad \tilde{h}_k[0, N_f - 1] \mathbf{1}_{N_t}^T \right]^T \quad (6.53)$$

$$\approx \left[\hat{h}_k[0,0] \mathbf{1}_{N_t}^T \quad \cdots \quad \hat{h}_k[0, N_f - 1] \mathbf{1}_{N_t}^T \right]^T \quad (6.54)$$

that is $\tilde{\mathbf{h}}_{k,n} = \tilde{h}_k[0, n] \mathbf{1}_{N_t}$. In (6.54), we used the fact that $\tilde{h}_k[0, n] = \hat{h}_k[0, n]$ for FS channels. To recognize this fact, substitute $\tilde{c}_k(t, f) = \tilde{c}_k(0, f)$ and $\tilde{C}_k(\theta, f) = \tilde{c}_k(0, f) \delta(\theta)$ in (6.12) and (6.30), respectively, where $\delta(\cdot)$ is the Dirac-delta function. Now, from (6.32), in a Case 3 MC-DS-CDMA system,

$$\hat{\mathbf{g}}_{k,n}^{(f)} = \hat{\mathbf{q}}_{k,n}^{(f)} \hat{h}_k[0, n] \quad (6.55)$$

$$= \begin{bmatrix} \hat{\mathbf{q}}_{k,n}^{(f)} & \mathbf{X}_{k,n} \end{bmatrix} \begin{bmatrix} \hat{h}_k(0, n) \\ \mathbf{0}_{N_t-1} \end{bmatrix} \quad (6.56)$$

$$= \bar{\mathbf{Q}}_k^{(f)}(n) \mathbf{D}_{N_t}^H \hat{h}_k(0, n) \mathbf{1}_{N_t} \quad (6.57)$$

$$\approx \bar{\mathbf{Q}}_k^{(f)}(n) \mathbf{D}_{N_t}^H \tilde{\mathbf{h}}_{k,n} \quad (6.58)$$

where in (6.56), $\mathbf{X}_{k,n}$ is any appropriately sized matrix. In (6.57),

$$\bar{\mathbf{Q}}_k^{(f)}(n) = \begin{bmatrix} \hat{\mathbf{q}}_{k,n}^{(f)} & \mathbf{X}_{k,n} \end{bmatrix} \text{ and we used the fact that } \mathbf{D}_{N_t} \begin{bmatrix} \hat{h}_k[0, n] & \mathbf{0}_{N_t-1}^T \end{bmatrix}^T = \hat{h}_k[0, n] \mathbf{1}_{N_t}.$$

In (6.58), we used the BF assumption in (6.53). Now in (6.58) choose $\mathbf{X}_{k,n}$ so that

$\bar{\mathbf{Q}}_k^{(f)}(n)$ is circulant. Hence,

$$\begin{aligned} \mathbf{D}_{N_t} \hat{\mathbf{g}}_{k,n}^{(f)} &\approx \mathbf{D}_{N_t} \bar{\mathbf{Q}}_k^{(f)}(n) \mathbf{D}_{N_t}^H \tilde{\mathbf{h}}_{k,n} \\ &= \ddot{\mathbf{Q}}_{k,n} \tilde{\mathbf{h}}_{k,n}. \end{aligned} \quad (6.59)$$

That is,

$$\bar{\mathbf{D}}_{N_t} \hat{\mathbf{g}}^{(f)} \approx \ddot{\mathbf{Q}}_k \tilde{\mathbf{h}}_k = \ddot{\mathbf{g}}_k \quad (6.60)$$

Again, one can see that $\tilde{\mathbf{g}}_k$ in (6.16) for the FS channel is equal to $\ddot{\mathbf{g}}_k$ in (6.60) provided that $\tilde{\mathbf{q}}_k = \bar{\mathbf{D}}_{N_t} \hat{\mathbf{q}}^{(f)}$ and the proof then follows. \square

We note that $\bar{\mathbf{D}}_{N_t}$ is a particular unitary transformation for Proposition 3 to hold in FS channel. In fact, under BF assumption, the proposition holds in a FS channel for

$$\text{any } \bar{\mathbf{F}}_{N_t} = \begin{bmatrix} \mathbf{F}_{N_t} & \mathbf{0} & \cdots & \mathbf{0} \\ \mathbf{0} & \mathbf{F}_{N_t} & \cdots & \mathbf{0} \\ \vdots & \ddots & \ddots & \vdots \\ \mathbf{0} & \cdots & \mathbf{0} & \mathbf{F}_{N_t} \end{bmatrix} \text{ where } \mathbf{F}_{N_t} \text{ is any } N_t \times N_t \text{ unitary transformation.}$$

To recognize this fact, we write

$$\bar{\mathbf{F}}_{N_t} \hat{\mathbf{g}}^{(f)} = \begin{bmatrix} \mathbf{F}_{N_t} \hat{\mathbf{q}}_{k,0}^{(f)} & \mathbf{0} & \cdots & \mathbf{0} \\ \mathbf{0} & \mathbf{F}_{N_t} \hat{\mathbf{q}}_{k,1}^{(f)} & \cdots & \mathbf{0} \\ \vdots & \ddots & \ddots & \vdots \\ \mathbf{0} & \cdots & \mathbf{0} & \mathbf{F}_{N_t} \hat{\mathbf{q}}_{k,N_f-1}^{(f)} \end{bmatrix} \hat{\mathbf{h}}_k^{(f)} \quad (6.61)$$

$$= \begin{bmatrix} \text{diag}\{\mathbf{F}_{N_t} \hat{\mathbf{q}}_{k,0}^{(f)}\} & \mathbf{0} & \cdots & \mathbf{0} \\ \mathbf{0} & \text{diag}\{\mathbf{F}_{N_t} \hat{\mathbf{q}}_{k,1}^{(f)}\} & \cdots & \mathbf{0} \\ \vdots & \ddots & \ddots & \vdots \\ \mathbf{0} & \cdots & \mathbf{0} & \text{diag}\{\mathbf{F}_{N_t} \hat{\mathbf{q}}_{k,N_f-1}^{(f)}\} \end{bmatrix} \times \begin{bmatrix} \hat{h}_k[0,0] \mathbf{1}_{N_t} \\ \vdots \\ \hat{h}_k[0, N_f - 1] \mathbf{1}_{N_t} \end{bmatrix} \quad (6.62)$$

$$\approx \check{\mathbf{Q}}_k \tilde{\mathbf{h}}_k \quad (6.63)$$

where in (6.63) we used the BF assumption in (6.53) and $\check{\mathbf{Q}}_k = \text{diag}\{\bar{\mathbf{F}}_{N_t} \hat{\mathbf{q}}_k^{(f)}\}$. Again the right hand side in (6.63) is $\tilde{\mathbf{g}}_k$ provided that $\tilde{\mathbf{q}}_k = \bar{\mathbf{F}}_{N_t} \hat{\mathbf{q}}_k^{(f)}$. Another way to look at this fact is to consider (6.43). In this case, the channel matrices for MC-DS-CDMA Case 3 and MC-CDMA systems are,

$$\hat{\mathbf{H}}_k = \begin{bmatrix} \hat{h}_k[0,0] \mathbf{I}_{N_t} & \mathbf{0} & \cdots & \mathbf{0} \\ \mathbf{0} & \hat{h}_k[0,1] \mathbf{I}_{N_t} & \cdots & \mathbf{0} \\ \vdots & \ddots & \ddots & \vdots \\ \mathbf{0} & \cdots & \mathbf{0} & \hat{h}_k[0, N_f - 1] \mathbf{I}_{N_t} \end{bmatrix} \text{ and}$$

MC-DS-CDMA ⇕ MC-CDMA	MC-CDMA ⇕ DS-CDMA	DS-CDMA ⇕ MC-DS-CDMA
$\tilde{\mathbf{q}}_k = \left\{ \begin{array}{l} \bar{\mathbf{D}}_{N_t} \hat{\mathbf{q}}_k^{(f)}, B_o > \Delta f_c \\ \bar{\mathbf{F}}_{N_t} \hat{\mathbf{q}}_k^{(f)}, B_o \ll \Delta f_c \\ \text{and BF} \end{array} \right\}$	$\mathbf{q}_k = \mathbf{D}_N^H \tilde{\mathbf{q}}_k$	$\hat{\mathbf{q}}_k^{(f)} = \left\{ \begin{array}{l} \bar{\mathbf{D}}_{N_t}^H \mathbf{D}_N \mathbf{q}_k, B_o > \Delta f_c \\ \bar{\mathbf{F}}_{N_t}^H \mathbf{D}_N \mathbf{q}_k, B_o \ll \Delta f_c \\ \text{and BF} \end{array} \right\}$

Table 6.1. Equivalence results for FS channel

$$\tilde{\mathbf{H}}_k = \begin{bmatrix} \tilde{h}_k[0,0] & 0 & \cdots & 0 \\ 0 & \tilde{h}_k[0,1] & \cdots & 0 \\ \vdots & \ddots & \ddots & \vdots \\ 0 & \cdots & 0 & \tilde{h}_k[0, N_f - 1] \end{bmatrix} \text{ respectively.} \quad (6.64)$$

It is then clear that under BF assumption, $\hat{\mathbf{H}}_k = \bar{\mathbf{F}}_{N_t}^H \tilde{\mathbf{H}}_k \bar{\mathbf{F}}_{N_t}$ for any $\bar{\mathbf{F}}_{N_t}$. An interesting special case of $\bar{\mathbf{F}}_{N_t}$ is to be \mathbf{I}_N , that is, the MC-DS-CDMA and the MC-CDMA systems are also equivalent under BF if $\tilde{\mathbf{q}}_k = \hat{\mathbf{q}}_k^{(f)}$.

The results obtained in this section are summarized in Table 6.1. Note that the third column in Table 6.1 is obtained by combining the results in the first two columns.

6.4.2. Equivalences in TS Channel

Building on the intuition in Section 6.3, a similar set of results analogous to that in Section 6.4.1 can be obtained in TS channel. We recall from Section 6.2.4, that in TS channel, The MC-DS-CDMA system only have Case 2 in (6.2.3.2) and Case 3 in (6.2.3.3). In this case, Proposition 1 shows the sufficient condition for a DS-CDMA and a MC-CDMA systems to be equivalent. Proposition 2 shows the sufficient condition for a DS-CDMA system and a MC-DS-CDMA Case 2 system to be equivalent. Proposition 3 shows the sufficient condition for a DS-CDMA system and a MC-DS-

CDMA Case 3 system to be equivalent. The sufficient conditions for a MC-CDMA system to be equivalent to a MC-DS-CDMA system Cases 2 and 3 then follow. The proofs of Propositions 1, 2 and 3 in TS channel are analogous to those introduced in the previous section for FS channel under the following mappings:

MC-CDMA \longrightarrow DS-CDMA

MC-DS-CDMA Case1 \longrightarrow MC-DS-CDMA Case2

$\mathbf{q}_k \longrightarrow \tilde{\mathbf{q}}_k$

$\tilde{\mathbf{q}}_k \longrightarrow \mathbf{q}_k$

$\hat{\mathbf{q}}_k^{(f)} \longrightarrow \hat{\mathbf{q}}_k^{(t)}$

$\tilde{\mathbf{h}}_{k,n} \longrightarrow \mathbf{h}_{k,p}$ where $\mathbf{h}_{k,p} = \left[\tilde{h}_k[pN_f, 0] \ \dots \ \tilde{h}_k[(p+1)N_f - 1, 0] \right]$ is the p^{th} segment of \mathbf{h}_k of length $N_f \times 1$

$N_t \longrightarrow N_f$

$N_f \longrightarrow N_t$

$l \longrightarrow m$

$L \longrightarrow 2M + 1$

$L_o \longrightarrow 2M_o + 1$

$x^{(f)} \longrightarrow x^{(t)}$ for any quantity x

$\mathbf{D}_N \longrightarrow \mathbf{D}_N^H$

$\mathbf{D}_{N_t} \longrightarrow \mathbf{D}_{N_f}^H$

$\bar{\mathbf{D}}_{N_t} \longrightarrow \bar{\mathbf{D}}_{N_f}^H$ where $\bar{\mathbf{D}}_{N_f}$ is similar to $\bar{\mathbf{D}}_{N_t}$ except for replacing \mathbf{D}_{N_t} with \mathbf{D}_{N_f} .

$\bar{\mathbf{F}}_{N_t} \longrightarrow \bar{\mathbf{F}}_{N_f}^H$ where $\bar{\mathbf{F}}_{N_f}$ is similar to $\bar{\mathbf{F}}_{N_t}$ except for replacing \mathbf{F}_{N_t} with \mathbf{F}_{N_f} and \mathbf{F}_{N_f}

is any unitary transformation of dimension N_f .

Table 6.2 summarizes the equivalence results in TS channel. Again, the third column in the table is obtained by combining the results in columns one and two.

MC-DS-CDMA ⇕ DS-CDMA	DS-CDMA ⇕ MC-CDMA	MC-CDMA ⇕ MC-DS-CDMA
$\mathbf{q}_k = \begin{cases} \bar{\mathbf{D}}_{N_f}^H \hat{\mathbf{q}}_k^{(t)}, T_o > \Delta t_c \\ \bar{\mathbf{F}}_{N_f}^H \hat{\mathbf{q}}_k^{(t)}, T_o \ll \Delta t_c \\ \text{and BF} \end{cases}$	$\tilde{\mathbf{q}}_k = \mathbf{D}_N \mathbf{q}_k$	$\hat{\mathbf{q}}_k^{(t)} = \begin{cases} \bar{\mathbf{D}}_{N_f} \mathbf{D}_N^H \tilde{\mathbf{q}}_k, T_o > \Delta t_c \\ \bar{\mathbf{F}}_{N_f} \mathbf{D}_N^H \tilde{\mathbf{q}}_k, T_o \ll \Delta t_c \\ \text{and BF} \end{cases}$

Table 6.2. Equivalence results for TS channel

There is though a subtle point that needs to be explained when equivalent proofs to those in Section 6.4.1 are derived. That is, in FS channel, l only takes positive values and the one-sided DFT operation was used in the obtained results. In TS channel, as stated above, l maps to m which takes symmetric values around 0 as seen in (6.12) and (6.25). Now, using a single-sided DFT operation as done before in the proofs in Section 6.4.1 will imply a phase shift. That is, the analogous equations to (6.45) and (6.50) are

$$\mathbf{D}_N^H(1 : 2M + 1) \tilde{\mathbf{h}}_k = \mathbf{h}_k \odot \mathbf{e}_{M,N} \text{ and} \quad (6.65)$$

$$\mathbf{D}_{N_f}^H(1 : 2M_o + 1) \hat{\mathbf{h}}_{k,p}^{(t)} = \tilde{\mathbf{h}}_{k,n} \odot \mathbf{e}_{M_o, N_f} \quad (6.66)$$

respectively, where $\mathbf{e}_{M,N} = \begin{bmatrix} 1 & e^{j\frac{2\pi M}{N}} & \dots & e^{j\frac{2\pi(N-1)M}{N}} \end{bmatrix}$. A proof for the relation in (6.65) is provided in Appendix D. Similar proof for (6.66) can be deduced. We note that the presence of phase shift does not change the equivalence condition since it does not affect the SINR value. Starting from this point, the phase shift will be ignored in the analysis.

6.4.3. Equivalences in TFS Channel

In this section we prove Propositions 1,2 and 3 for the general case of TFS channel. In TFS channel, the MC-DS-CDMA system have the three cases described in Sec-

tion 6.2.3. In this case, Proposition 1 shows the sufficient condition for a MC-CDMA and a DS-CDMA systems to be equivalent. Proposition 2 shows the sufficient condition for a MC-CDMA system and a MC-DS-CDMA Case 1 system as well as the condition for a DS-CDMA system and a MC-DS-CDMA Case 2 system to be equivalent. Proposition 3 shows the sufficient condition for a MC-CDMA system and a MC-DS-CDMA Case 3 system to be equivalent.⁶ The remaining equivalence cases then follow.

6.4.3.1. Proof of Proposition 1

Before proving Proposition 1 for TFS channel, we first introduce the following lemma.

Lemma 1:

$$h_k[p, l] = \sum_{m=-M}^M H_k[m, l] e^{j \frac{2\pi m(p+1/2)}{N}} \quad (6.67)$$

where $h_k[p, l]$ is given in (6.4) and

$$H_k[m, l] = \int_0^{T_m} \int_{-B_d}^{B_d} C(\theta, \tau) \text{sinc}(m - \theta T) \text{sinc}(l - B\tau) e^{-j\pi(m - \theta T)} e^{-j\pi(l - B\tau)} d\theta d\tau \quad (6.68)$$

where $C(\theta, \tau) = \int c(t, \tau) e^{-j2\pi\theta t} dt$.

⁶An equivalent proof is also provided for the sufficient condition to have a DS-CDMA system and a MC-DS-CDMA Case 3 system equivalent.

Proof:

See Appendix E.

Now recall (6.7) and (6.8), one can write \mathbf{g}_k as

$$\mathbf{g}_k = \sum_{l=0}^L \mathbf{Q}_k(l) \mathbf{h}_{k,l} \quad (6.69)$$

$$= \sum_{l=0}^L \mathbf{Q}_k(l) \sum_{m=-M}^M H_k(m, l) \mathbf{e}_{m,N}(l) \quad (6.70)$$

$$= \sum_{m=-M}^M \sum_{l=0}^L H_k(m, l) (\mathbf{q}_k(l) \odot \mathbf{e}_{m,N}(l)) \quad (6.71)$$

$$= \sum_{m=-M}^M \acute{\mathbf{Q}}_{k,m} \acute{\mathbf{h}}_{k,m} \quad (6.72)$$

where in (6.70) we used Lemma 1, in (6.71) (recall $\mathbf{Q}_k(l)$ in (6.7) is diagonal) we replaced $\mathbf{Q}_k(l) \mathbf{e}_{m,N}(l)$ by $\mathbf{q}_k(l) \odot \mathbf{e}_{m,N}(l)$, and in (6.72)

$\acute{\mathbf{Q}}_{k,m} = \begin{bmatrix} \mathbf{q}_k(0) \odot \mathbf{e}_{m,N}(0) & \cdots & \mathbf{q}_k(L) \odot \mathbf{e}_{m,N}(L) \end{bmatrix}$ (recall that $\acute{\mathbf{Q}}_{k,m}$ is Toeplitz) and $\acute{\mathbf{h}}_{k,m} = \begin{bmatrix} H_k[m, 0] & \cdots & H_k[m, L] \end{bmatrix}^T$. Using the same approach as in Appendix C, one can show that

$$\acute{\mathbf{h}}_{k,m} = \mathbf{D}_N^H \tilde{\mathbf{h}}_{k,m} \quad (6.73)$$

where $\tilde{\mathbf{h}}_{k,m}$ is given in (6.15). Using (6.73) in (6.72), then

$$\mathbf{D}_N \mathbf{g}_k = \sum_{m=-M}^M \mathbf{D}_N \acute{\mathbf{Q}}_{k,m} \mathbf{D}_N^H \tilde{\mathbf{h}}_{k,m} \quad (6.74)$$

$$= \sum_{m=-M}^M \bar{\mathbf{Q}}_k(m) \tilde{\mathbf{h}}_{k,m} = \bar{\mathbf{g}}_k \quad (6.75)$$

where $\bar{\mathbf{Q}}_k(m) = \text{diag}\{D_N[\mathbf{q}_k \odot \mathbf{e}_m]\} = \text{diag}\{[D_N \mathbf{q}_k](m)\}$ and the second equality is obtained from the properties of DFT. One can see that $\bar{\mathbf{g}}_k$ in (6.75) is basically $\tilde{\mathbf{g}}_k$ in (6.16) for TFS channel provided that $\tilde{\mathbf{q}}_k = \mathbf{D}_N \mathbf{q}_k$. hence, Proposition 1 is proved for TFS channel.

6.4.3.2. Proof of Proposition 2

In TFS channel, we need to prove the following to prove Proposition 2:

1. MC-DS-CDMA Case 1 system in Section 6.2.3.1 is equivalent to MC-CDMA system provided that $\tilde{\mathbf{q}}_k = \bar{\mathbf{D}}_{N_r} \hat{\mathbf{q}}_k$.
2. MC-DS-CDMA Case 2 system in Section 6.2.3.2 is equivalent to DS-CDMA system provided that $\mathbf{q}_k = \bar{\mathbf{D}}_{N_f}^H \hat{\mathbf{q}}_k$.

The first proof can be deduced by noting that in MC-DS-CDMA Case1 system, per sub-band there exists L_o multipath due to frequency selectivity and per path, each chip is faded differently due to time selectivity. This scenario per sub-band is similar to that in Section 6.4.3.1. The proof is obtained by mimicking the proof in Section 6.4.3.1 per sub-band parallel to the proof of Proposition 2 in Section 6.4.1.

The second proof can be directly obtained analogous to the first one using the mappings in Section 6.4.2.

6.4.3.3. Proof of Proposition 3

In TFS channel, Proposition 3 addresses the equivalence conditions between a MC-DS-CDMA Case3 system in Section 6.2.3.3 and, a MC-CDMA and DS-CDMA systems. Starting with a MC-CDMA system in TFS channel. Under BF assumption, the noise-free received signal in (6.11) can be written as (recall (4.46))

$$\tilde{\mathbf{x}}_k(t) \approx \sum_{i=1}^{N_f} \sum_{m=-M}^M \tilde{h}_k[m, i] \sum_{n \in \Omega_i} \tilde{q}_k[n] e^{j \frac{2\pi(n+1/2)t}{T}}. \quad (6.76)$$

In view of (6.76), the MC-CDMA system in TFS channel under BF encounters multiple Doppler components per sub-band. As discussed in Section 6.3, to diagonalize

the system, we decrease T_o and increase B_o such that the resulting TF-CDMA basis waveforms encounter non-selective fading. One can see that this scenario is analogous to the way MC-CDMA system diagonalizes MC-DS-CDMA Case 1 system in the proof of Proposition 2 Section 6.4.1. In fact, the proof of Proposition 3 in TFS channel is analogous to that of Proposition 2 in Section 6.4.1 except for interchanging time and frequency domains and the same condition $\tilde{\mathbf{q}}_k = \bar{\mathbf{D}}_{N_t} \hat{\mathbf{q}}_k^{(f)}$ for equivalence hold.

We note that, analogous proof to Proposition 3 in TFS channel can be obtained starting with DS-CDMA system and using the mappings in Section 6.4.2. The corresponding condition for equivalence is $\mathbf{q}_k = \bar{\mathbf{D}}_{N_f}^H \hat{\mathbf{q}}_k^{(t)}$.

We also note that in TFS channel as oppose to FS (TS) channel, not any $\bar{\mathbf{F}}_{N_t}$ ($\bar{\mathbf{F}}_{N_f}$) unitary transformation satisfies equivalence. The reason is that in TFS channel the channel matrix in MC-CDMA (DS-CDMA) system is no longer diagonal but rather Toeplitz due to time (frequency) selectivity. Hence, there will always be a DFT operation between the channel coefficients of MC-DS-CDMA Case3 system and those of MC-CDMA (DS-CDMA) system.

The equivalence results obtained in Section 6.4.3 are summarized in Tables 6.3 and 6.4. In both tables, the last column is obtained by combining the results in the first two columns. We note that from Tables 6.3 and 6.4, given \mathbf{q}_k , we have two possible conditions for MC-DS-CDMA Case 3 system to be equivalent to DS-CDMA system:

1. $\hat{\mathbf{q}}_k^{(f)} = \bar{\mathbf{D}}_{N_t} \mathbf{D}_N \mathbf{q}_k$.
2. $\hat{\mathbf{q}}_k^{(t)} = \bar{\mathbf{D}}_{N_f} \mathbf{q}_k$.

One can show that both unitary transformations $\mathbf{F}_1 = \bar{\mathbf{D}}_{N_t} \mathbf{D}_N$ and $\mathbf{F}_2 = \bar{\mathbf{D}}_{N_f}$ satisfy (6.43) when systems x and y are MC-DS-CDMA Case 3 and DS-CDMA respectively.

A similar argument holds for MC-DS-CDMA Case 3 and a MC-CDMA systems.

MC-DS-CDMA ⇕ MC-CDMA	MC-CDMA ⇕ DS-CDMA	DS-CDMA ⇕ MC-DS-CDMA
$\tilde{\mathbf{q}}_k = \left\{ \begin{array}{l} \bar{\mathbf{D}}_{N_t} \hat{\mathbf{q}}_k^{(f)}, B_o > \Delta f_c, \\ T_o \ll \Delta t_c \\ \bar{\mathbf{D}}_{N_t} \hat{\mathbf{q}}_k^{(f)}, B_o \ll \Delta f_c, \\ T_o \ll \Delta t_c \\ \text{and BF} \end{array} \right\}$	$\mathbf{q}_k = \mathbf{D}_N^H \tilde{\mathbf{q}}_k$	$\hat{\mathbf{q}}_k^{(f)} = \left\{ \begin{array}{l} \bar{\mathbf{D}}_{N_t}^H \mathbf{D}_N \mathbf{q}_k, B_o > \Delta f_c, \\ T_o \ll \Delta t_c \\ \bar{\mathbf{D}}_{N_t}^H \mathbf{D}_N \mathbf{q}_k, B_o \ll \Delta f_c, \\ T_o \ll \Delta t_c \\ \text{and BF} \end{array} \right\}$

Table 6.3. Equivalence results for TFS channel-Part 1

MC-DS-CDMA ⇕ DS-CDMA	DS-CDMA ⇕ MC-CDMA	MC-CDMA ⇕ MC-DS-CDMA
$\mathbf{q}_k = \left\{ \begin{array}{l} \bar{\mathbf{D}}_{N_f}^H \hat{\mathbf{q}}_k^{(t)}, \\ T_o > \Delta t_c, \\ B_o \ll \Delta f_c \\ \bar{\mathbf{D}}_{N_f}^H \hat{\mathbf{q}}_k^{(t)}, \\ T_o \ll \Delta t_c, \\ B_o \ll \Delta f_c \text{ and BF} \end{array} \right\}$	$\tilde{\mathbf{q}}_k = \mathbf{D}_N \mathbf{q}_k$	$\hat{\mathbf{q}}_k^{(t)} = \left\{ \begin{array}{l} \bar{\mathbf{D}}_{N_f} \mathbf{D}_N^H \tilde{\mathbf{q}}_k, \\ T_o > \Delta t_c, \\ B_o \ll \Delta f_c \\ \bar{\mathbf{D}}_{N_f} \mathbf{D}_N^H \tilde{\mathbf{q}}_k, \\ T_o \ll \Delta t_c, \\ B_o \ll \Delta f_c \text{ and BF} \end{array} \right\}$

Table 6.4. Equivalence results for TFS channel-Part 2

6.5. Numerical Results

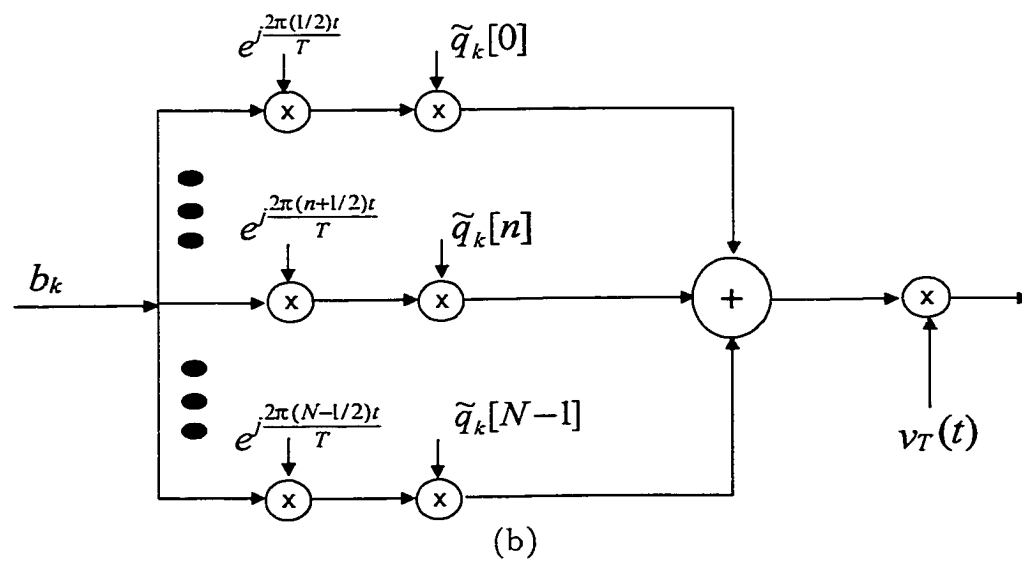
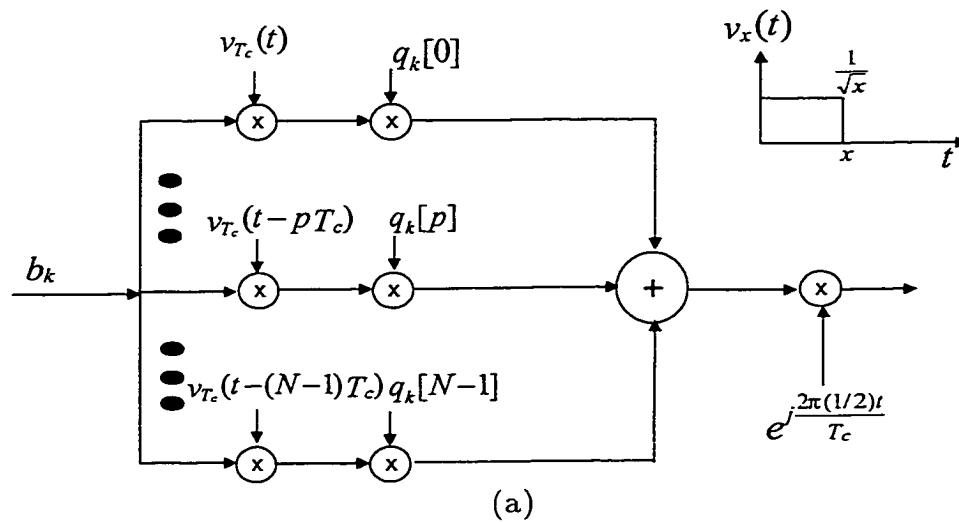
In this section we illustrate the results obtained in Section 6.4. We consider a system of $K = 20$ users, and a WSSUS channel model with $L = 4$ resolvable paths. Each user uses a distinct Gold code of length $N = 32$ for signal spreading and the receiver employs a MMSE detector. We use SINR and P_e defined in Section 6.4 as measures for performance and adopt the equivalence conditions stated in Tables 1,2,3 and 4.

Figure 6.7(a) and (b) show the performance of the different CDMA systems in FS channel. In these figures we show the performance of the three systems considered in this paper. In particular, we show the performance of MC-DS-CDMA system for its two cases. First, Case 1 where we choose $N_f = 2$ so that $L_o = 2$. Second, Case 3 where two different values of N_f are considered, $N_f = 8, 16$. We also show the performance of the DS-CDMA and MC-CDMA systems. Figure 6.7(a) shows the SINR performance for the different systems as well as the Signal to Noise Ratio (SNR) in absence of interference which is a bound on the SINR. Figure 6.7(b) shows the P_e for the different systems. As expected from Propositions 1,2 and 3, the performance of the different systems is virtually indistinguishable.

Figure 6.8(a) and (b) show the $SINR$ and P_e respectively for the MC-CDMA, DS-CDMA and MC-DS-CDMA Case 3 systems in TFS channel with $B_d T = 0.2$. For the MC-DS-CDMA Case 3 system, we take $N_f = 8$ and ideally assume that under this choice every time-frequency basis waveform encounters non selective fading in time and frequency. Again the performance of the three systems is virtually identical.

6.6. Conclusion

In this chapter we studied MMSE multiuser detection for a class of CDMA systems in FS, TS, and TFS channels. We drew a complete duality between systems operating over time and frequency selective channels. We also use this duality to divide the systems operating over TFS channel into sub-groups that either resemble some of the systems operating over FS or TS channels. Building on the time-frequency duality, we showed the sufficient conditions for the different systems to be equivalent in FS, TS, and TFS channels. Numerical results that support our analysis were also provided.



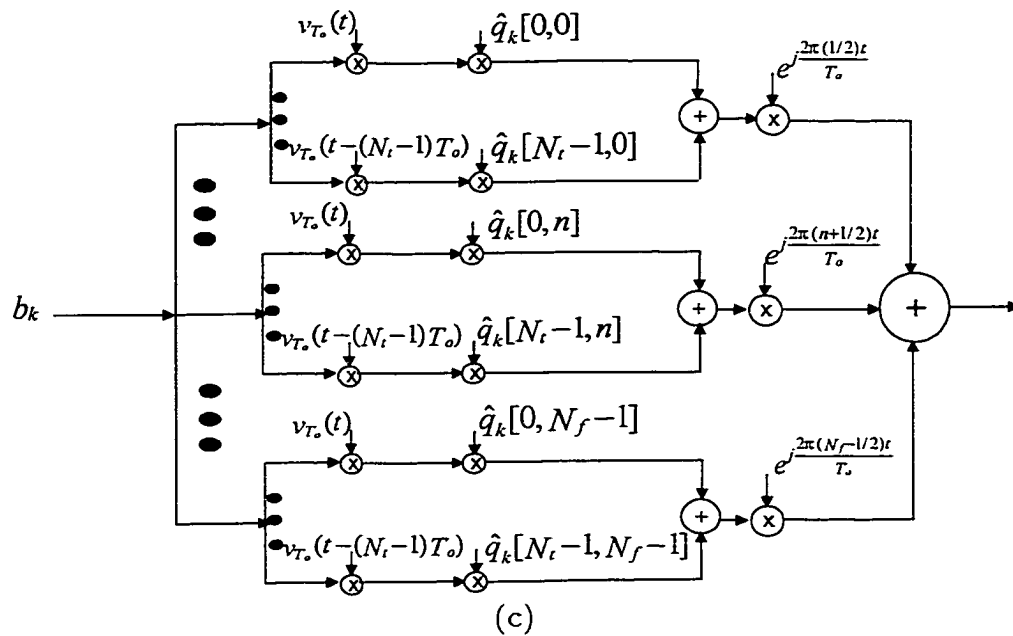
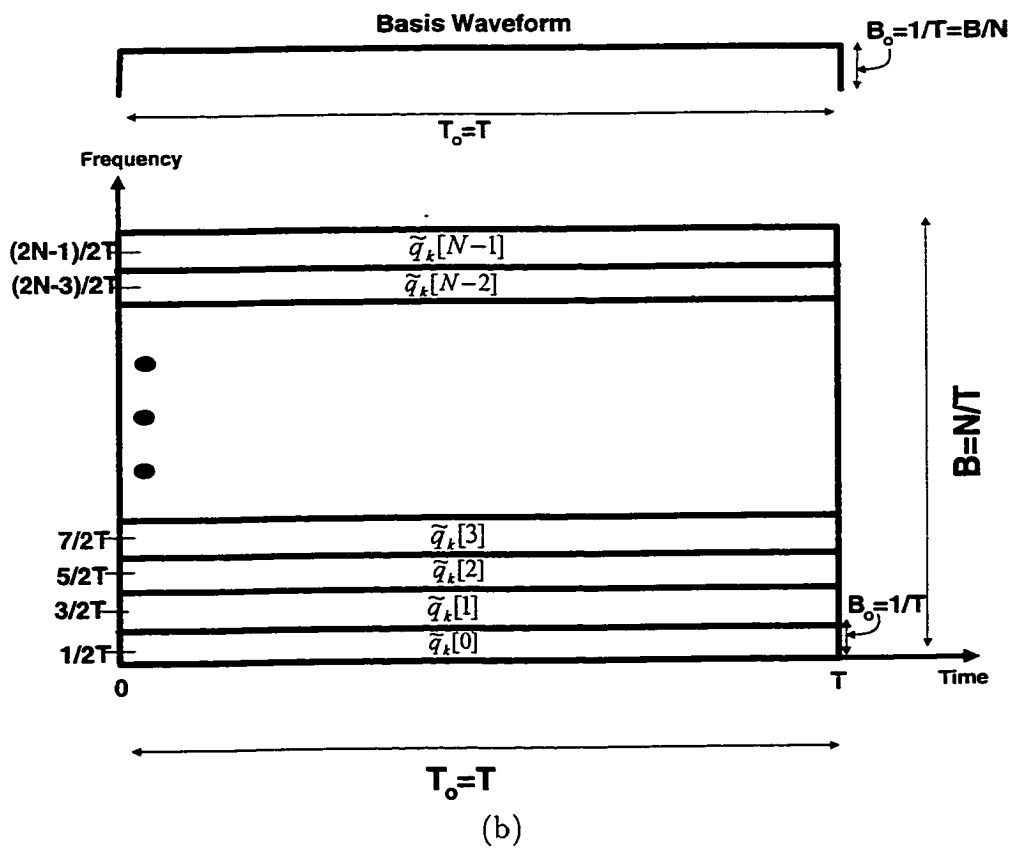
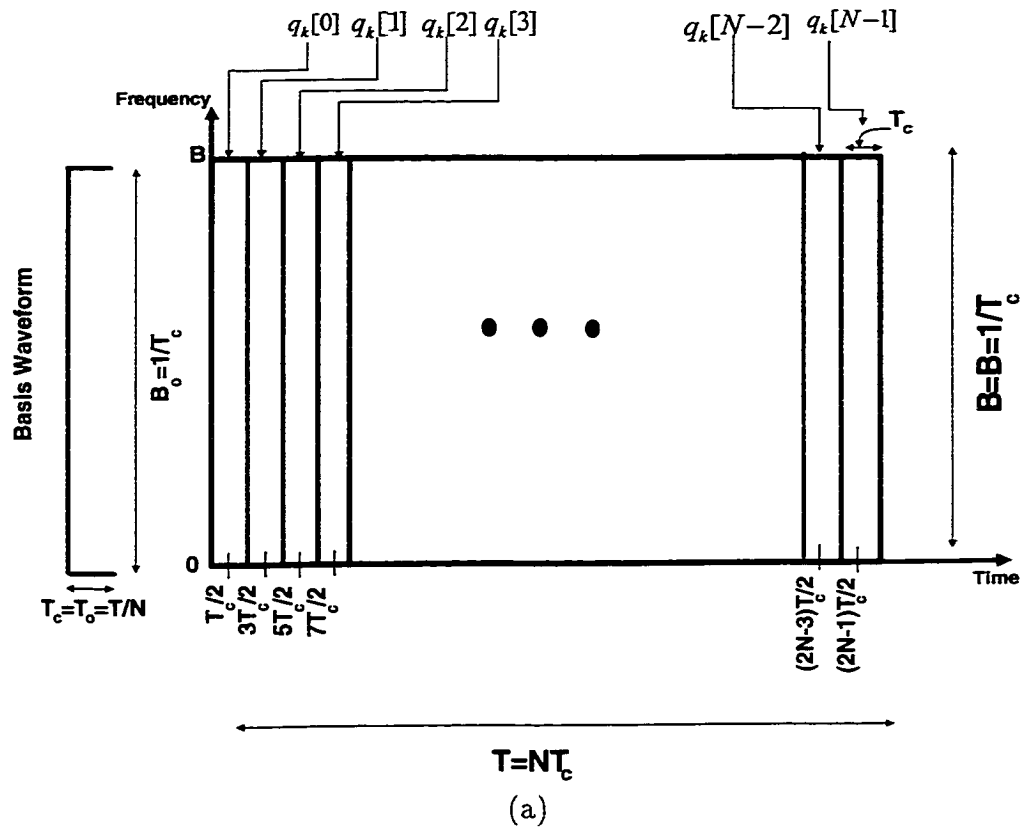
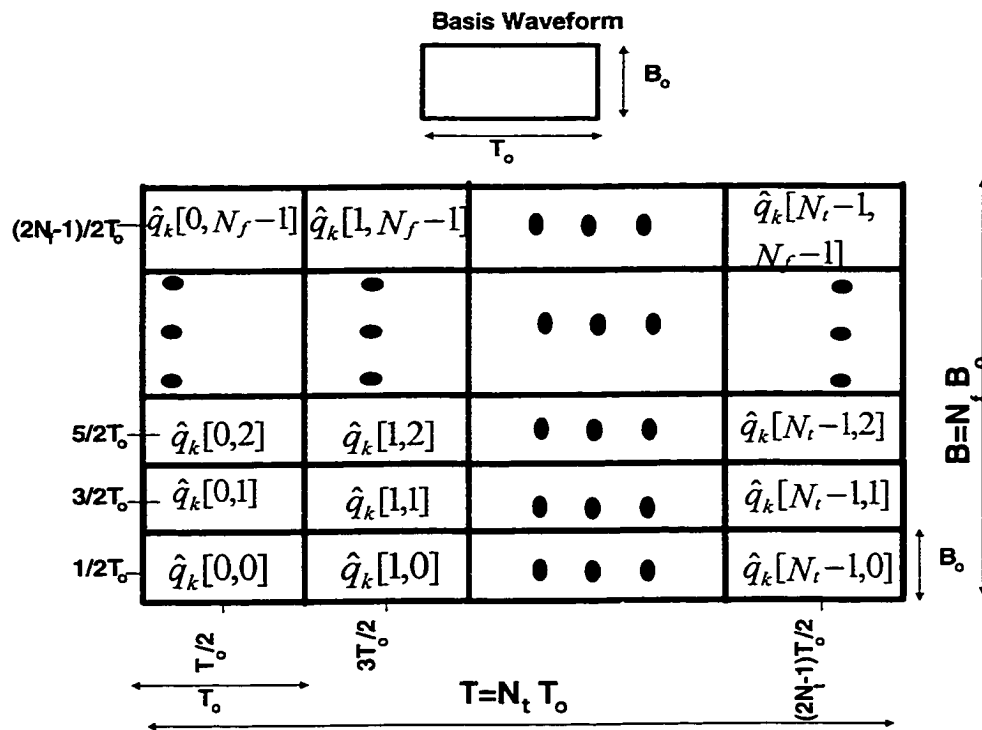


Figure 6.1. The transmitter structure for different CDMA systems. (a) DS-SS-CDMA system where $q_k[p]$ is the p^{th} entry of the k^{th} user signature code. (b) MC-SS-CDMA system where $\tilde{q}_k[n]$ is the n^{th} entry of the k^{th} user signature code. (c) MC-DS-SS-CDMA system where $\hat{q}_k[p, n]$ is the $(p, n)^{\text{th}}$ entry of the k^{th} user signature code.





(c)

Figure 6.2. The code distribution in time and frequency domains. (a) DS-CDMA system. (b) MC-CDMA system. (c) MC-DS-CDMA system.

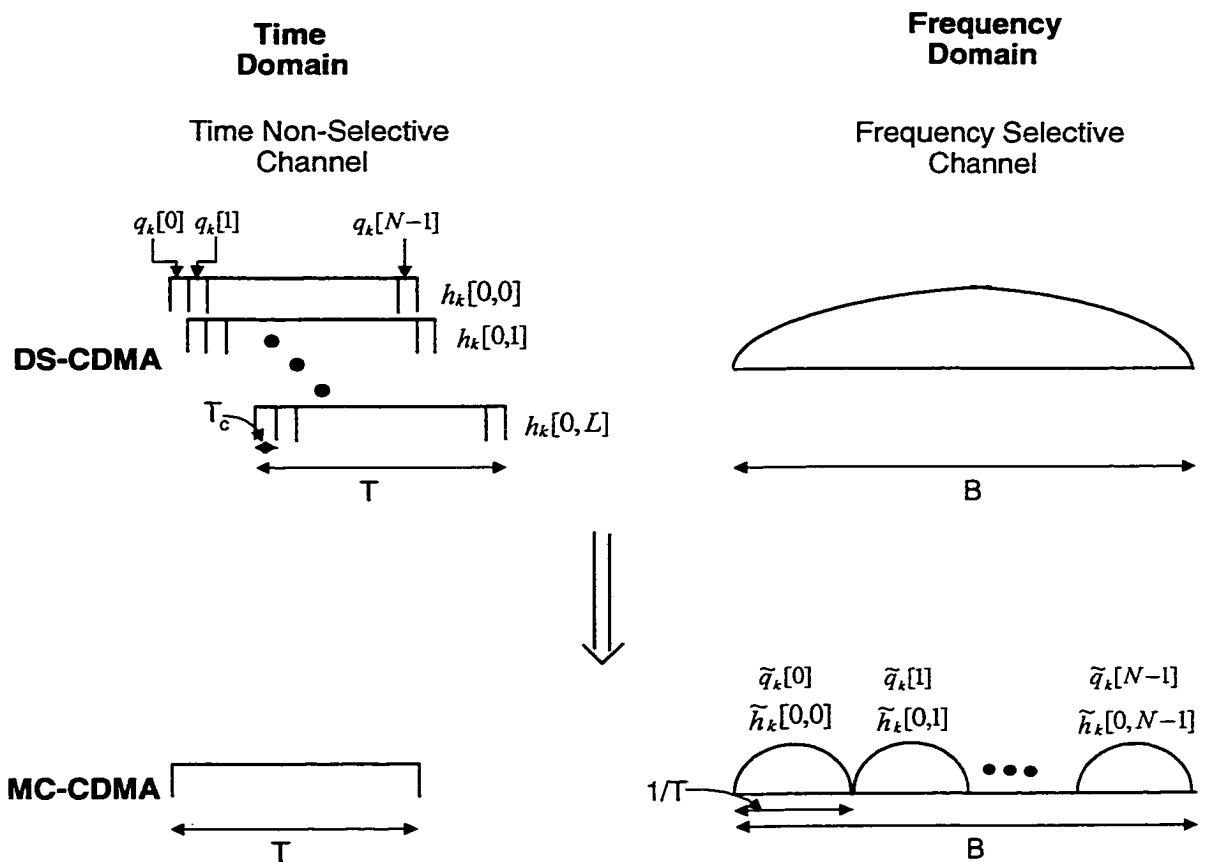


Figure 6.3. DS-CDMA and MC-CDMA systems in FS channel. The DS-CDMA system exhibits multipath in time domain due to frequency selectivity. The MC-CDMA system is diagonal since each subcarrier encounters non selective fading in the frequency domain.

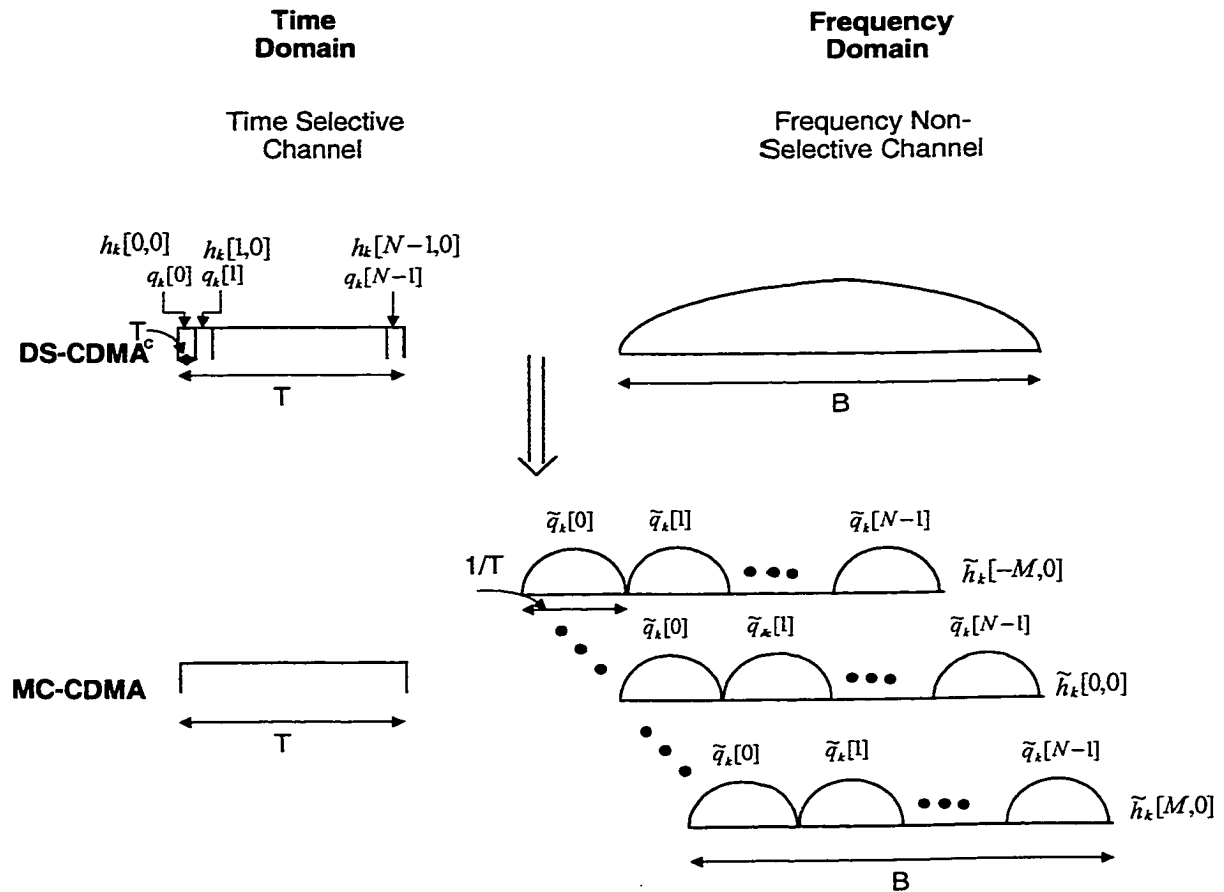


Figure 6.4. DS-CDMA and MC-CDMA systems in a TS channel. The MC-CDMA system exhibits multiple Doppler components in the frequency domain due to time selectivity. The DS-CDMA system is diagonal since each basis waveform (chip) encounters non selective fading in the time domain.

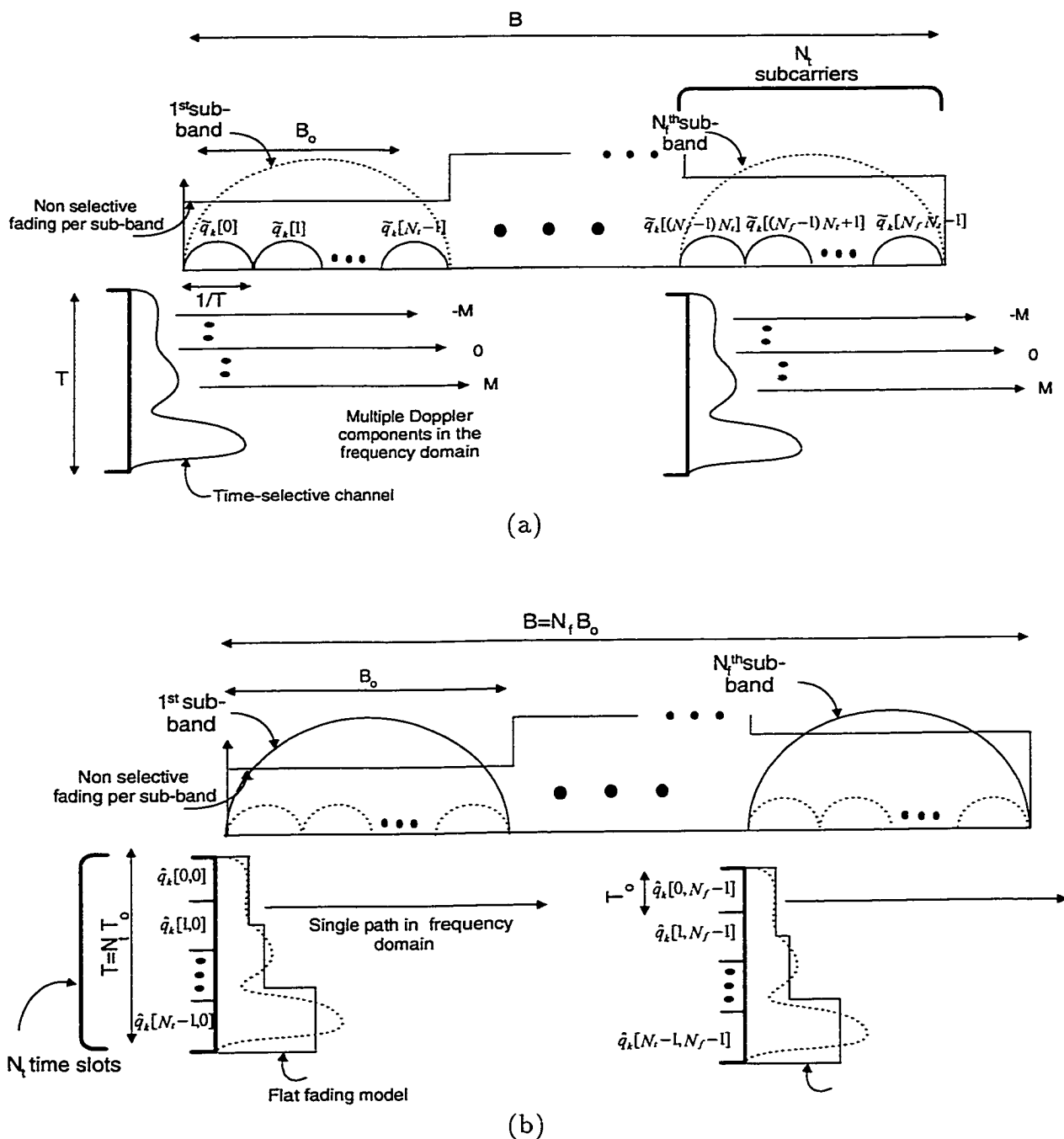


Figure 6.5. Diagonalizing a TFS channel via a TF-CDMA system starting from a MC-CDMA system. The bandwidth is divided into N_f sub-bands each contains N_t subcarriers that are faded similarly. To diagonalize TFS channel, each basis waveform duration is reduced by N_t , its bandwidth is increased by N_t so as the new basis waveforms encounter non selective fading in time and frequency. (a) MC-CDMA system. (b) TF-CDMA.

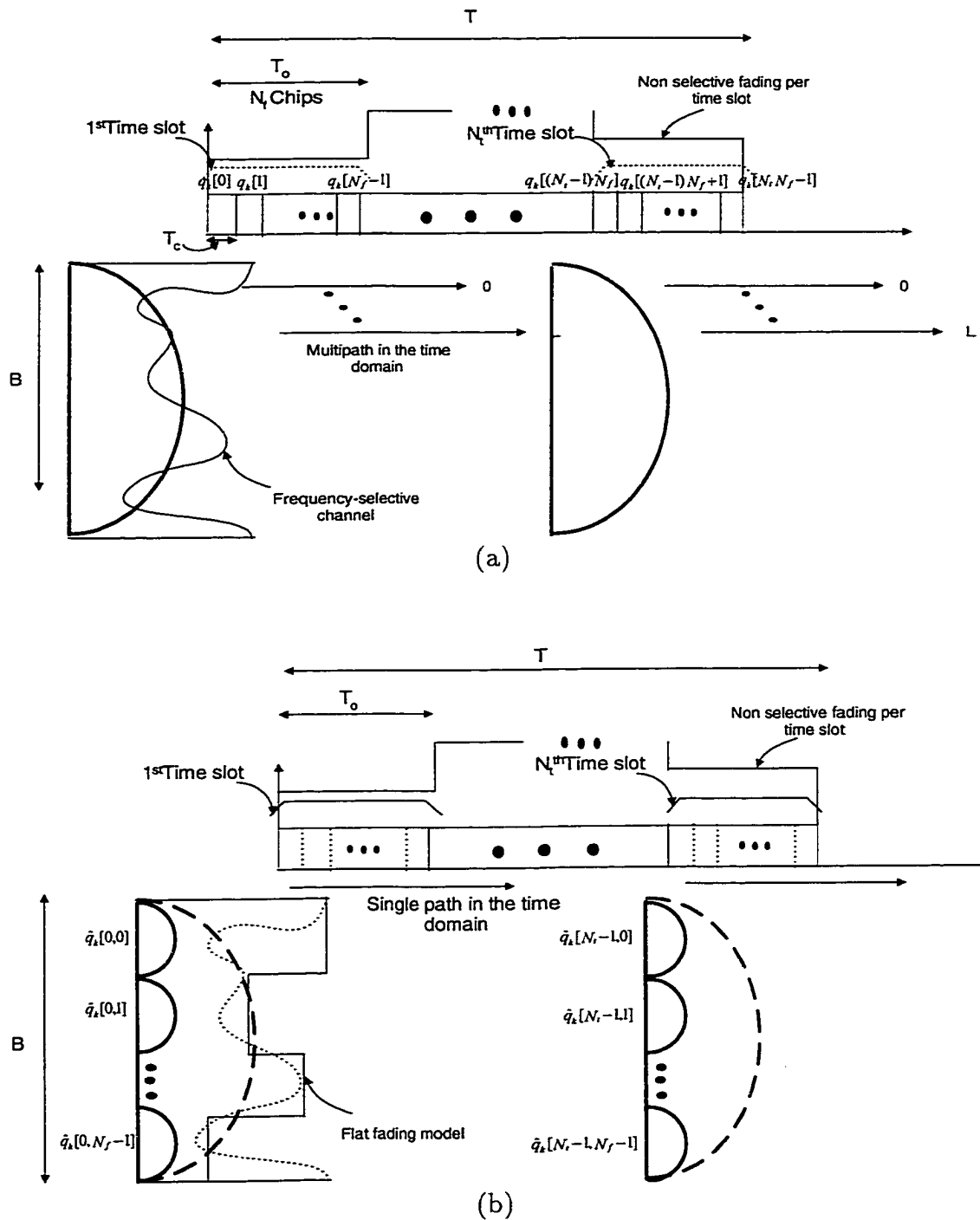


Figure 6.6. Diagonalizing TFS channel via TF-CDMA system starting from a DS-CDMA system. The symbol duration is divided into N_f time slots each contains N_f time samples that fade similarly. To diagonalize the TFS channel, each basis waveform bandwidth is reduced by N_f , its duration is increased by N_f so as the new basis waveforms encounter flat fading in time and frequency. (a) DS-CDMA system. (b) TF-CDMA.

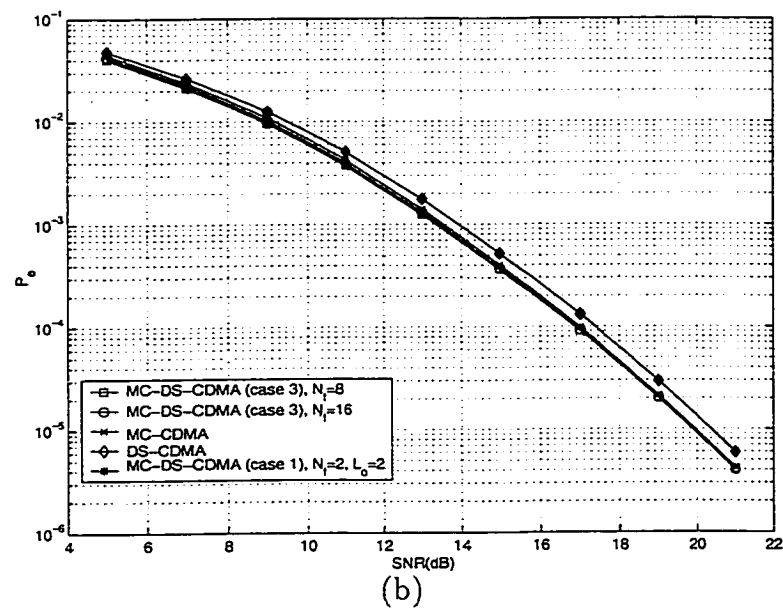
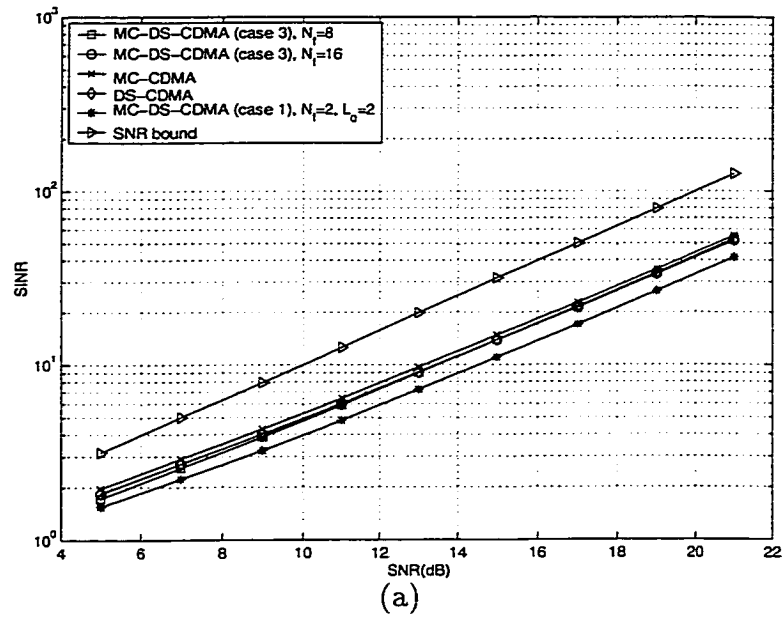


Figure 6.7. Various systems performance over FS channel for $K = 20$ as a function of SNR . (a) $SINR$. (b) P_e .

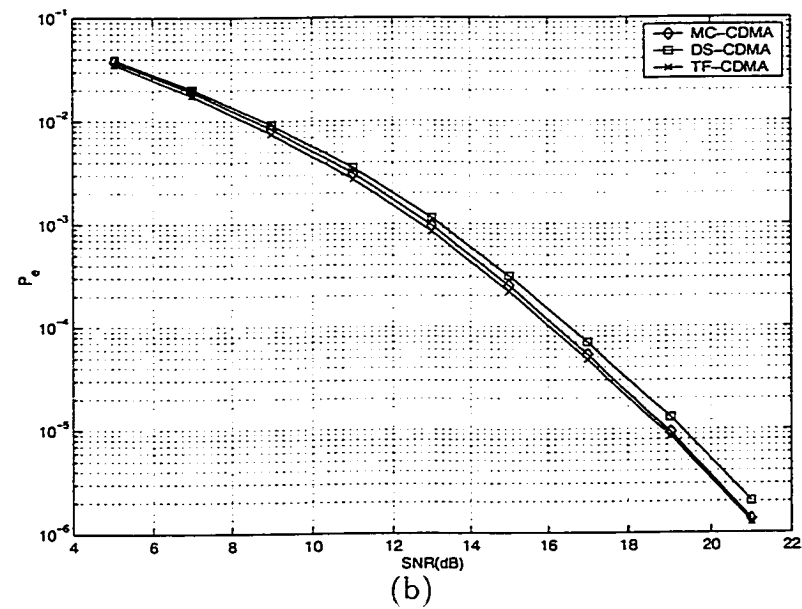
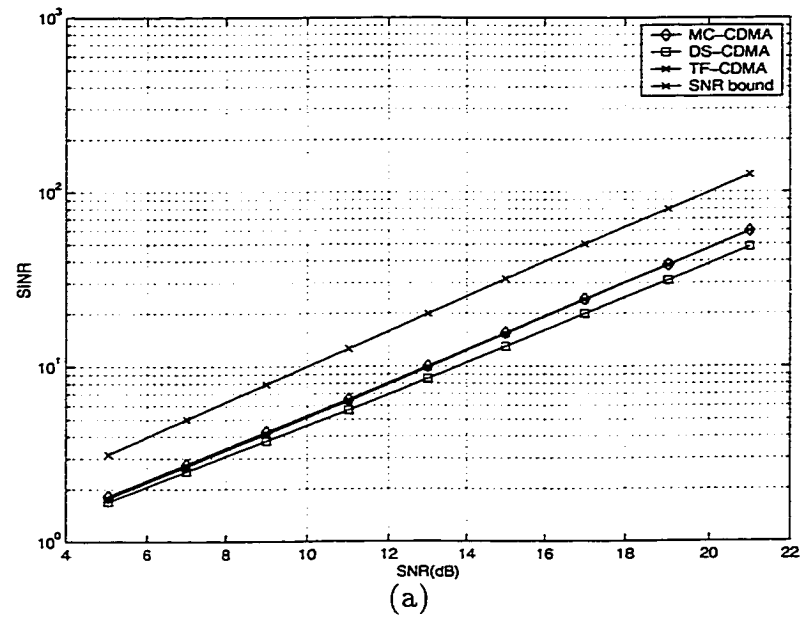


Figure 6.8. The performance of MC-CDMA, DS-CDMA and TF-CDMA systems over TFS channel for $K = 20$ as a function of SNR and at $B_d T = 0.2$. (a) $SINR$. (b) P_e .

CHAPTER 7

CONCLUSIONS AND FUTURE RESEARCH

This thesis has proposed some innovations in the design of CDMA systems operating over time and frequency selective channels. CDMA are MAI-limited systems. MAI causes an irreducible bit error rate (interference floor) even at high SNR. We studied interference suppression technique based on Minimum Mean Square Error (MMSE) criterion. The receiver building blocks are the canonical multipath-Doppler coordinates that enable us to naturally partition the signal space into primary and secondary coordinates. The detector employs a number N_{tot} of primary plus secondary coordinates that define the detector subspace. To suppress N_i interferers, the detector subspace should have a dimension $N_{tot} \geq N_i + 1$. Primary coordinates only carry desired signal and secondary coordinates are added progressively until necessary dimensions are attained to suppress interference. The proposed receiver can achieve near-optimal performance with minimal complexity. The receiver also lends itself easily to adaptive implementations that only require the knowledge of the desired user's signature code. In Chapter 4, we studied the MC-CDMA system over multipath channels in the presence of imperfections, such as fast fading, frequency offsets and phase noise. The MC-CDMA system diagonalizes slow fading channels, however it suffers severe performance degradation in the presence of imperfections. Imperfections destroy orthogonality between subcarriers, thereby introducing ICI. We introduced a unified signal model that captures the different types of imperfections. Analytical expressions for the imperfections coefficients as well as an estimate to the number of strong coefficients were also provided. We then proposed a Rake receiver-like detector that captures the energy loss due to imperfections and exploits Doppler diversity.

In Chapter 5, we proposed signaling scheme and corresponding transceiver structure that diagonalizes time and frequency selective channels. The proposed scheme employs short-time Fourier basis waveforms as information-bearing signals. The aim is to have each basis waveform encounter flat fading. The conditions necessary for diagonalization to hold as well as a near-optimal choice of the basis waveforms was provided.

The thesis culminated with a general framework that includes the different CDMA systems under consideration as special cases. This framework exploited time-frequency duality to establish an equivalence between systems operating over purely frequency selective channels and those operating over purely time selective channels. We then generalized these results to include the different CDMA systems operating over time and frequency selective channels. Sufficient conditions for all systems to perform almost in a similar fashion over the different types of channels were derived. The different aspects of the results developed in this thesis suggest several promising directions for future research, some of which we discuss next.

- **Adaptive implementation to the MMSE detector in Chapter 3.**

In Chapter 3 we provided two possible adaptive implementation based on minimizing the output energy subject to constraining the desired component to a constant. One direction for future research is to consider adaptive implementation of the receiver. This include finding a suitable algorithm as well as addressing problems such as convergence rate, algorithm initialization, algorithm robustness, etc. We note that even though many papers have addressed adaptive implementation for multiuser detectors in slow fading channel [54, 23, 55, 56, 57], the performance of these adaptive

schemes in the presence of rapid temporal variations, as well as complexity issues remain an open issue.

- **Extending the scheme in Chapter 4 for other imperfections.**

Basically there exist two other main imperfections that severely degrade the performance of MC-CDMA systems – Inter Symbol Interference (ISI) and high Peak to Average Ratio (PAR). As mentioned before, the problem of ISI due to multipath is solved by appending a cyclic prefix at the end of each data frame. Cyclic prefix absorbs the channel echoes and restores orthogonality between the different subcarriers. A crucial condition for cyclic prefix to work is that it be longer than the number of multipaths L . In some scenarios this condition is not satisfied and again the orthogonality is destroyed creating ICI and energy leakage. The PAR problem is due to the nature of MC signal as a sum of sinusoids – so that its sampled amplitude has almost Gaussian distribution and can get high enough to be susceptible to non-linear distortion by power amplifiers. Non-linearities also destroy orthogonality and create ICI. An extension to our research is to find an equalizer for these imperfections parallel to the schemes introduced in Chapter 4. For instance, it could be possible to cast the ISI and PAR problems in the same unified framework introduced in Chapter 4.

- **Pulse shaping for improved channel diagonalization.** In Chapter 5, we derived the conditions necessary for the basis waveforms to diagonalize time- and frequency-selective channels. It is clear that better diagonalization is achieved if the basis waveform is well-localized in time and frequency. In the results in Chapter 5, we adopted the rectangular

pulse shape for simplicity. An interesting future research direction is to try to find better pulse shapes for improved channel diagonalization. For example, the Gaussian pulse was tested in [52]. This pulse is well-localized in time and frequency such that it meets the Hiesenberg uncertainty principle limit. However, there is no easy way of extracting data from those basis waveforms since they are non-orthogonal.

- **Finding the eigenfunctions for space-time scenarios.** In Chapter 5, we showed how to find an approximate eigenfunctions for time-and frequency-selective channels. A more challenging problem is to find the eigenfunctions for space-time channels as well. In scenarios where multiple antennas are used at the transmitter and/or the receiver and if the channel state information is a priori known at the transmitter, diagonalizing the channel is feasible. However, the eigenfunctions change with the spatial channel coefficients. A very challenging problem is to find *fixed* space-time basis functions that approximately diagonalize the space-time channel.

APPENDIX A

THE NECESSARY CONDITION FOR (3.47) TO HOLD

Recall that $\mathbf{R}_{e,e} = \mathbf{g}_1 \mathbf{g}_1^H + \mathbf{R}_{\epsilon,\epsilon}$. It follows from the matrix inversion lemma [31] that

$$\mathbf{R}_{e,e}^{-1} = \mathbf{R}_{\epsilon,\epsilon}^{-1} - \frac{\mathbf{R}_{\epsilon,\epsilon}^{-1} \mathbf{g}_1 \mathbf{g}_1^H \mathbf{R}_{\epsilon,\epsilon}^{-1}}{1 + \mathbf{g}_1^H \mathbf{R}_{\epsilon,\epsilon}^{-1} \mathbf{g}_1}. \quad (\text{A.1})$$

To characterize the eigenvector corresponding to the minimum eigenvalue we study the Rayleigh quotient $(\mathbf{x}^H \mathbf{R}_{e,e}^{-1} \mathbf{x}) / \|\mathbf{x}\|^2$. From (A.1) it follows that

$$\mathbf{x}^H \mathbf{R}_{e,e}^{-1} \mathbf{x} = \frac{\sigma^2 \mathbf{x}^H \mathbf{R}_{\epsilon,\epsilon}^{-1} \mathbf{x}}{\sigma^2 + \sigma^2 \mathbf{g}_1^H \mathbf{R}_{\epsilon,\epsilon}^{-1} \mathbf{g}_1} + \frac{\sigma^2 (\mathbf{g}_1^H \mathbf{R}_{\epsilon,\epsilon}^{-1} \mathbf{g}_1) (\mathbf{x}^H \mathbf{R}_{\epsilon,\epsilon}^{-1} \mathbf{x})}{\sigma^2 + \sigma^2 \mathbf{g}_1^H \mathbf{R}_{\epsilon,\epsilon}^{-1} \mathbf{g}_1} - \frac{\sigma^2 |\mathbf{x}^H \mathbf{R}_{\epsilon,\epsilon}^{-1} \mathbf{g}_1|^2}{\sigma^2 + \sigma^2 \mathbf{g}_1^H \mathbf{R}_{\epsilon,\epsilon}^{-1} \mathbf{g}_1}. \quad (\text{A.2})$$

Recall from (3.27) that

$$\mathbf{R}_{\epsilon,\epsilon}^{-1} = \mathbf{V}_{I,p} \tilde{\Lambda}^{-1} \mathbf{V}_{I,p}^H + \frac{1}{\sigma^2} \mathbf{V}_{\perp,p} \mathbf{V}_{\perp,p}^H, \quad (\text{A.3})$$

from which we conclude that as $\sigma^2 \rightarrow 0$, $\mathbf{R}_{\epsilon,\epsilon}^{-1} \approx \frac{1}{\sigma^2} \mathbf{P}_{\perp,p} = \frac{1}{\sigma^2} \mathbf{V}_{\perp,p} \mathbf{V}_{\perp,p}^H$. Combining this fact with (A.2) we conclude that for $\sigma^2 \rightarrow 0$

$$\mathbf{x}^H \mathbf{R}_{e,e}^{-1} \mathbf{x} \approx \frac{\mathbf{x}^H \mathbf{P}_{\perp,p} \mathbf{x}}{\sigma^2 + \mathbf{g}_1^H \mathbf{P}_{\perp,p} \mathbf{g}_1} + \frac{1}{\sigma^2} \frac{(\mathbf{g}_1^H \mathbf{P}_{\perp,p} \mathbf{g}_1) (\mathbf{x}^H \mathbf{P}_{\perp,p} \mathbf{x})}{\sigma^2 + \mathbf{g}_1^H \mathbf{P}_{\perp,p} \mathbf{g}_1} - \frac{1}{\sigma^2} \frac{|\mathbf{x}^H \mathbf{P}_{\perp,p} \mathbf{g}_1|^2}{\sigma^2 + \mathbf{g}_1^H \mathbf{P}_{\perp,p} \mathbf{g}_1}. \quad (\text{A.4})$$

From (A.4) we conclude that in order to keep $\mathbf{x}^H \mathbf{R}_{e,e}^{-1} \mathbf{x}$ from blowing up (as $\sigma^2 \rightarrow 0$), we need to have the second term on the right-hand side equal to zero. Clearly, the choice $\mathbf{x} = \alpha \mathbf{g}_1$ accomplishes this and it follows that

$$\lim_{\sigma^2 \rightarrow 0} \frac{\alpha \mathbf{g}_1^H \mathbf{R}_{e,e}^{-1} \alpha \mathbf{g}_1}{\|\alpha \mathbf{g}_1\|^2} = \frac{1}{\|\mathbf{g}_1\|^2}. \quad (\text{A.5})$$

However, $\mathbf{x} = \mathbf{g}_1$ may not be the unique choice unless $\mathbf{P}_{\perp,p}$ has rank D_p (full-rank). Since $\mathbf{V}_{\perp,p}$ is $D_p \times (N_{tot} - N_i)$, a necessary condition for $\mathbf{P}_{\perp,p}$ to be full-rank is that

$N_{tot} - N_i = D_p + D_s - N_i \geq D_p$, or equivalently, $D_s \geq N_i$. Thus, we conclude that a necessary condition for the least (most) dominant eigenvector of $\mathbf{R}_{\mathbf{e},\mathbf{e}}^{-1}$ ($\mathbf{R}_{\mathbf{e},\mathbf{e}}$) to converge to $e^{j\phi}\mathbf{g}_1/\|\mathbf{g}_1\|$ in the limit of high SNR (with $1/\|\mathbf{g}_1\|^2$ as the corresponding eigenvalue¹) is that $D_s \geq N_i$. This proves (3.47).

¹The remaining $D_p - 1$ eigenvalues of $\mathbf{R}_{\mathbf{e},\mathbf{e}}^{-1}$ ($\mathbf{R}_{\mathbf{e},\mathbf{e}}$) $\rightarrow +\infty(0)$.

APPENDIX B

THE PROOF OF PROPOSITION 1, CHAPTER 5

Using (2.2) in (5.14) we get $\rho = 1 - xy$ where

$$x = \frac{1}{(T_0)^2} \int_{-T_0/2}^{T_0/2} \int_{-T_0/2}^{T_0/2} R_1(t_1 - t_2) dt_1 dt_2 \quad (\text{B.1})$$

$$y = \frac{1}{(B_0)^2} \int_{-B_0/2}^{B_0/2} \int_{-B_0/2}^{B_0/2} R_2(f_1 - f_2) df_1 df_2. \quad (\text{B.2})$$

Using (5.7), (B.1) becomes

$$x \approx 2\text{sinc}(B_d T_0) - \text{sinc}^2(B_d T_0) \quad (\text{B.3})$$

by using the approximation $\frac{1}{a} \int_0^a \text{sinc}(l) dl = \text{sinc}(a/2)$ that is justified by **C1**. A similar expression for y can be obtained by replacing $2B_d$ with T_m and T_0 with B_0 and using the fact that $e^{-j\pi T_m \Delta f} \approx 1$ in (5.7) for $|\Delta f| < B_0$ (due to **C2**). Thus,

$$\rho = 1 - \left[1 - (1 - \text{sinc}(B_d T_0))^2\right] \left[1 - (1 - \text{sinc}(T_m B_0/2))^2\right] \quad (\text{B.4})$$

which can be further simplified to

$$\rho = K((B_d T_0)^6 + (T_m B_0)^6) - K^2(B_d T_m)^6 \quad (\text{B.5})$$

by using the fact that $1 - \text{sinc}(a) \approx \frac{\pi}{3!} a^3$ for $x \ll 1$, where $K = \frac{\pi^2}{(3!)^2 2^6}$. Since $(B_d T_0)^6 (T_m B_0)^6 = (T_m B_d)^6$ is a constant, we deduce that ρ has a minimum at $B_d T_0 = T_m B_0$ by using the inequality $\frac{a+b}{2} \geq \sqrt{ab}$ for $a > 0$ and $b > 0$.

APPENDIX C

THE PROOF OF (6.43)

Recall from (6.12) that in FS channel, (i.e. $M=0$ in (6.11)), $\tilde{h}_k(0, n) = \tilde{C}_k(0, (n + 1/2)/T)$. For (6.45) to hold, it suffices to prove that $\tilde{h}_k(0, n)$ is the n^{th} component of the DFT of $\{h_k(0, l), l = 0, 1, \dots, L\}$, from which

$$\begin{aligned}
 \sum_{l=0}^L h_k[0, l] e^{-j\frac{2\pi ln}{N}} &= \sum_{l=0}^L e^{-j\frac{2\pi ln}{N}} \int_0^{T_m} c_k(0, \tau) \text{sinc}(l - B\tau) e^{j\pi(l - B\tau)} dt \\
 &= \int_0^{T_m} c_k(0, \tau) e^{-j\pi B\tau} \sum_{l=0}^L \text{sinc}(l - B\tau) e^{-j2\pi l(n/N + 1/2)} dt \\
 &= \int_0^{T_m} c_k(0, \tau) e^{-j\pi B\tau} e^{-j2\pi(n/N + 1/2)B\tau} dt \\
 &= \int_0^{T_m} c_k(0, \tau) e^{-j\frac{2\pi n\tau}{T}} dt \\
 &= \tilde{C}_k(0, n/T) \\
 &= \tilde{h}_k(0, n) \square \tag{C.1}
 \end{aligned}$$

APPENDIX D

THE PROOF OF (6.63)

Recall from (6.4) that in TS channel (i.e. $L=0$ in (6.3)), $h_k(p, 0) \approx c_k((p + 1/2)T_c, 0)$.

Note also from (6.12) that in TS channel,

$$\tilde{h}_k(m, 0) = \int_{-B_d}^{B_d} \tilde{C}_k(\theta, 0) \text{sinc}(m - \theta T) e^{-j\pi(m - \theta T)} d\theta. \quad (\text{D.1})$$

Let $v = M + m$, for (6.65) to hold, it suffices to prove that $e^{j\frac{2\pi Mp}{N}} h_k(p, 0)$ is the p^{th} component of the Inverse (I) DFT of $\{\tilde{h}_k(v, 0), v = 0, 1, \dots, 2M\}$, from which

$$\sum_{v=0}^{2M} \tilde{h}_k(v, 0) e^{j\frac{2\pi vp}{N}} = \int_{-B_d}^{B_d} \tilde{C}_k(\theta, 0) e^{j\pi(M + \theta T)} \sum_{v=0}^{2M} \text{sinc}(v - M - \theta T) e^{-j\pi v} e^{j\frac{2\pi vp}{N}} d\theta \quad (\text{D.2})$$

$$= \int_{-B_d}^{B_d} \tilde{C}_k(\theta, 0) e^{j\pi(M + \theta T)} e^{j2\pi(p/N - 1/2)(M + \theta T)} d\theta \quad (\text{D.3})$$

$$= e^{j\frac{2\pi Mp}{N}} \int_{-B_d}^{B_d} \tilde{C}_k(\theta, 0) e^{j2\pi p T_c \theta} d\theta \quad (\text{D.4})$$

$$= e^{j\frac{2\pi Mp}{N}} h_k(p, 0) \square. \quad (\text{D.5})$$

APPENDIX E

THE PROOF OF LEMMA 1

Starting with the right hand side of (6.67),

$$\sum_{m=-M}^M H_k(m, l) e^{j \frac{2\pi m(p+1/2)}{N}} = \int_0^{T_m} \int_{-B_d}^{B_d} C(\theta, \tau) \text{sinc}(l - B\tau) e^{-j\pi(l-B\tau)} e^{j\pi(\theta T)} \times \sum_{m=-M}^M \text{sinc}(m - \theta T) e^{-j\pi m} e^{j \frac{2\pi m(p+1/2)}{N}} d\theta d\tau \quad (\text{E.1})$$

$$= \int_0^{T_m} \int_{-B_d}^{B_d} C(\theta, \tau) \text{sinc}(l - B\tau) e^{-j\pi(l-B\tau)} e^{j\pi(\theta T)} e^{j\pi M} \times e^{-j \frac{2\pi M(p+1/2)}{N}} \sum_{v=0}^{2M} \text{sinc}(v - M - \theta T) e^{-j\pi v} e^{j \frac{2\pi v(p+1/2)}{N}} d\theta d\tau \quad (\text{E.2})$$

$$= \int_0^{T_m} \int_{-B_d}^{B_d} C(\theta, \tau) \text{sinc}(l - B\tau) e^{-j\pi(l-B\tau)} e^{j\pi(\theta T)} \times e^{j\pi M} e^{-j \frac{2\pi M(p+1/2)}{N}} e^{j2\pi(\frac{p+1/2}{N}-1/2)(M+\theta T)} d\theta d\tau \quad (\text{E.3})$$

$$= \int_0^{T_m} \int_{-B_d}^{B_d} C(\theta, \tau) \text{sinc}(l - B\tau) e^{-j\pi(l-B\tau)} \times e^{j2\pi\theta T(\frac{p+1/2}{N})} d\theta d\tau \quad (\text{E.4})$$

$$= \int_0^{T_m} c((p+1/2)T_c, \tau) \text{sinc}(l - B\tau) e^{-j\pi(l-B\tau)} d\tau \quad (\text{E.5})$$

$$= h_k(p, l) \quad (\text{E.6})$$

where in (E.2), we did a change of variables $v = m + M$. \square

BIBLIOGRAPHY

- [1] J. G. Proakis, *Digital Communications*. New York: McGraw Hill, 3rd ed., 1995.
- [2] T. S. Rappaport, *Wireless Communications*. New Jersey: Prentice Hall, 1996.
- [3] A. M. Sayeed and B. Aazhang, "Joint multipath-Doppler diversity in mobile wireless communications," *IEEE Trans. Commun.*, vol. 47, pp. 123–132, Jan. 1999.
- [4] R. Lupas and S. Verdu, "Near-far resistance of multiuser detectors in asynchronous channels," *IEEE Trans. Commun.*, vol. 38, pp. 496–508, Apr. 1990.
- [5] S. Hara and R. Prasad, "Overview of multicarrier CDMA," *IEEE Commun. Magazine*, pp. 126–133, Dec. 1997.
- [6] K. Fazel and L. Papke, "On the performance of orthogonal multicarrier CDMA in a multipath fading channel," in *Proc. IEEE PIMRC*, pp. 468–472, Sept. 1993.
- [7] E. Sourour and M. Nakagawa, "Performance of orthogonal multicarrier CDMA in a multipath fading channel," *IEEE Trans. Commun.*, vol. 44, pp. 356–367, Mar. 1996.
- [8] V. Dasilva and E. Sousa, "Performance of orthogonal CDMA codes for quasi-synchronous communication systems," in *Proc. IEEE ICUPC '93*, (Ottawa, Canada), pp. 995–999, Oct. 1993.
- [9] T. Lok and T. Wong, "Transmitter and receiver optimization in multicarrier CDMA systems," *IEEE Trans. Commun.*, vol. 48, pp. 1197–1207, July 2000.
- [10] T. Kadous and A. Sayeed, "Progressively powerful multiuser detection over time-varying multipath channel," in *proc. IEEE GLOBECOM '1999.*, (Rio de-Janeiro, Brazil), Dec. 1999.
- [11] T. A. Kadous and A. M. Sayeed, "Decentralized multiuser detection for time-varying multipath channels," *IEEE Trans. Commun.*, vol. 48, pp. 1840–1852, Nov. 2000.
- [12] A. M. Sayeed, "Canonical multipath-Doppler coordinates in wireless communications," in *36th Annual Allerton Conference on Communication, Control and Computing*, 1998.
- [13] A. M. Sayeed, A. Sendonaris, and B. Aazhang, "Multiuser detection in fast fading multipath environments," *IEEE J Select. Areas Commun.*, vol. 16, pp. 1691–1701, Dec. 1998.

- [14] P.A.Bello, "Measurement of random time-variant linear channels," *IEEE Trans. Commun.*, vol. 15, pp. 469–475, July 1969.
- [15] Y. Li, L. Cimini, and N. R. Sollenberger, "Robust channel estimation for OFDM systems with rapid dispersive fading channels," *IEEE Trans. Commun.*, vol. 46, pp. 902–915, July 1998.
- [16] D. Slepian, "On bandwidth," *Proc. IEEE*, vol. 64, pp. 292–300, Mar. 1976.
- [17] S. Verdu, *Multuser Detection*. Cambridge University Press, 1998.
- [18] in *Wireless Communications: Signal Processing Perspectives* (H. V. Poor and G. W. Wornell, eds.), Prentice Hall, 1998.
- [19] U. Madhow, "Blind adaptive interference suppression for direct-sequence CDMA," *Proc. IEEE (Special Issue on Blind System Identification and Estimation)*, vol. 86, pp. 2049–2069, Oct. 1998.
- [20] G. Woodward and B. Vucetic, "Adaptive detection of DS-CDMA," *Proc. IEEE*, vol. 86, pp. 1413–1434, July 1998.
- [21] I. Ghauri and D. T. M. Slock, "Blind channel and linear MMSE receiver determination in DS-CDMA systems," in *Proc. ICASSP'99*, pp. 2699–2702, Mar. 1999.
- [22] M. K. Tsatsanis and Z. Xu, "Performance analysis of minimum variance CDMA receivers," *IEEE Trans. Signal Processing*, vol. 46, pp. 3014–3022, Nov. 1998.
- [23] X. Wang and H. V. Poor, "Blind adaptive multiuser detection in multipath CDMA channels based on subspace tracking," *IEEE Trans. Signal Processing*, vol. 46, pp. 3030–3044, Nov. 1998.
- [24] H. Liu and M. D. Zoltowski, "Blind equalization in antenna array CDMA systems," *IEEE Trans. Signal Processing*, vol. 45, pp. 161–172, Jan 1997.
- [25] T. F. Wong, T. M. Lok, J. S. Lehnert, and M. D. Zoltowski, "A linear receiver for direct-sequence spread-spectrum multiple-access systems with antenna arrays and blind adaptation," *IEEE Trans. Inform. Theory*, vol. 44, pp. 659–676, Mar. 1998.
- [26] T. Kailath, "Sampling models for linear time-variant filters," Tech. Rep. 352, MIT Research Laboratory of Electronics, May 1959.
- [27] G. H. Golub and C. F. V. Loan, *Matrix Computations*. John Hopkins, 1996.

- [28] U. Madhow and M. L. Honig, "MMSE interference suppression for direct-sequence spread-spectrum CDMA," *IEEE Trans. Commun.*, vol. 42, pp. 3178–3188, Dec. 1994.
- [29] X. Wang and H. V. Poor, "Blind multiuser detection: A subspace approach," *IEEE Trans. Inform. Theory*, vol. 44, pp. 677–690, Mar. 1998.
- [30] H. V. Poor and S. Verdu, "Probability of error in MMSE multiuser detection," *IEEE Trans. Inform. Th.*, vol. 43, pp. 858–871, May 1997.
- [31] S. Haykin, *Adaptive Filter Theory*. Prentice Hall, 3 ed., 1996.
- [32] S. Verdu, "Optimum multi-user asymptotic efficiency," *IEEE Trans. Commun.*, vol. 38, pp. 496–508, Apr. 1990.
- [33] B. D. Van Veen, A. M. Sayeed, and E. N. Onggosanusi, "Interference resistant blind acquisition and channel estimation for CDMA communication systems," in *Proc. 2000 IEEE Int. Conf. on Acoust., Speech and Signal Proc. — ICASSP '00*, 2000.
- [34] S. Bhasyam, A. M. Sayeed, and B. Aazhang, "Time-selective signaling and reception for communication over multipath fading channels," *IEEE Trans. Commun.*, vol. 48, pp. 83–94, Jan 2000.
- [35] A. M. Sayeed, E. N. Onggosanusi, and B. D. Van Veen, "A canonical space-time characterization of mobile wireless channels," *IEEE Communications Letters*, pp. 94–96, Apr. 1999.
- [36] E. N. Onggosanusi, A. M. Sayeed, and B. D. Van Veen, "Canonical space-time coordinates for multiuser wireless communications," in *Proc. 2nd IEEE Wksp. on Signal Proc. Adv. Wireless Commun. — SPAWC '99*.
- [37] E. N. Onggosanusi, B. D. Van Veen, and A. M. Sayeed, "Multi-access interference suppression in canonical space-time coordinates: A decentralized approach," *submitted to IEEE Trans. Commun.*
- [38] S. Hara and R. Prasad, "Design and performance of multicarrier CDMA system in frequency-selective Rayleigh fading channels," *IEEE Trans. Veh. Technol.*, vol. 48, pp. 1584–1595, Sept. 1999.
- [39] T. Pollet, M. V. Bladel, and M. Moeneclaey, "BER sensitivity of OFDM systems to carrier frequency offset and wiener phase noise," *IEEE Trans. Commun.*, vol. 43, pp. 191–193, Feb./Mar./Apr. 1995.
- [40] P. Robertson and S. Kaiser, "Analysis of the effect of phase-noise in orthogonal frequency division multiplex (OFDM) systems," in *proc. IEEE ICC '95.*, (Seattle, WA), pp. 1652–1657, June 1995.

- [41] L. Tomba and W. A. Krzymien, "Sensitivity of the MC-CDMA access scheme to carrier phase noise and frequency offset," *IEEE Trans. Veh. Technol.*, vol. 48, pp. 1657–1665, Sept. 1999.
- [42] T. Pollet, M. Moeneclaey, I. Jeanclaude, and H. Sari, "Effect of carrier phase jitter on single-carrier and multi-carrier QAM systems," in *Proc. ICC 1995*, (Seattle, Washington), pp. 1046–1050, IEEE, June 1995.
- [43] C. Muschallik, "Influence of RF oscillators on an OFDM signal," *IEEE Trans. Consumer Elect.*, vol. 41, pp. 592–603, Aug. 1995.
- [44] P. Robertson and S. Kaiser, "Analysis of the loss of orthogonality through Doppler spread in OFDM systems," in *Proc. GLOBECOM 99*, (Brazil), pp. 1–10, IEEE, DEC. 1999.
- [45] X. Gui and T. S. Ng, "Performance of asynchronous orthogonal multicarrier CDMA system in frequency selective fading channel," *IEEE Trans. Commun.*, vol. 47, pp. 1084–1091, July 1999.
- [46] H. Steendam and M. Moeneclaey, "Analysis and optimization of the performance of OFDM on frequency-selective time-selective fading channels," *IEEE Trans. Commun.*, vol. 47, pp. 1811–1819, Dec. 1999.
- [47] J. Armstrong, "Analysis of new and existing methods of reducing intercarrier interference due to carrier frequency offset in OFDM," *IEEE Trans. Commun.*, vol. 47, pp. 365–369, March 1999.
- [48] G. J. Foschini and G. Vannucci, "Characterizing filtered light waves corrupted by phase noise," *IEEE Trans. Inform. Theory*, vol. IT-34, pp. 1437–1448, Nov. 1988.
- [49] A. Papoulis, *Probability, Random Variables and Stochastic Processes*. New York: McGraw Hill, 3rd ed., 1991.
- [50] L. Cimini, "Analysis and simulations of a digital mobile channel using orthogonal frequency division multiplexing," *IEEE Trans. Commun.*, vol. 33, pp. 665–674, July 1985.
- [51] W. Kozek, "On the transfer function calculus for under-spread LTV channels," *IEEE Tran. Sig. Proc.*, Jan. 1997.
- [52] K. Liu, T. A. Kadous, and A. M. Sayeed, "Orthogonal time-frequency signaling in doubly dispersive channels," *to be submitted to IEEE Trans. Inform. Theory*.
- [53] M. K. Simon and M. S. Alouini, "A unified approach to the performance analysis of digital communication over generalized fading channels," *Proc. IEEE*, vol. 86, pp. 1860–1877, Sept. 1998.

- [54] M. Honig, U. Madhow, and S. Verdu, "Blind adaptive multiuser detection," *IEEE Trans. Inform. Theory*, vol. 41, pp. 944–960, July 1995.
- [55] D. Chen and S. Roy, "An adaptive multiuser receiver for CDMA systems," *IEEE JSAC*, vol. 12, pp. 808–816, June 1994.
- [56] J. Caire, "Two-stage nondata-aided adaptive linear receivers for DS/CDMA," *IEEE Trans. Commun.*, vol. 48, pp. 1712–1724, Oct. 2000.
- [57] U. Madhow, "Blind adaptive interference suppression for the near-far resistant acquisition and demodulation of direct-sequence CDMA systems," *IEEE Trans. Signal Processing*, vol. 45, pp. 124–136, Jan. 1997.